Investigations of Charge Carrier Complexes in CdSe Nanocrystals Using State-Selective Ultrafast Spectroscopy

Samuel L Sewall

Department of Chemistry

McGill University

Montreal, Quebec

Canada

January 2010

A Thesis submitted to McGill University
In partial fulfillment of requirements for the degree of
Doctor of Philosophy

Table of Contents

Abstract

This thesis is about the use of exciton selective ultrafast spectroscopic techniques in investigations of state-to-state dynamics and biexcitonic interactions in CdSe nanocrystals (NCs). Close to the band edge the electronic states are well-defined spectrally, and can be excited using different pump pulse wavelengths generated using tunable optical parametric amplifiers (OPAs). In chapter 3 the response of nanocrystals samples when excited into the three lowest energy states is compared with traditional UV excitation. This reveals how powerful state-selective techniques are in measurement of intraband relaxation dynamics and state-specific biexciton interaction strengths. The next chapter uses these techniques to investigate the electronic structure of the both the single exciton and biexciton manifold of states in CdSe nanocrystals. The lowest energy states of the biexciton spectrum are characterized, which shows a measurable dependence on the configuration of the component charge carriers.

The size dependence of different biexciton states is then explored, both those of intrinsic states measurable at early times after optical pumping and a mixed phase biexciton observable at later times when hole trapping has occurred. The dynamics of this trapping process are shown to be state dependent, occurring much faster from higher excited states. The ground state biexciton can be explored in some detail, and it is revealed to be split into different states by various asymmetries of the nanocrystal lattice and shape. This allows absorption into and emission from the biexciton to occur at different energies, which manifests itself as Stokes shift of the band edge biexciton.

Résumé

Cette thèse porte sur l'étude de la dynamique des transitions quantiques et des interactions biexcitoniques dans des nanocristaux de CdSe (NCS) par des techniques spectroscopiques ultra-rapides à excitation sélective. Les états électroniques situés à la frontière de la bande sont bien résolus spectralement et peuvent être excités à différentes longueurs d'onde par des impulsions pompes générées par des amplificateurs paramétriques optiques à fréquence ajustable (OPAs). Le chapitre 3 présente la réponse des nanocristaux lorsqu'ils sont excités dans les trois premiers niveaux d'énergie les plus faibles comparativement à leur réponse via une excitation dans l'UV, plus couramment employée. Cette étude démontre l'efficacité des techniques d'excitations sélectives quant à la caractérisation de la dynamique de relaxation inter-bandes et de la force des interactions biexcitoniques d'états spécifiques. Dans le chapitre suivant, ces même techniques sont utilisées pour étudier la structure électronique des états excitoniques et biexcitoniques des nanocristaux de CdSe. La caractérisation des niveaux de plus basses énergies du spectre des biexcitons démontre que la réponse de ces derniers dépend, de façon mesurable, de la configuration des transporteurs de charges.

La dépendance de la taille des états biexcitoniques est ensuite explorée. Pour ce faire, les états intrinsèques sont mesurés immédiatement après le pompage optique ainsi qu'un état mixte de type biexcitonique apparaissant après le piégeage des trous. La dynamique de ce processus, appelé "piégeage de trou", dépend de l'état quantique et est beaucoup plus rapide pour les états excités supérieurs. L'étude détaillée de l'état biexcitonique fondamental démontre que ce dernier se divise en différents états distincts. Ce phénomène est dû aux multiples asymétries apparaissant dans la forme et dans le

réseau du nanocrystal, ce qui permet aux biexcitons d’absorber et d’émettre des photons d’énergies différentes, tel que reflété par le déplacement de Stokes de la bande biexcitonique.

Statement of Originality

The author claims that the following aspects of the thesis constitute original scholarship and an advancement of knowledge:

Chapter 3: The non-linear optical response of CdSe nanocrystals samples measured by pump/probe, when excited into the three lowest energy states is compared with UV excitation. The dynamics of the band edge bleach was shown to be state dependent in a predictable manner based upon the electronic structure of the system, and it was conclusively shown to be completely determined by electron populations with no contribution of hole states. This allowed a subtractive method using the $1P_e$ and $1S_e$ data to obtain the electronic intraband relaxation dynamics with very high precision. Similarly, by examining the A1 region sub-resonant to the band edge, state specific biexciton signals were observed for the first time in high quality colloidal samples. This gives a signal sensitive to the full eigenstates of the system, revealing state dependent interaction strengths and dynamics. By taking advantage of these biexcitonic signals, a direct measurement of hole relaxation between well defined states was made which showed ultrafast relaxation in the valence band overcoming the phonon bottleneck.

Chapter 4: This examines electronic structure of the both the single exciton and biexciton manifold of states in CdSe nanocrystals. The assignments of the symmetry of the 4 lowest energy transitions are made experimentally for the first time, and they disagree with the conventional EMA results. This is an important result for the design and interpretation of many ultrafast experiments. The lowest energy states of the biexciton spectrum are characterized for the first time also, showing how the different configurations of charges making up these complexes affect the interaction strength.

Chapter 5: The size dependence of two different excited biexciton states is explored. One is the intrinsic state measurable at early times after excitation into the 1S-2S$_{3/2}$ state, and the other a mixed phase biexciton observable at later times (~50 ps) when hole trapping has occurred. Both types of biexcitons show an increase in binding energies as the size of the nanocrystal is decreased, which sets an experimental benchmark for theoretical treatments of these complex systems. The dynamics of the hole trapping process are shown to be state dependent, occurring much faster from higher excited states.

Chapter 6: The ground state biexciton is explored, as it is the most important state for applications in gain and quantum computing. Measurements of the biexciton binding energy using states selective absorptive and emissive techniques reveal large inconsistencies in the measured values, well outside experimental error. These can be resolved by showing that the band edge biexciton level is split into different states by the wurzite lattice and shape asymmetry of the nanocrystal. This allows absorption into and emission from this state to occur at different energies, which manifests itself as a previously unobserved biexciton Stokes shift.

Portions of this thesis contains material that has been published previously by the author, please see the appendix for the copyright permission forms.

Ultrafast spectroscopy requires is inherently a collaborative effort, so much of the data presented here was obtained while working in tandem Ryan Cooney. He performed the following procedures without the help of the author:

1. Fitting the ΔΔOD Dynamics shown in Figure 3.7

2. Measuring the Non-linear Spectra shown in Figure 4.3
3. Modeling of Charge Carrier Wavefunctions displayed in Figure 5.4

All nanocrystal samples which were not purchased commercially were synthesized by Eva Dias (used in Chapters 3 and 5).

Acknowledgements

A PhD is not something that can be undertaken without the knowledge, expertise, and support of many people, both inside and outside of the academic community. I would like to take this opportunity to thank as many as possible.

Firstly, I must thank my supervisor, Dr. Patanjali Kambhampati, for taking a chance on a pretty wild looking guy to recruit for his first PhD student. A good scientist must have patience, imagination and insight, and Pat has helped me immensely in each of these areas. He was incredibly patient with me as I developed my skills in setting up optics and running experiments, and has shown me there is always a new way to attack a problem or analyze a data set. Thank you for all your help and encouragement.

The other graduate students I worked with in the Kambhampati group are an amazing collection of people and personalities. In my "generation", I had the pleasure of working with Kevin Anderson from the outset, and the work he did on setting up our data acquisition program puts me forever in his debt. Ryan Cooney and I have in many ways done a joint project, working with each other on all aspects of research including the design and construction of the spectrometer, instrument maintenance, and daily operation. We were constantly bouncing ideas off each other during analysis, writing manuscripts and during preparation of our theses. Eva Dias has put up with all of our shenanigans with grace and good humor, and has contributed an incredible amount in terms of materials synthesis and characterization. Thanks also to Dr. Sagar, a post-doc with our group.

The newest generation of the group- Jon Saari, Jon Mooney and Pooja Tyagi- have made the final year of graduate school a real treat with their enthusiasm for taking over the reigns, it's comforting to leave with the future in good hands. There are too many other graduate students who I would like to thank, so I will restrict myself to only mentioning Adil Kassam, David Kolin, Finlay MacNabb, Chris Maclaughlin, Matt Hassler, Chris Godbout, Robert Chatelain, and Vance Morrison.

I have been incredibly lucky to work in the last year in collaboration with Alex Zunger and Alberto Franceschetti at NREL in Colorado; I offer them many thanks for sharing their expertise with us.

There are also several wonderful professors and educators in this department with whom I would like to thank for many wonderful conversations on a range of topics, including Prof. David Ronis, Prof. William Galley, Dr. Grazyna Wilczek, Prof. Gonzalo Cosa, Pr. Christopher Barrett, and Pr. Brad Siwick. Prof. Paul Wiseman has been on my committee from the start of my degree, serving in this regard despite our fierce hockey rivalry. Prof. Anthony Mittermaier also deserves special thanks for his friendship, and all his help understanding the off-diagonals of the density matrix. I would also like to thank Chantal Marotte for everything she does to help graduate students navigate the bureaucratic elements of the university, I don't think anyone would ever graduate without her.

I received substantial financial assistance from the James Macfee and J.W. McConnell Fellowships during my studies, for which I am very grateful.

My parents have given me unconditional love and support throughout all my many years of studies, along with my sister and the rest of my family. My beautiful wife Wendy Evans inspired me throughout, and I couldn't have done it without her.

Peace, and thanks to all!

Chapter 1 Introduction

Advances in material science have driven humankind's progress from time immemorial. As the modern science of chemistry developed in the 19th and 20th centuries, research into matter and its constituents led to an explosion of new discoveries which has given us the capabilities to meet the various needs of modern civilization.

In order to understand the motions of electrons and holes which give rise to the electronic and optical properties of bulk semiconductor materials, the fields of solid-state physics and chemistry were developed from newly discovered principles of quantum theory. This allowed researchers to design revolutionary new devices such as the transistor based upon the physical understanding of charge dynamics in different structures. An incredible range of technologies developed in the last century, including laser diodes, solar electricity cells, and microprocessors all arose from these principles.

Despite these tremendous achievements further progress in materials science is now called for to meet new challenges facing the developed world, especially to meet energy production/consumption goals and to increase information processing power for computer technologies. Nanotechnology hopes to make these further scientific and technological advances by engineering the physical size of the material in order to tailor their properties. Their technological importance makes semiconductor materials one of the most intensely investigated aspects of the burgeoning nanoscience field.

Nanometer scale semiconductor crystals, referred to as nanocrystals (NCs), have great potential to revolutionize many fields such as solar energy conversion, quantum computing, and laser light sources. Their promise arises from intriguing new electronic and optical properties that develop in nanocrystals due to the development of discrete states, which is caused by an increase in the prominence of intrinsically quantum mechanical effects as the physical size of the crystal approaches the volume which electrons and holes tend to occupy inside a semiconductor. Despite almost 30 years of research, there is not the necessary depth of knowledge about how various processes occur in semiconductor nanocrystals to allow for their successful incorporation into many new technologies.

Many of the most critical advances will depend on engineering electron and hole behavior on the natural timescale of their dynamics- the femtosecond (10^{-15} sec). This requires studying these systems using modern optical techniques which have this ultrafast time resolution. This thesis contains a systematic investigation of the nonlinear optical properties of colloidal CdSe nanocrystals when excited into the different available electronic states. Time resolved ultrafast spectroscopy combined with spectral selection of excitation and probe wavelength was used to characterize the level structure, interaction strength and dynamics of different types of complexes consisting electrons and holes confined inside the nanocrystal.

The following section will describe the spectroscopic techniques and principles behind the ultrafast experiments used in this thesis. The next section will describe semiconductor nanocrystals, and review the literature regarding charge carrier dynamics and interaction strengths in colloidal nanocrystals.

1.1 Ultrafast Pump/Probe Spectroscopy

Many of the most interesting processes following the interaction of light with matter occur on the femtosecond to picosecond timescale (10^{-15} sec = 1 fs, 10^{-12} sec = 1 ps), characteristic of electronic transition times and nuclear motion. State of the art laser systems developed over the past two decades are capable of producing light pulses of femtosecond duration which can be used to observe many of the elementary events following photoexcitation in different materials, such as dissociation, vibrational relaxation, and wavepacket formation[1-3].

Spectroscopic techniques in chemistry measure changes to the properties of light when passing through a medium which contains a sample of interest. These changes are caused mainly by the interaction of the electric field component of electromagnetic radiation with the medium. This results in changes to the polarization of the medium, determined by the electric field strength of the light and the susceptibility of the material.

In techniques which use low intensity light sources, such as the measurement of an absorption spectrum, the field strength is in the regime where the macroscopic polarization of the sample is linear in the applied field strength. In ultrafast measurement the instantaneous field strength is much higher and the polarization becomes a nonlinear function of the electric field strength. For this reason, time resolved techniques fall under the domain of non-linear optics.

In nonlinear optics, the Polarization must be expanded as a Taylor series in powers of E (the electric field),

$$\vec{\mathrm{P}} \propto \chi^{(1)} \cdot \vec{\mathrm{E}} + \chi^{(2)} : \vec{\mathrm{E}}\vec{\mathrm{E}} + \chi^{(3)} \vdots\, \vec{\mathrm{E}}\vec{\mathrm{E}}\vec{\mathrm{E}} + \ldots \tag{1.1}$$

In this equation, the susceptibility of the different orders is responsible for effects that can be measured using different optical setups. The third order susceptibility determines the polarization response in the pump/probe techniques which are used to take direct time domain measurements of the ultrafast changes which occur after photon absorption in this thesis.

Pump/probe spectroscopy is therefore a third order nonlinear optical technique, in which the recovery of a system is measured by a probe pulse after being perturbed by a pump pulse. When compared with other ultrafast techniques, such as the transient grating or photon echo measurements, pump/probe is often advantageous because the data does not need to be fit into complicated models of time dependent response functions in order to correspond to a physical observable. Described on a simple level, the technique allows users to directly measure changes to the absorption spectrum of the sample during different photophysical processes. The generated data can be interpreted relative to the sample's linear absorption spectrum to give information about both how different states are populated over time and any new transitions available to the system after photoexcitation.

The data in time-resolved absorption (TA) experiments measures the response of a sample to optical excitation by using a relatively strong pump pulse followed by a weak probe pulse, hence the name pump-probe spectroscopy. The data in this measurement compares the absorbance of the probe pulse beam with the pump pulse on with the absorbance of the probe pulse with the pump pulse off:

$$\Delta \mathrm{OD}(\lambda) = \mathrm{OD}^{\mathrm{on}}(\lambda) - \mathrm{OD}^{\mathrm{off}}(\lambda) \tag{1.2}$$

In this equation $\Delta \mathrm{OD}(\lambda)$ is the change in absorbance of a sample at wavelength λ, $\mathrm{OD}^{\mathrm{on}}(\lambda)$ is the measured absorbance of the sample with the pump on, and $\mathrm{OD}^{\mathrm{off}}(\lambda)$ is the absorbance of the sample with the pump off.

With the pump pulse off the absorbance of the probe pulse can be described as

$$\mathrm{OD}^{\mathrm{off}}(\lambda) = \sigma_{0\to 1}(\lambda) * \mathrm{N} * \ell \tag{1.3}$$

In this equation $\mathrm{OD}^{\mathrm{off}}(\lambda)$ is the absorbance of a probe pulse with wavelength λ without the pump, $\sigma_{0\to 1}(\lambda)$ is the absorption cross section of the sample at that wavelength (the 0→1 subscript denotes the transition from the initial ground state, with zero excitations, to the final state in which there has been 1 excitation), N is the number density of the species being studied in the sample, and ℓ is the path length of the sample. This is simply the linear absorption spectrum of the sample, as shown in figure 1.1a.

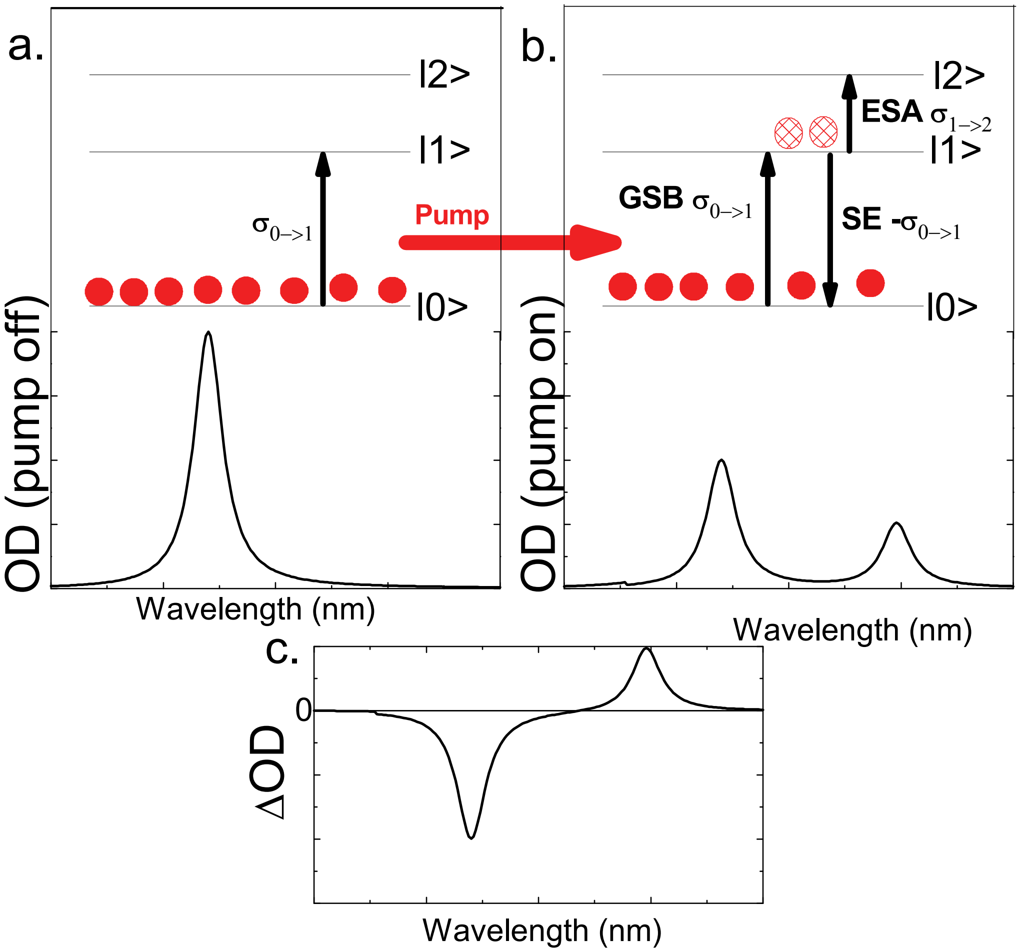

Figure 1.1: a. Sample with the pump off. Nanocrystals in their ground state (zero excitations) are represented by solid red circles. They absorb light at probe wavelengths described by $\sigma_{0\to1}(\lambda)$, the absorption cross section for single excitation, yielding the absorption spectrum shown.

b. Sample after optical excitation with pump pulse. Nanocrystals in ground state are represented by solid red circles, nanocrystals that have absorbed a photon to create a single exciton are represented by cross-hatched circles. GSB and SE attenuate absorption spectrum of the sample, ESA leads to new peaks in the spectrum (described in text).

c. Transient Absorption Spectrum, a plot of the change in absorbance as a function of wavelength. It is equal to the subtraction of the absorption spectrum with pump off (1a) from the spectrum with pump on (1b).

The path length does not change in these measurements, so this equation can be simplified by combining the concentration and path length together

$$n = N * \ell \tag{1.4}$$

Here n refers to number density of particles per unit area. Using this substitution the probe pulse absorbance in the absence of the pump is then

$$OD^{off}(\lambda) = \sigma_{0\to1}(\lambda) * n \tag{1.5}$$

With pulses that are well separated in time, there are 3 effects that pumping the sample can have on the absorbance of the probe pulse, and these are illustrated in figure 1.1b for a simple system:

1. Ground State Bleaching (GSB): Transfer of population from ground to excited state by the pump pulse leads to state filling due to Pauli blocking (limits on the number of electrons which can occupy a state), decreasing the absorbance of the sample in the pumped area.
2. Stimulated Emission (SE): The probe pulse can induce stimulated emission from the excited state to the ground state, which increases the probe beam intensity and manifests itself as a decrease in the absorbance.
3. Excited State Absorption (ESA): If there are transitions into states accessible only from the excited state resonant with the probe wavelength, then excited particles can absorb the probe light to make such a transition, increasing the absorbance of the sample when pumped.

These effects combine to give an expression for the absorbance of the probe pulse after the pump pulse has excited some fraction of the particles:

$$\mathrm{OD}^{\mathrm{on}}(\lambda) = \sigma_{0\rightarrow1}(\lambda) * (\mathrm{n} - 2\mathrm{N}_1) + \sigma_{1\rightarrow2}(\lambda) * \mathrm{N}_1 \tag{1.6}$$

In this equation is this equation $\mathrm{OD}^{\mathrm{on}}(\lambda)$ is the absorbance of the probe beam at wavelength λ with the pump on, $\sigma_{0\rightarrow1}(\lambda)$ is the absorption cross section of the sample at that wavelength, n is the total concentration of all particles per unit area, N_1 is the number density of excited particles per unit area, and $\sigma_{1\rightarrow2}(\lambda)$ is the absorption cross section for the transition from the singly excited state to a higher excited state (subscripts referring to the number of excitation events). Figure 1.1b displays $\mathrm{OD}^{\mathrm{on}}(\lambda)$.

An expression for $\Delta\mathrm{OD}(\lambda)$, the experimentally measured transient absorption signal, is obtained by inserting equations (1.5) and (1.6) into equation (1.2):

$$\Delta\mathrm{OD}(\lambda) = \sigma_{0\rightarrow1}(\lambda) * (-2\mathrm{N}_1) + \sigma_{1\rightarrow2}(\lambda) * \mathrm{N}_1 \tag{1.7}$$

Linking the terms in this equation to the 3 processes which contribute is straightforward: GSB and SE each act to lower the concentration of particles absorbing at the transition frequency measured in the absorption spectrum, which lowers the absorbance in the presence of the pump pulse and manifests itself as a negative going bleach in a transient absorption data. These effects are accounted for in first term on the RHS of equation (1.7). ESA leads to induced absorptions, whose spectral position depends on the relative spacing of energy levels accessible to an excited particle, the second term on the RHS of equation (1.7).

Measurement of $\Delta\mathrm{OD}$ over a range of wavelengths gives a transient absorption (TA) spectrum showing whether the absorbance has increased or decreased at each position as shown in panel c of figure 1.1. In essence this is taking a snapshot of the system as it evolves. Negative going features show which states are populated and positive going features indicate absorptive transitions available to the excited fraction of the sample.

To examine how ΔOD varies in time as relaxation processes occur, one can take a series of measurements of the TA spectra at different time delays between pump and probe. The time delay, which is often referred to using τ, is defined as

$$\tau = t_{probe} - t_{pump} \tag{1.8}$$

The convention shown here would give negative values for τ when the probe arrives at the sample position before the pump pulse and positive values when the probe pulse arrives after the pump. When $\tau = 0$, the pulses arrive at the sample simultaneously- this time delay is known as time zero.

An example of a series of TA spectra is given in figure 1.2a. Before time zero one measures a baseline of zero, since the probe measures an undisturbed sample regardless of whether pump pulse is on or off. At early times one generally sees features develop into various maxima, evolving and eventually decaying over different timescales as the excited particles undergo relaxation processes. As shown in equation (1.7), these features give information about the population of the states and the absorption spectrum of excited particles. Here the bleaching feature and the induced absorption have been labeled, B1 and A1 respectively.

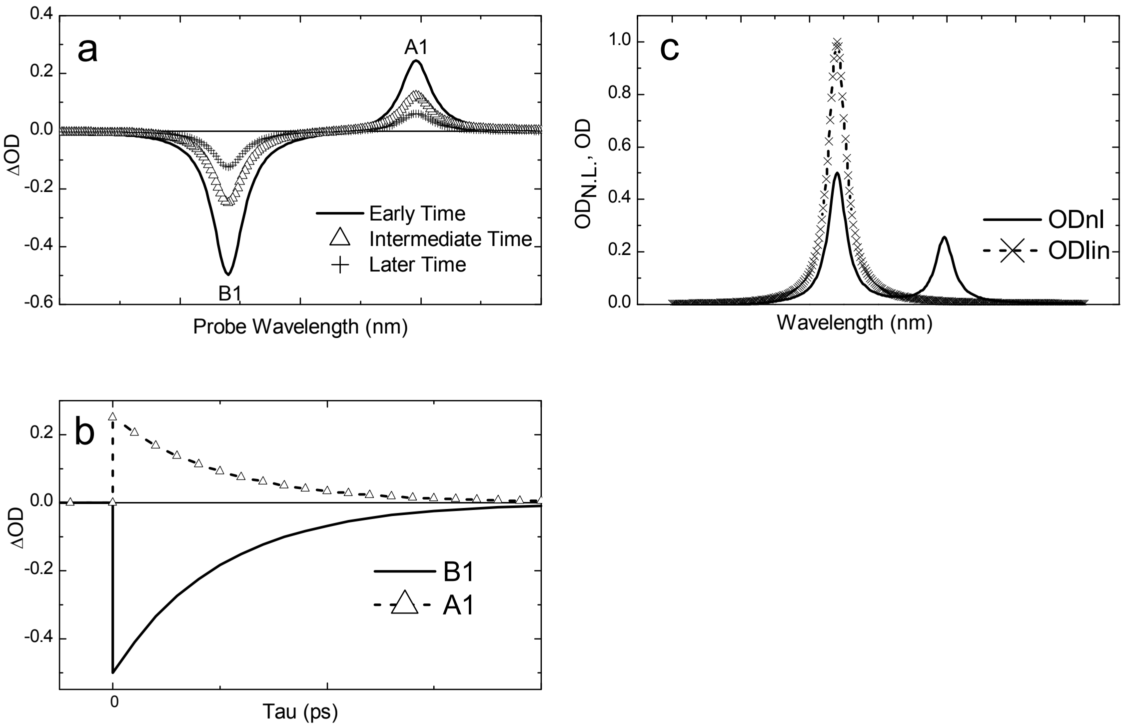

Figure 1.2: a). TA spectra taken at different time delays for the same sample used in figure 1.1. TA spectra are helpful for looking at level shifting and populations at a specific time delay. The features are labeled as a bleach (B1) or induced absorption (A1)

b). Kinetic transients of the B1 and A1 features, which plot ΔOD at one energy over a range of time delays. This is useful for examining dynamics of different processes.

c.) The non linear spectrum ($OD_{N.L.}$) compared to the linear absorption spectrum of the sample. This is normally done to examine how heavily transitions are bleached and to monitor the development of optical gain, which would be manifested as negative going portions of the non-linear spectrum.

It is often judicious experimentally and analytically to measure ΔOD only at one probe wavelength in order to clearly examine the time evolution of a specific feature. In this case the data is presented as ΔOD versus τ, known as a pump/probe transient and illustrated in figure 1.2b. For B1, the bleaching feature, the signal goes negative to a maximum and relaxes over the following picoseconds reflecting the dynamics of excited particles relaxing back to the ground state. A1, the photoinduced absorption, begins positive and relaxes with the same dynamics. More complicated systems will have much more complex dynamics; this is only a simple example for illustrative purposes.

In some pump/probe experiments relating to optical gain, it useful to plot OD_{on}, the actual absorbance of the sample following excitation with the pump pulse. This is obtained by adding the measured TA spectrum with the linear absorption spectrum of the sample, and is referred to as the non-linear spectrum (OD_{NL}).

$$OD_{NL} = OD_0 + \Delta OD \tag{1.9}$$

It is illustrated in figure 1.2c compared to the linear absorption of the sample. Regions where bleaching occurs in the OD_{NL} are due to lowered sample absorbance, depending on how fully populated the energy levels of the different electronic transitions are.

With high fluence pumping it is possible to saturate a transition so that no further probe pulse absorption can occur and the sample reaches optical transparency, $OD_{NL} = 0$. If a population inversion can be supported it is possible to have OD_{NL} lower than zero, as the sample begins to transmit more probe light than entered it via stimulated emission in the negative portions.

The various ways of portraying pump/probe data illustrated in this section are used throughout this thesis. The TA spectrum and kinetic transients shown here for a simple 3 level system are relatively straightforward to interpret. In semiconductor nanocrystals the level structure is much more complex, but overall the experimental data can be interpreted in the same manner. The next section described the electronic structure of nanoscale semiconductor systems, focusing on CdSe. The last section of the introduction examines how ultrafast spectroscopy has been applied to these systems.

1.2 Colloidal CdSe Nanocrystals

In atoms and small molecules, the various electronic configurations that gave rise to states which could be coupled by light have been examined from the beginning of the development of quantum mechanics. The processes which follow photoexcitation in these systems are well characterized, relaxation phenomena such as internal conversion and intersystem crossing were thoroughly understood in various molecules before pulsed laser technology had developed enough to measure such processes in real time. Analysis of the early ultrafast measurements in those types of systems benefited from having both a well understood manifold of available states and a good understanding of the dynamical processes which were accessible in each system.

Semiconductor nanocrystals do not have such a well developed theoretical literature. We review semiconductor nanocrystals in terms of electronic structure and ultrafast dynamics. We begin by looking at the bulk phase properties of CdSe, to understand how these are modified in nanocrystalline systems.

1.2.1 Comparison of Bulk and Nanocrystalline CdSe

The properties of both small CdSe molecules/clusters and large crystals of the same material are well understood. Molecular Orbital theory (MO theory) gives a thorough understanding of the discrete energy levels of the former, while the latter are described using continuous solid state bands. In between these two extremes lies the nanoscale regime, where CdSe materials exhibit properties intermediate between bulk and molecular systems. Nanocrystals (NCs) are large enough to be considered to have an organized lattice structure, but they behave very differently than the bulk phase material. In order to understand nanocrystals more thoroughly, it is helpful to first examine the bulk system.

Bulk CdSe is a direct gap II-VI semiconductor, not in widespread use in current technologies. The most stable phase is the wurzite (hexagonal) crystal structure[4]. It is a wide gap semiconductor with an energy gap (E_g) ~1.75 eV[5], which separates the conduction band (CB) made up of Cd 5*s* orbitals, and the valence band (VB) which arises from Se 4*p* orbitals[6]. The band structure in the region of the band gap is shown in figure 1.3.

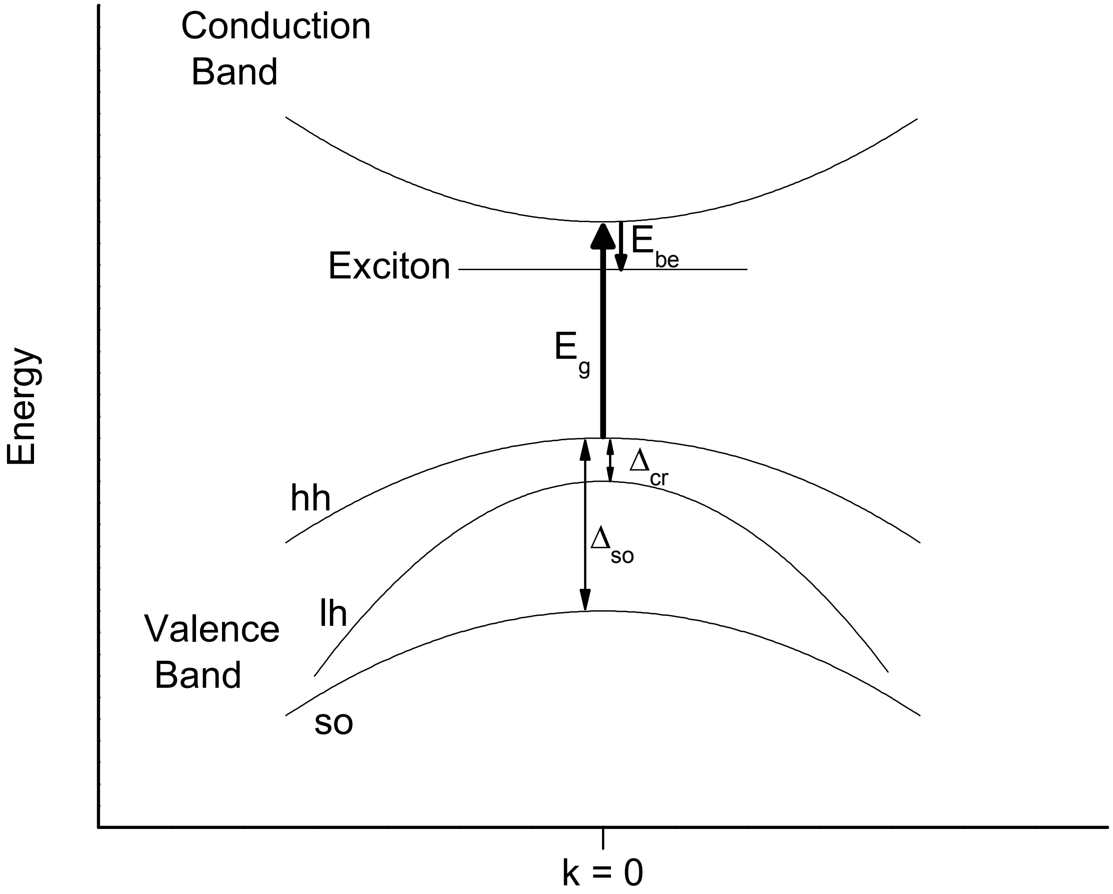

Figure 1.3: The Band Structure of Bulk CdSe (not to scale). The valence band is split into the heavy-hole, light-hole, and split-off-hole subbands. Δ_{so} is the energy splitting from spin orbit coupling, while Δ_{cr} is the crystal field splitting caused by interactions from beyond the nearest neighbors in a wurzite lattice crystal. The valence band and conduction band are separated by a large energy gap, E_g, for the formation of a free electron and hole. Slightly subresonant to this transition, a bound electron/hole pair called an exciton maybe formed, this transition is lowered by the binding energy (E_{be}), arising from stabilization due to the Coulombic attraction between the charge carriers.

The 3 subbands of the valence band arise from different forces at work which lift the degeneracy of the different 4*p* orbitals. Strong spin-orbit coupling lowers one band by an amount Δ_{so} as indicated in the figure, 0.42 eV in CdSe[4]. This band is fairly far removed from the band edge, and is known as the split-off-hole subband. The remaining subbands in figure 1.3 are split only by a small amount, Δ_{cr}, the crystal field splitting caused by forces on electrons due to asymmetry of the crystal lattice. This splitting is only 0.041 eV in wurzite CdSe[4, 7], and disappears in zinc blende samples because of the less complicated unit cell symmetry. These bands are the light-hole (lh) and heavy-hole (hh) subbands, in reference to the different effective masses of holes between them. The effective mass is inversely proportional to the curvature of the subband:

$$\frac{1}{m_{eff}} = \frac{1}{\hbar^2}\frac{d^2E}{dk^2} \tag{1.10}$$

It is used to account for the interaction of the electrons and holes with the ions of the lattice, by assuming that they can be treated as free particles of different masses instead of incorporating the rather complex periodic potential they actually experience.

The absorption spectrum of bulk CdSe is mostly featureless, smoothly increasing with energy. The absorption onsets of the three subbands are resolvable from curvature changes near the band edge[4, 8]. Upon excitation with light slightly lower in energy than E_g, it is possible to form a bound electron hole pair known as an exciton. Exciton formation is observable as a distinct peak distinct near the red edge of the absorption onset in bulk samples. In CdSe, Wannier type excitons form- in which the electron and hole execute orbits around their center of mass, attracted to each other by the Coulombic forces between them[9]. Excitons form a discrete state below the conduction band, allowing the binding energy of the exciton to be measured as shown in figure 1.3 (0.0167 eV in CdSe[4]).

The motions of charge carriers in semiconductors are mainly determined by their effective masses, which are proportional to the curvature of the band they populate as shown in equation (1.10). The overall "size" of the exciton is its Bohr radius (a_b), in analogy to the hydrogen atom[6]:

$$a_B = \frac{4\pi\varepsilon\hbar^2}{\mu\ e^2} \tag{1.11}$$

In this equation ε is the dielectric constant of the material, $\hbar$ is the reduced Plank's constant, e is the charge of an electron, and μ is the reduced mass of the exciton. The reduced mass of the exciton is the reduced mass calculated from the effective masses of the electron and hole

$$\frac{1}{\mu} = \frac{1}{m_{eff}^{e}} + \frac{1}{m_{eff}^{h}} \tag{1.12}$$

For CdSe, the excitonic Bohr radius is approximately 5 nanometers[10].

Nanoscale effects become important as the size of the crystal becomes comparable to Bohr radius of an exciton. For CdSe, nanocrystals normally have radii from ~1-4 nm[11]. The charges can no longer move freely throughout the lattice, they are now confined within a small volume and experience quantization of their translational energy levels caused by the boundary conditions imposed by the geometry of the nanocrystal. This is known as "quantum confinement", so particles which exhibit such effects are also known as quantum dots (QDs). For the purposes of this thesis, quantum dot and nanocrystal are used interchangeably.

In semiconductor nanocrystals quantum confinement causes a blueshift of the energy gap and increased spacing between adjacent energy levels as the particle size is decreased. These effects can be understood by considering the common particle-in-a-box problem from introductory quantum mechanics courses, used to show how particle eigenfunctions depend on the box size and geometry. This problem shows how the quantum mechanical treatment of a particle confined by a potential leads to quantization of its energy levels and allowed motions.

For spherical nanocrystals (NCs) the particle radius thus controls the colour of light which the material absorbs, and this parameter can be controlled during synthesis. Similar control over carrier wavefunctions can be exerted by changing particle geometry, for example creating rod like structures by tuning the synthesis conditions. This has led to nanocrystals to be referred to as “artificial atoms”, with the possibility of ordering them into form “artificial solids” whose properties could be tailored to create new materials customized for different processes[12, 13].

1.2.2 Synthesis and Characterization of Semiconductor Nanocrystals

The interesting properties of the semiconductor crystals were realized in the early 1980's[14-16]. The most common earlier types of semiconductor nanocrystals were made via precipitation of precursor compounds inside a silicate matrix[17, 18]. Often the samples were simply coloured glass filters[19, 20]. These samples are interesting for historical purposes, but this technique results in nanocrystals of limited quality due to the large size dispersion of particle radii and their poorly passivated surfaces. This made early investigations of the underlying physics of nanocrystals very difficult.

Wet chemical techniques were developed, and gave much better results for synthesis of nanocrystals as colloidal particles[21]. These techniques depend on a controlled precipitation event followed by a time of crystal growth to achieve the desired particle radius. Early methods involved dangerous organometallic compounds such as $Cd(CH_3)_2$ dissolved in coordinating solvents at high temperatures (~300 C), and required completely air and water free conditions. The nanocrystals synthesized this way had much better surface quality, but still required size-selective precipitation to obtain samples of appropriate size dispersion to resolve transitions clearly.

The safety concerns involved with the organometallic synthesis led to investigations of alternative routes[22-24]. The modern synthesis of colloidal nanocrystals is much safer, and results in samples with the low size dispersion (5-10%), so that size selective precipitation is not necessary. The cadmium precursor used is normally a salt or metal oxide, dissolved in a mixture of solvent, surface ligands and a long chain phosphonic acid (it is possible but not necessary for the solvent to be a surface ligand)[25]. At high temperatures a complex of the phosphonic acid and Cadmium ions forms. When a Selenium solution is injected, the Se displaces the phosphonic acid and CdSe crystals form and begin to grow[23]. Growth is stopped at the desired crystallite size by cooling the reaction mixture quickly, and the nanocrystals are collected by flocculation and centrifugation.

A selection of absorption and emission spectra are shown in figure 1.4 for 3 different sizes of high quality CdSe nanocrystals. There are several absorption features resolvable in the visible region, due states arising from quantum confinement of charge carriers. The energy gap and the spacing between adjacent energy levels increasing in the smaller particles, as expected. At higher energies the absorption spectrum is almost featureless, resembling the continuum of states in bulk CdSe. This is most likely because the highly energetic charges resulting from excitations in this region have significant tunneling outside of the crystalline core, rendering the size of the crystal not adequate to set the boundary conditions which lead to discreet energy levels[26, 27].

The emission spectrum is a single, symmetric Gaussian corresponding to radiative recombination of electrons and holes from their band edge states, discussed further in section 1.2.4. Poor surface quality would be indicated by significant amounts of emission on the red edge of the visible spectrum. This is called deep trap emission, resulting from recombination involving charge carriers trapped in some type of unpassivated surface states[27-29]. The samples shown here are well passivated, there is no sign of deep trap emission.

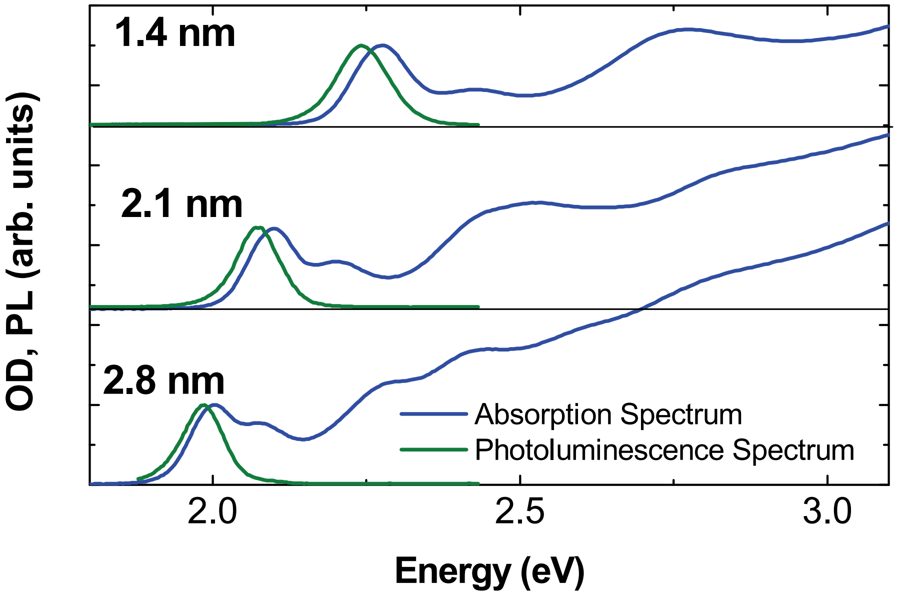

Figure 1.4: Absorption and Photoluminescence Spectra for 3 different sizes of CdSe Nanocrystal (denoted by radius). The development of distinct states is clear by the different resolvable features in the absorption spectra for each size of NC. The band edge transition and spacing between energy levels becomes larger as the radius is decreased due to stronger confinement, just as in the particle-in-a-box problem. The P.L. Spectra are a single peak, with a size dependent Stokes shift which increases in smaller samples.

The sizes can be verified by TEM, though now well developed sizing curves are available[11, 30]. The size dispersion can be measured directly from TEM images, or extrapolated from the spectral width of the absorption and emission features. The best quality samples still have significant spectral widths, approximately 25 nm FWHM for emission or 14 nm HWHM for the band edge absorption feature[11, 22, 25].

1.2.3 Electronic Structure of Semiconductor Nanocrystals

In quantum confined systems, optical excitation creates a nanoscale exciton comprised of an electron and hole each populating one of the available eigenstates. Because the size of the particle is smaller than the excitonic Bohr radius, a nanoscale exciton is not at all equivalent to the Wannier type bulk exciton described earlier by equation (1.11). Coulombic interactions of the electrons and holes bind bulk excitons, in nanoscale excitons quantum confinement is the dominant contribution to their sum energy. In order to describe the features observed in the absorption spectra shown in figure 1.4 we must examine the types of states which arise from quantum confinement of charges. These states make up the electronic structure of semiconductor nanocrystals.

The charge carriers in CdSe nanocrystals belong to the "strong confinement regime", where the nanocrystal radius so small that the boundary conditions effect the motions of the electrons and holes themselves. In the strong confinement regime, both the electrons in the conduction band and the holes in the valence band will then have quantized energy levels and can be treated somewhat independently of each other as confinement effects overwhelm the Coulombic attractions between the charges[31]. Optical transitions will occur when an electron is promoted from a distinct state in the valence into another distinct state in the conduction band. Just as in the particle-in-a-box problem, both the energy gap and the spacing between adjacent energy levels in each band are size dependent, and CdSe NCs exhibit multiple resolvable transitions in contrast to the mostly featureless bulk absorption spectrum.

The most complete measurement of the different excitonic energy levels over a wide size range of CdSe nanocrystals was published by the Bawendi group at MIT in 1996, using photoluminescence excitation spectra (PLE)[32]. There have been a number of different theoretical approaches applied to the complicated problem of understanding these energy levels[33]. The most widely used in the literature is the effective mass approximation (EMA)[31], based on perturbation theory applied to the bulk band structure of CdSe. The EMA yields a relatively simple level structure for the level structure of the conduction and valence band, with states which can be described using term symbols that denote features of the wavefunctions such as the carrier envelope function symmetry and angular momentum components[34].

Other theoretical treatments use computational approaches developed for molecular systems modified to handle the large number of atoms required to derive the level structure of nanoscale clusters. The most well developed set of results of this kind use computational techniques based upon density functional theory known as the Direct Diagonalization Method (DDM), pioneered by the Zunger group at NREL[35]. These types of calculations give somewhat different predictions for some of the details of the electronic structure of semiconductor nanocrystals when compared to the EMA results, with a more congested valence band and greater mixing of different types of states[36, 37].

There has been some debate in the literature about the best technique for the treatment of nanoscale systems[38-40]. One of the most concerning elements of the EMA technique is that it does not include a realistic surface for the nanocrystal. The EMA approach assumes an infinite confining potential, with bulk like crystal structure throughout the nanocrystal. Computational methods have shown that surface reconstruction and passivation plays an important role in the optical properties of the nanocrystals[41-46]. With these atomistic approaches, one is able to treat many parts of this problem in a manner which corresponds more strongly to the physical conditions present in real systems, but the solutions acquire a similar level of complexity and are less straightforward to work with as an experimentalist.

Both the analytic EMA and computational DDM each have many merits, but the DDM calculations yield states with a much more complex character which are difficult to assign concise term symbols relating to underlying observables. On the other hand, the term symbols describing the excitonic wavefunctions of the various energy levels described using the EMA approach have a relatively simple interpretation and have become the vernacular of the quantum dot field. This nomenclature adequately describes many characteristics of nanocrystal absorption and emission spectra for the purposes of this thesis. We will therefore briefly describe the EMA approach as it provides insight into how quantum confined electronic states arises from bulk systems as the dimensions are reduced, with the caveat that the resulting wavefunctions are much too simple to accurately describe the distribution of charge in real nanocrystals. More thorough treatments of the EMA are available in the literature[31, 34]

On the simple level, what is done is to replace the continuous bands which were used to describe bulk CdSe with discrete transitions based upon hydrogenic wavefunctions arising from the spherically symmetric potential experienced by the charge carriers. This involves composing the excitonic energy levels from wavefunctions in which electron and hole act as free particles (appropriate in the strong confinement regime), each with an effective mass approximated from the curvature of the appropriate subband (from which the EMA derives its name).

With this framework in place, strongly confined charges can be treated independently of each other, with Coulombic effects treated as a first order perturbation[6, 31]. This is justified by the $1/r^2$ dependence of confinement effects when compared to the $1/r$ dependence of Coulomb terms. EMA includes spin-orbit coupling effects in the valence band, but does not include splitting from the crystal field of wurzite lattice. It also assumes that the particle is perfectly spherical, in order to limit the solution to ones with proper symmetry. Crystal field and shape asymmetry are treated in deriving the exciton fine structure, as will be shown in section 1.2.4.

The eigenfunctions for each charge carrier consist of an envelope function, describing the confinement induced quantization of the translational degree of freedom of its motion into a Hydrogenic-like wavefunction, mixed with the orbital symmetry of the band it occupies. The predicted level structure is plotted in figure 1.5a, showing several charge carrier states in each band.

It can be seen in figure 1.5a that the conduction band near the band edge collapses into widely spaced energy levels made up electrons with wavefunctions consisting of an envelope function constructed using a Cd 5*s* orbital basis[32]. The term symbols for the electronic states are $1S_e$, $1P_e$, $1D_e$, etc., with the format nL_e describing the principal quantum number, *n*, and the lowest dominant angular symmetry of the envelope function, L (there is some mixing with the state of higher angular momentum L+2 caused by confinement, known as S-D mixing)[6]. The subscript is to be clear it is describing an electron.

The higher degeneracy of the Se 4*p* orbitals which make up the valence band, and the larger effective mass of the hole compared with the electron, result in more densely packed energy levels near the band edge in the valence band as compared with the conduction band[6, 32], shown in figure 1.5. Confinement leads to quantum mechanical mixing of the subbands, known as valence band mixing (VB mixing), in addition to S-D mixing[6].

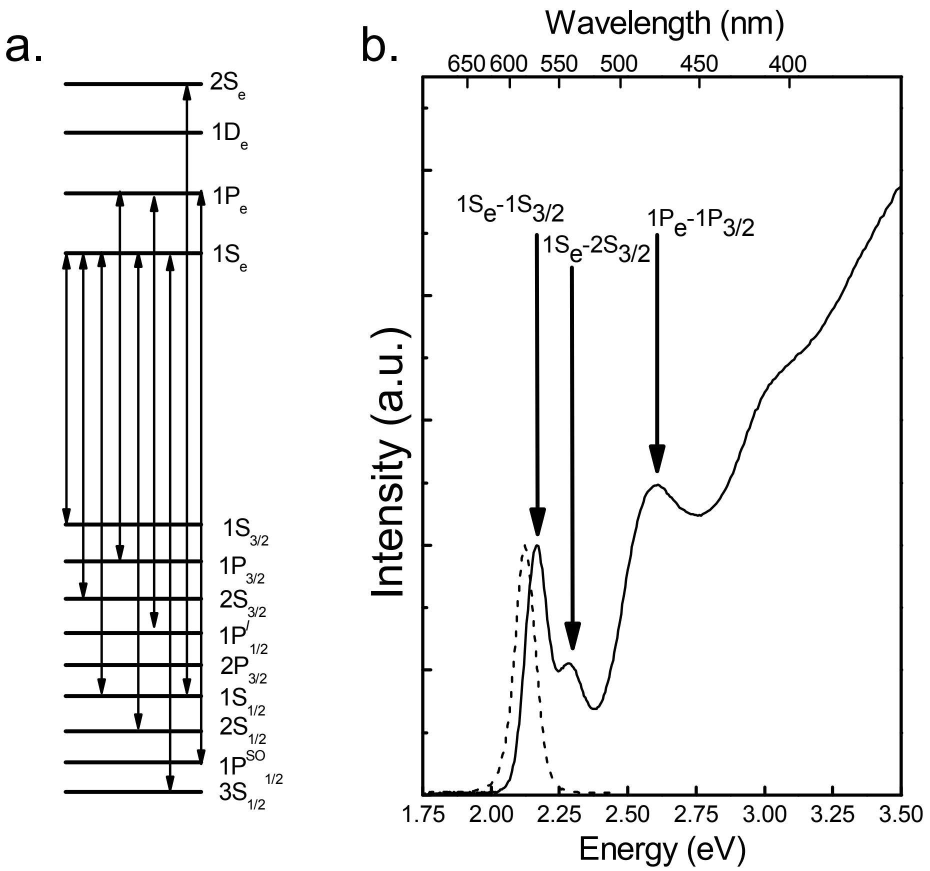

Figure 1.5: Results of EMA calculations. a.) The energy levels predicted for when quantum confinement of charges occurs in CdSe nanocrystals, collapsing the valence band and conduction band into discrete states (the level splittings are not to scale). The arrows denote the possible transitions as predicted from the calculated energy levels.

b). The absorption (solid line) and emission (dashed line) spectrum for a CdSe NC sample with the three lowest transitions of appreciable oscillator strength labeled. At higher energies the energy levels become quite congested, making it difficult to have clear assignments much past the $1P_e$-$1P_{3/2}$ transition.

The hole wavefunctions are then designated by the term symbols $1S_{3/2}$, $1P_{3/2}$, $2S_{3/2}$, $1S_{1/2}$, etc. The *n*L portion is the same as in the electronic wavefunctions. The subscript gives F_h, the total hole angular momentum. F is the sum of the unit cell angular momentum, J, and the envelope function angular momentum, L:

$$F_h = J_h + L_h \tag{1.13}$$

L is zero for S-type states, 1 for P-type, etc. J is simply the sum of carrier spin, S, and its atomic orbital angular momentum, ℓ:

$$J_h = \ell_h + S_h \tag{1.14}$$

Strong spin orbit coupling means that states arising from the split-off-hole subband will have $J_h = 1/2$, those from light-hole and heavy-hole subbands will have $J_h = 3/2$. Recall that this ignores the crystal field splitting, which will be added as a perturbation to examine emissive properties. The subscripts simply denote that we are considering hole states, the same quantities (F, L, J, ℓ, S) can be defined for the electronic wavefunctions.

Calculating selection rules shows that strongly allowed transitions couple hole states n_hL_{Fh} to electronic states with the same envelope function angular momentum L, and the total excitonic wavefunction is designated as $n_eL_en_hL_{Fh}$. For example, the first two strongly allowed transitions in the absorption spectrum are $1S_e$-$1S_{3/2}$ and $1S_e$-$2S_{3/2}$ respectively (see figure 1.5). In the first transition, the hole is formed at the top of the valence band when an electron is excited into the lowest electronic state of the conduction band. In the second transition, the electron populates the lowest conduction band state, but originates much deeper in the valence band.

These excitonic states lead to the features seen in the linear absorption spectrum of a CdSe nanocrystal shown, in figure 1.5b with the assignments of the 3 lowest energy strongly allowed transitions based up EMA calculations of selection rules. Most of the work presented in this thesis exploits the differences between these three states to systematically explore the photophysics of nanoscale charge carriers, so they are very important in the following chapters.

As discussed, the first two transitions populate the lowest energy electronic state, the 2 fold spin degenerate $1S_e$ state. The second transition results in a hole with excess energy below the valence band edge. The next transition in the spectrum promotes an electron from the $1P_{3/2}$ valence band state, much closer to the top of the valence band than the $2S_{3/2}$ state, into the highly excited $1P_e$ conduction band state. In this the initial excess energy is mostly from the electron above the conduction band edge.

It should be noted that there remains some controversy as to the correct character assignment of different envelope functions for the higher excited states[36]. Both theory and experiment have shown that the spacing between adjacent energy levels becomes congested in the high energy portion of the spectrum. There is some indication that a manifold of continuum like state may be available at higher energies[27].

As described earlier, there are shortcomings of the EMA method, so the results present here should be used to understand nomenclature and the relevant energy levels but should not be considered a complete picture or overly precise.

1.2.4: Nanocrystal Emission: Fine Structure of the Band Edge State

The previous results are able to predict the absorption spectrum of a nanocrystal sample from simple confinement of charges inside the particle volume. In order to understand the emissive properties of semiconductor nanocrystals it is necessary to explore the band edge state in more detail. Early investigators were surprised by the rather long radiative lifetime of CdSe nanocrystals, on the order of a few microseconds when normally fluorescence occurs on the nanosecond timescale[47, 48]. It was also noted that the Stokes shift between the absorption and emission peak increased as the nanocrystal radius is reduced, and was shown to be insensitive to surface ligands and solvent, indicating it was an intrinsic property of the nanocrystal and not due to reconstruction of solvent shells or ligand structures[49]. These properties can explained by the splitting of degenerate energy levels induced by factors ignored in the calculations present in the previous section[50]- resulting in what is called "fine structure" of the exciton state, shown in Figure 1.6.

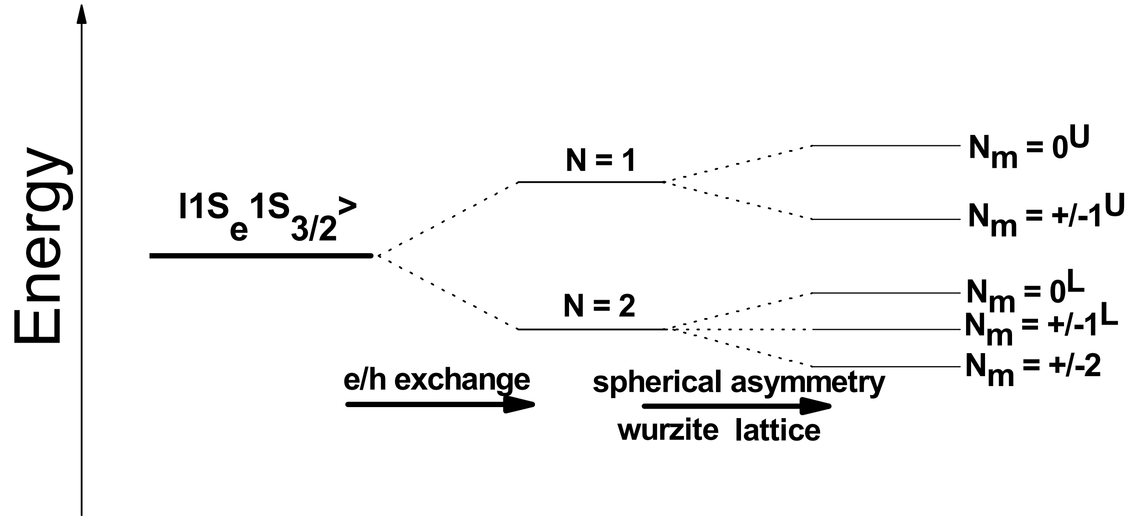

Figure 1.6: Fine Structure of the band edge state in CdSe nanocrystals. The state would be considered to be 8 fold degenerate in the absence of any perturbations. The electron/hole exchange interaction is enhanced by quantum confinement, and splits the state based upon N, the total angular momentum of the e/h pair, into a 3 fold degenerate upper state (N=1) and 5 fold degenerate lower state (N=2). These levels are then split by the deviations from a true spherical shape in a real nanocrystal (which is slightly elliptical) and the crystal field present in a wurzite lattice structure into states characterized by their angular momentum projection along the unique crystal axis, N_m. For $N_m = 0$ and $N_m = 1$, states are distinguished according to whether they arise from the N = 1 or N = 2 manifolds by using superscripts of U and L respectively. States with $N_m = 1$ or $N_m = 2$ are 2 fold degenerate, while those of Nm = 0 are singly degenerate.

For cubic lattice, spherical CdSe nanocrystals in the absence of any exchange interaction, the band edge $1S_e1S_{3/2}$ is 8 fold degenerate (including spin)[51]. For a band edge exciton there is a spin correlation interaction between the electron and the hole, the e/h exchange interaction, which is proportional to the overlap integral of their wavefunctions[52]. The interaction is negligible in the bulk but is large in nanocrystals due to their small size, and increases as the radius of the dots decreases. This splits the 8 states into 2 levels distinguished by the exciton total angular momentum (N), comprised of the angular momenta of both charge carriers as described in equation (1.13):

$$N = F_h \pm F_e \qquad (1.15)$$

F_h = 3/2 for the band edge hole state, and F_e = 1/2, so that N may take a value of 1 or 2. Just as in singlet-triplet multiplicity splitting in molecular systems, the upper energy state has N=1 and the lower energy level with N = 2.

CdSe quantum dots normally have a wurtzite lattice structure. This has a unique crystal axis (the c-axis) that splits the valence band edge light-hole and heavy-hole subbands due to anisotropy of fields in the crystal as described by Δ_{cr} discussed in section 1.2.1. In CdSe nanocrystals this splitting is further enhanced due to shape asymmetry, because crystals tend to be elongated along the c-axis which lifts the degeneracy of different orientations of the total angular momentum of the exciton for different projections along the crystal axis. In real quantum dots the crystal field and shape asymmetry will therefore split the upper N = 1 and lower N = 2 levels by their projections along the c-axis (N_m), so that the band edge exciton ends up being comprised of 5 distinct energy levels characterized by N_m and which level they arise from as shown in figure 1.6.

Calculations show that optical transitions are allowed to the 1^L, 1^U and 0^U states, but forbidden from the vacuum state directly the 0^L and 2 states[50, 51]. However, emission tends to come from N_m = 2 state as it is lowest in energy. The emissive state is known then as the dark exciton because it is not accessible by direct optical excitation, and it does not contribute to the linear absorption spectrum. The large Stokes shift and its size dependence is then a product of the fine structure splitting between the bright and dark states, along with the anomalously long fluorescence lifetime and its inverse dependence on magnetic field strength[53].

Section 1.3 : Ultrafast Spectroscopy of Semiconductor Nanocrystals

As shown in section 1.2.3, the features in the linear absorption spectrum of nanocrystals are due to the discrete eigenstates in both the conduction and valence band (figure 1.5). This thesis shows how using state specific pump/probe pulses to measure transient absorption features in CdSe nanocrystals uncovers new and important results. There is some nomenclature for the features observed with pump/probe method when applied to these systems, which will be reviewed briefly.

Consider a sample as shown in figure 1.7a, with the $1P_e$-$1P_{3/2}$ and $1S_e$-$1S_{3/2}$ transitions labeled. The TA spectrum is shown in figure 1.7b, pumping into the $1P_e$-$1P_{3/2}$ excited state (τ = 175 fs). Four distinct bleaching features (B1-B4) can clearly be seen at probe energies where there is a pump induced decrease in absorbance, and are labeled using the notation developed by Klimov et al[26]. The spectral positions of the bleach have a clear energy correspondence to the eigenstates of the quantum dot seen in the linear absorption spectrum, and they can be assigned to state filling of various excitonic transitions. These features are very useful in determining the dynamics of intraband relaxation of charges within their respective bands to the band edge[54, 55] and their eventual recombination[56].

Primarily it is the B1 feature which is monitored, as it measures the state filling of the band edge state ($1S_e$-$1S_{3/2}$). Intraband relaxation will be reviewed in section 1.3.2.

There are also two regions where induced absorption can be seen (A1 and A2), which arise due to ESA processes. In this case, these are the formation of biexcitons. When a nanocrystal absorbs two photons, the result is that there are two excitons (4 total charge carriers) forced to remain inside a volume which significantly smaller than what would be occupied by a bulk phase exciton (as described by the Bohr radius in equation (1.11)), enhancing the various interactions of the charge carriers. Higher order multiexcitons are possible using more intense pumping.

Multiexciton formation is a natural process in pump/probe measurements due to sequential absorption of photons from each pulse[57]. When the pump beam populates a given eigenstate, absorption of the probe beam then can follow transitions into a new many-body eigenstate. At low fluence the probe then creates a biexciton state, while at high fluence there are many possibilities depending on the average number of excitations per particle. Due to the small size of the particles there is forced overlap of the charges carrier wavefunctions[58], leading to larger multiparticle interaction strengths which can shift the energy of different transitions due to biexciton binding energy, Δ_{xx}, as illustrated in fig 1.7c.

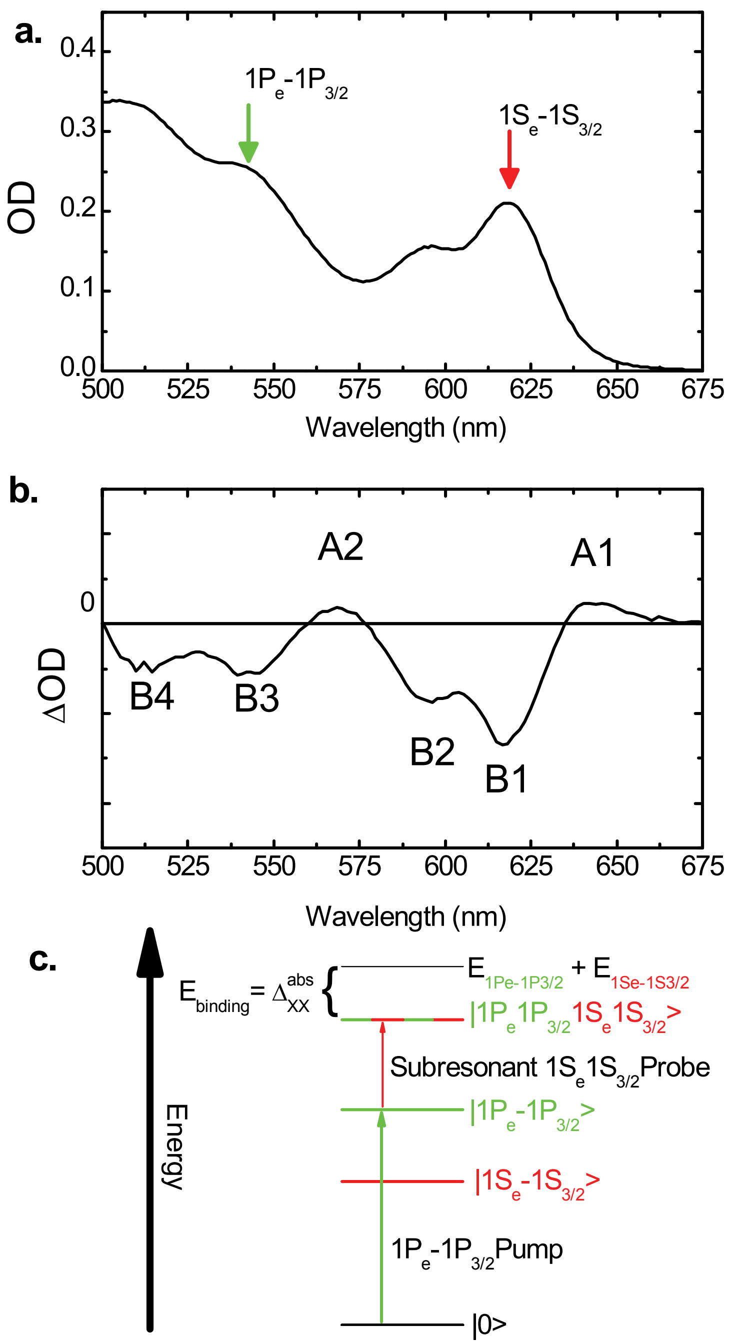

Figure 1.7. a. Linear absorption spectrum of PL spectrum of CdSe quantum dots with radius = 2.8 nm b. TA Spectra of sample taken at 175 fs time delay. The bleach features (B1-B4) and absorption features (A1-A2) are labeled. c. Schematic showing biexciton formation processes in pump/probe measurements, using the $1P_e1P_{3/2}$ pump and sub-resonant $1S_e1S_{3/2}$ probe. The shifting of the energy levels for eigenstates creating the biexciton are manifested as positive signals in the A1 and A2 regions of the TA spectrum.

As shown, a nanocrystal first absorbs a pump pulse photon, creating a $1P_e$-$1P_{3/2}$ exciton. The presence of this exciton then shifts the energy necessary to create a second exciton, in this example a $1S_e$-$1S_{3/2}$ exciton, when they form a biexcitonic complex. The magnitude of the energy shift is the biexciton binding energy, Δ_{xx}. It is defined as the energy difference between the biexciton (XX) and the sum of its component excitons ($X1 = 1P_e$-$1P_{3/2}$ and $X2 = 1S_e$-$1S_{3/2}$):

$$\Delta_{xx} = (E_{X1} + E_{X2}) - E_{XX} \tag{1.16}$$

If the energy E_{X1} is supplied by the absorption of a pump photon, the energy of the probe photon necessary to excite the second transition into the biexciton state can be calculated by rearrangement of (1.16) to yield

$$E_{XX} = (E_{X1})_{\text{pump}} + (E_{X2} - \Delta_{XX})_{\text{probe}} \tag{1.17}$$

The excited nanocrystals will therefore exhibit pump induced absorption at probe wavelengths subresonant to the $1S_e$-$1S_{3/2}$ transition, leading to the A1 feature seen in figure 1.7b.

The binding energies of the biexcitons in nanocrystals can be quite large[20, 59], so they heavily influence the nonlinear optical response of these systems[60-62]. This thesis presents a thorough study of the state dependence of the biexciton binding energy, showing that Δ_{xx} is sensitive to the exact configuration of it component charge carriers- there is a biexciton spectrum which determines the level shifting. This level shifting is important in a variety of applications for nanocrystals, including optical gain[63], quantum cryptography[64], and non classical photon sources[65].

The next section presents a review of literature of biexcitons in colloidal nanocrystals, followed by a review of exciton dynamics.

1.3.1 Investigations of Biexcitons

It is of great interest to see how biexciton interaction strengths as characterized by the biexciton binding energy described by equation (1.16), compare in nanoscale systems to those in bulk systems, which are quite weak (~4.5 meV in bulk CdSe[66]). In a nanoscale system, the Hamiltonian of a biexciton complex has seven terms[67]

$$H = H_e + H_h + V_{ee} + V_{hh} + V_{eh} + \delta V(\varepsilon_1, \varepsilon_2, r_e, r_h) + V_{e,h}^{conf} \qquad (1.18)$$

In this equation H_e and H_h are the kinetic energies of the electrons and holes respectively, while V_{ee}, V_{hh}, V_{eh} are the Coulombic terms describing the magnitude of electrical charge interactions. $\delta V(\varepsilon_1, \varepsilon_2, r_e, r_h)$ is a corrective term to the Coulomb potential due to the difference in the dielectric constant of the interior of the crystal and the barrier environment (changes to the dielectric constant will effect the screening of the powerful Coulombic interactions between the charges). $V_{e,h}^{conf}$ is the confining potential.

Solving equation (1.18) to find the energy of the biexciton levels requires a number of inputs which are not well known, and this has led to some confusion in the theoretical literature beginning in the late 1980's. One of the earliest treatments calculated repulsive interactions (negative values of the binding energy), which became stronger as the size of the nanocrystal decreases[68]. This disagreed with another in depth theoretical study that used a variational approach to examine the biexciton binding energy as a function of the size of the nanocrystal, and examined how this was effected by the ratio of the effective masses of the charge carrier and the ratio of the dielectric constants of the nanocrystal interior to the surrounding medium[69]. These results predicted that the binding energy would be increased in smaller samples, until the Coulombic interactions begin to overwhelm any compensatory effects caused by changes to the shape of the wavefunction in the four particle states when compared to single exciton (two particle states). It was also shown that the dielectric constants of the core and surrounding play a large role in determining the maximum binding energy and shape of the size dependent trend. Further treatments in this time period predicted positive binding energies which continuously increased as a function of size[57].

The theoretical consensus that finally emerged from all the different treatments is that the biexciton binding energy will likely increase as the radius of the nanocrystal is decreased, but the radius dependence of the increase and over what size range this holds depends on the several factors that are not well known-such as any size dependent variation of the dielectric constant or exchange forces between charge carriers[70-72]. Electron correlation has also been shown to be a large contribution to the biexciton binding energy[73].

The early theories predicted there would be observable induced absorptions to both the low energy and high energy side of the bleaches in transient absorption data, caused by bound and excited states of the biexciton[57, 59, 69, 74-77]. However, the samples available at that time were not of sufficient quality to do a thorough investigation in order to validate any of the different treatments.

In general, the size dispersion was very high, and it was shown that inhomogeneous broadening will overwhelm the induced absorptions by obscuring level shifting[57].

Higher energy induced absorptions assigned to blueshifted band edge transitions were observed in glass samples[57], assigned to excited states of the biexciton. With higher quality samples that had lower size dispersion it became possible to observe redshifting of the band edge transitions[20, 59, 77, 78]. One report calculated that the biexciton binding energy increases when electrons and holes in excited states are combined with charge carriers in the band edge, and they were able to back up these calculations by using different pump energies and observing changes to the induced absorptions in the measured TA spectra of a mixed composition glass sample[79]. This is the only report where any care was taken to examine biexciton complexes where it is well known which states the charge carriers populate, but unfortunately the poor surface quality of the $CdS_{0.6}Se_{0.4}$ NCs in a glass matrix hindered detailed analysis.

Higher quality samples greatly facilitated the observation of induced absorptions by lowering the size dispersion of the sample. The most thorough study of biexcitonic interactions using pump/probe on high quality colloidal CdSe NCs used 400 nm light to excite a range of sizes[10, 80]. This group measured binding energies ~12 meV in NC samples with radii ranging from 1-4 nm, measuring no size dependence to the biexciton binding energy. They measured the level shifting at early times when the charge carriers have not relaxed[10]. It is therefore not clear what state the excited electron and hole occupy[10], so it is unclear which part of the biexcitonic spectrum is being measured in each size of nanocrystal.

Limitations in state resolution in TA methods are not as severe when time resolved photoluminescence is used. These techniques involve ultrafast resolution of the emission spectrum of nanocrystal sample. Emission from the biexciton state can be observed in the early time photoluminescence of a highly excited sample of nanocrystals[58, 81-84], and this technique has become prevalent in investigations of multiexciton interaction strengths in nanocrystals over the past 5 years.

Achermann et al first reported biexciton emission as a shoulder on the red edge of the single exciton PL spectrum, only observable at early times and having a supra linear power dependence[58]. When examining the size dependence of the shifting, they obtained a somewhat complicated trend which showed the binding energy increasing up to 35 meV as the size of the nanocrystals was decreased until a critical size of ~ 2 nm in radius, at which point the binding energy drops sharply with further confinement. They explained the data by dividing the NC size into two regimes: between 3.5 and 2 nm in radius Δ_{xx} increases roughly as 1/R as expected for Coulombic interactions, below 2 nm interparticle repulsions take over which lower the binding energy. Certain theoretical work had predicted such a size dependence[69]. They also observed an emission peak positioned at much higher energy than the band edge emission, which was assigned to a charged biexciton with emission from an electron in the $1P_e$ electron energy level.

In 2004-2005 several reports followed up upon the Achermann data. One group was able to measure similar binding energies for the biexciton emission from the band edge state, and also measured a higher energy emission peak[82, 85]. By incorporating the NCs into a TiO_2 host matrix, they were able to observe amplified spontaneous emission from both peaks, which led them to assign the higher energy peak to a triexciton as opposed to a charged biexciton[85, 86]. They were also able to measure ordered photon emission from the different multiexciton states in single particle measurements of these systems[87]. Another group used a combination of time resolved emission and lifetimes at different probe energies to resolve multiexciton peaks[81]. They resolve positively charged biexcitons with huge binding energies (~120 meV), neutral biexcitons with binding energies ~30-40 meV in agreement with the other reports, and they also observe the higher energy multiexciton emission which they attribute to a neutral triexciton.

There is a large body of literature which studies the types of multiexcitons which may be formed in quantum dots grown on substrates using epitaxial techniques, known as self assembled quantum dots (SAQDs). In these types of systems, the biexciton is often investigated using polarized light in order to take advantage of selection rules of these types of systems[67, 88], or using single particle measurements[89-91]. These systems also allow for interesting types of multiexcitons to be formed by charging the structures, allowing measurements of the emission spectra of these complexes[92-94]. However, there are very important differences between the SAQDs and colloidal nanocrystals (also sometimes called “free standing” in contrast) in energy level spacing, selection rules, relaxation dynamics, particle geometry and size dispersion. This makes comparisons between the two types of systems quite difficult.

1.3.2 Relaxation Dynamics

As discussed, the hallmark feature of quantum confinement is the distinct states which arise. One of the most active areas of research in nanoscale systems is the dynamics of charge carrier relaxation. It is important to measure these dynamics both as a test-bed of how well the physics of nanoscale systems are understood, and because relaxation dynamics are intimately related to various potential applications for next generation technologies, especially those related to solar energy conversion[95].

In bulk systems photoexcited charge carriers relax very quickly to the band edge via the emission of LO-phonons[96, 97]. This mechanism should become very inefficient in nanoscale systems, as the charges must relax between states whose energy spacing is much larger than the phonon frequency. This would require multiphonon emission for each step of relaxation, and it was predicted that relaxation would only be able to proceed on the multipicosecond timescale due to a “phonon bottleneck”[98-101]. The signature of this feature would be that the increased energy level spacing would lead to the longer intraband relaxation times as the radius of the nanocrystal is decreased.

Early ultrafast measurements never observed such an effect, and always measured very fast sub-picosecond relaxation of excitons to the band edge[54, 77].

These measurements were hampered somewhat by the quality of samples, using mainly glass precipitates with large size dispersion and poor surface quality. In 1999, Klimov et. al. presented the most complete set of data on high quality CdSe colloidal nanocrystals[102]. Using a 400 nm pump the excited a range of crystallite sizes and measured the dynamics of the B1 feature. By fitting the band edge bleaching dynamics to obtain relaxation rates, they showed that rate constants for $1P_e$-$1S_e$ relaxation ranges from 150 fs in the smallest dots up to 530 fs in larger samples, and that clearly somehow carriers were bypassing the phonon bottleneck. The relaxation rates were similar to those measured in glass sample, indicating that the surface does not play a role in the relaxation mechanism[26].

Theorists have developed a model for an Auger type of relaxation process in which an electron transfers its excess energy to the hole[99, 103, 104]. This process is unidirectional as the valence band has a much higher density of states so the hole can meet the energy conservation requirements easily, while the conduction band is relatively sparse. While negligible in the bulk phase, this process becomes important in nanocrystals since the wavefunction overlap of the electrons and holes is much larger.

The Auger mechanism was well supported by experiments in which the electron relaxation was measured in the absence of the hole[55, 105]. These experiments measure the relaxation of electrons re-excited to the $1P_e$ state from the $1S_e$ state using an IR pump after the hole has been spatially localized in a trap state, finding that intraband relaxation becomes much longer. The hole trapping effectively removes the Auger mechanism, but the relaxation was still relatively fast (3-30 ps). Guyot-Sionnest showed that the relaxation time in this case becomes very sensitive to the type of capping ligands used on the nanocrystal surface, implying that exciton-ligand coupling can occur effectively in colloidal nanocrystals[55, 106]. He was later able to demonstrate the existence of the phonon bottleneck in specially designed systems in which all competing relaxation mechanisms had been minimized, showing electronic relaxation taking place on the nanosecond timescale[107].

While the Auger mechanism explained electronic intraband relaxation, the relaxation of holes between states in the valence band was not well understood. Hole populations were not thought to contribute appreciably to the bleaches observed in pump probe experiments due to the higher density of states of the conduction band[108, 109]. Using NIR probes in transient absorption experiments different groups assigned some dynamics to hole relaxation into trap states[102, 110, 111], but the levels in the valence band are closely spaced so directly monitoring transitions between them would require far IR probe[31] so it is not entirely clear what these measurements correspond to.

Time resolved photoluminescence experiments from the Klimov group observed dynamics implying hole relaxation was hindered by a phonon-bottleneck at the later stages of relaxation when the valence band energy level separation is large[112]. These measurements showed holes reaching the band gap in ~1 ps. It was determined that the measured dynamics did not depend on surface passivation or solvent nature, so they concluded it was intrinsic to the nanocrystal. The relaxation rate was slower in the smallest dots, so they concluded that phonon assisted relaxation was the primary mechanism of hole relaxation.

THz probe experiments from another group were somewhat contradictory, showing hole relaxation taking place on the femtosecond or picosecond timescale depending on whether the electron coupled to the hole via the Auger effect[113]. However, these results depend strongly on both the approximations of the electronic structure used in the EMA technique discussed previously, and on the polarizability of different excitonic states in their interpretation, which is not well understood.

Section 1.4 Conclusions

It has been shown that despite intensive research by the international community, both the biexcitonic electronic structure and ultrafast processes in semiconductor nanocrystals are not well understood. This thesis shows that state selective measurements provide a straightforward technique with which to experimentally approach quantum confined systems. By investigating the distinct states of CdSe nanocrystals, we uncovered specific state-to-state relaxation dynamics, and were able to probe the electronic structure of the single exciton and biexciton manifold of states.

There had not been any investigation of the pump energy dependence of the dynamics of the electrons and holes in high quality colloidal samples. Measurements of electronic relaxation rates had used 400 nm pumps in their experiments, which excites different states in different sizes of nanocrystal. This obscures the actual states involved in relaxation, limiting how accurately the rate constants can be measured. Previous examinations had not clearly identified the mechanism or timescale of hole relaxation through the valence band, since no group had developed a technique which could reliably monitor which state the hole occupied.

The electronic structure of the biexciton levels determines the biexciton binding energy, and how this depends on size and state were also not well understood. There was no well developed basis for the comparison of results of investigations using ultrafast transient absorption techniques against those using time resolved photoluminescence.

This thesis systematically examines the state specificity of the transient absorption data in quantum dots, and shows that the excitonic state created by the pump is as important in design and interpretation of data as the size or composition of the nanocrystal. We show ultrafast state-selective spectroscopy can be used to yield relaxation time constants with very high precision by monitoring charge carrier relaxation between specific states of *both* electrons and holes, and that it naturally allows the measurement of the lowest energy multiexciton energy levels of the biexciton spectrum. It also reveals new types of dynamics involving relaxation into surface states from excited states. Finally, from careful study of the band edge biexciton, we show it has an electronic substructure which causes it to exhibit a Stokes shift between absorption and emission.

These results are important in understanding the electronic structure of excitons and multiexcitons in semiconductor nanocrystals and the relaxation processes of charge carriers between the available states. These are crucial factors which gives rise to almost all of the properties which make NCs of such great technological interest. Accurate experimental data can validate existing theories or instigate the creation of new theoretical work to describe these phenomena. With this understanding researchers can determine the optimal structures for tailoring these materials for their specific uses, fully harnessing the power of quantum confinement for use in nanotechnology. Without understanding of the basic photophysics of these structures, more empirical approaches would need to be used and some of the true power and beauty of these materials could go unutilized.

Our experimental setup is described in Chapter 2. Chapters 3 introduces state-selective spectroscopic measurements of as method of investigation of carrier dynamics and biexcitonic level shifting in nanoscale systems. Chapter 4 uses this method to experimentally investigate the electronic structure of the single exciton and biexciton states in CdSe nanocrystals. Chapter 5 looks at the binding energies of the excited biexciton states as function of size, along with investigating surface trapping rates. In Chapter 6 the band edge biexciton is explored revealing a Stokes shift due to splitting in a similar manner to the fine structure of the single exciton. The final chapter summarizes the thesis and suggests future work to be done. Appendices concerning copyright follow.

References

[1] Y. Yan, R. M. Whitnell, K. R. Wilson, et al., Chem. Phys. Lett. **193**, 402 (1992).

[2] P. K. Walhout, J. C. Alfano, K. A. M. Thakur, et al., in *Ultrafast Phenomena IX*, edited by P. F. Barbara, W. H. Knox, G. A. Mourou and A. H. Zewail (Springer-Verlag, Berlin, 1994), Vol. IX, p. 495.

[3] C. J. Bardeen, J. Che, K. R. Wilson, et al., J. Phys. Chem. A FIELD Full Journal Title:Journal of Physical Chemistry A **101**, 3815 (1997).

[4] B. Ray, *II-VI Compounds* (Pergamon Press, Oxford, 1969).

[5] L. I. Berger, *Semiconductor Materials* (CRC Press, 1997).

[6] J. Norris David, in *Semiconductor and Metal Nanocrystals: Synthesis and Optical Properties*, edited by I. Klimov Victor (Marcel Dekker, Inc. , New York, 2004), p. 65.

[7] M. Balkanski and R. F. Wallis, *Semiconductoc Physics and Applications* (Oxford University Press, New York, 2000).

[8] A. I. Ekimov, F. Hache, M. C. Schanne-Klein, et al., Journal of the Optical Society of America B: Optical Physics **10**, 100 (1993).

[9] B. Segall, in *Physics and Chemistry of II-VI Compounds*, edited by M. Aven and J. S. Prener (John Wiley and Sons, Inc. , New York, 1967).

[10] V. I. Klimov, Annual Review of Physical Chemistry **58**, 635 (2007).

[11] W. W. Yu, L. Qu, W. Guo, et al., Chemistry of Materials **15**, 2854 (2003).

[12] J. J. Shiang, J. R. Heath, C. P. Collier, et al., Journal of Physical Chemistry B **102**, 3425 (1998).

[13] M. Drndic, M. V. Jarosz, N. Y. Morgan, et al., Journal of Applied Physics **92**, 7498 (2002).

[14] A. I. Ekimov, A. A. Onushchenko, A. G. Plyukhin, et al., Zh. Eksp. Teor. Fiz. FIELD Full Journal Title:Zhurnal Eksperimental'noi i Teoreticheskoi Fiziki **88**, 1490 (1985).

[15] L. E. Brus, Journal of Chemical Physics **79**, 5566 (1983).

[16] A. Ekimov and A. A. Onushchenko, Soviet Phys.-Chem. Glass **16** (1982).

[17] A. I. Ekimov, I. A. Kudryavtsev, M. G. Ivanov, et al., Journal of Luminescence **46**, 83 (1990).

[18] U. Woggon, M. Mueller, U. Lembke, et al., Superlattices and Microstructures **9**, 245 (1991).

[19] Y.-N. Hwang, C. M. Kim, S. C. Jeoung, et al., Physical Review B: Condensed Matter and Materials Physics **61**, 4496 (2000).

[20] V. Klimov, S. Hunsche, and H. Kurz, Physical Review B: Condensed Matter and Materials Physics **50**, 8110 (1994).

[21] C. B. Murray, D. J. Norris, and M. G. Bawendi, Journal of the American Chemical Society **115**, 8706 (1993).

[22] Z. A. Peng and X. Peng, Journal of the American Chemical Society **123**, 183 (2001).

[23] Z. A. Peng and X. Peng, Journal of the American Chemical Society **124**, 3343 (2002).
[24] D. V. Talapin, A. L. Rogach, A. Kornowski, et al., Nano Letters **1**, 207 (2001).
[25] L. Qu, Z. A. Peng, and X. Peng, Nano Letters **1**, 333 (2001).
[26] V. I. Klimov, Journal of Physical Chemistry B **104**, 6112 (2000).
[27] W. Hoheisel, V. L. Colvin, C. S. Johnson, et al., Journal of Chemical Physics **101**, 8455 (1994).
[28] N. Chestnoy, T. D. Harris, R. Hull, et al., Journal of Physical Chemistry **90**, 6 (1986).
[29] G. Bawendi Moungi, M. Stiegerwald, and L. Brus, Annual Review of Physical Chemistry **41**, 19 (1990).
[30] W. W. Yu, L. Qu, W. Guo, et al., Chemistry of Materials **16**, 560 (2004).
[31] A. L. Efros and M. Rosen, Annual Review of Materials Science **30**, 475 (2000).
[32] D. J. Norris and M. G. Bawendi, Physical Review B: Condensed Matter **53**, 16338 (1996).
[33] D. E. Gomez, M. Califano, and P. Mulvaney, Physical Chemistry Chemical Physics **8**, 4989 (2006).
[34] D. J. Norris, Optical Engineering (New York, NY, United States) **87**, 65 (2004).
[35] A. Zunger, Physica Status Solidi B: Basic Research **224**, 727 (2001).
[36] L.-W. Wang and A. Zunger, Journal of Physical Chemistry B **102**, 6449 (1998).
[37] H. Fu, L.-W. Wang, and A. Zunger, Physical Review B: Condensed Matter and Materials Physics **57**, 9971 (1998).
[38] H. Fu, L.-W. Wang, and A. Zunger, Applied Physics Letters **71**, 3433 (1997).
[39] A. L. Efros and M. Rosen, Applied Physics Letters **73**, 1155 (1998).
[40] H. Fu, L.-W. Wang, and A. Zunger, Applied Physics Letters **73**, 1157 (1998).
[41] N. A. Hill and K. B. Whaley, J. Chem. Phys. FIELD Full Journal Title:Journal of Chemical Physics **100**, 2831 (1994).
[42] N. A. Hill and K. B. Whaley, Chem. Phys. FIELD Full Journal Title:Chemical Physics **210**, 117 (1996).
[43] K. W. Leung, K.B, Journal of Chemical Physics **110**, 11 (1999).
[44] M. Califano, A. Franceschetti, and A. Zunger, Nano Letters **5**, 2360 (2005).
[45] A. Franceschetti and A. Zunger, Physical Review B: Condensed Matter and Materials Physics **62**, R16287 (2000).
[46] M. C. Troparevsky and A. Franceschetti, Applied Physics Letters **87**, 263115/1 (2005).
[47] M. G. Bawendi, P. J. Carroll, W. L. Wilson, et al., Journal of Chemical Physics **96**, 946 (1992).
[48] M. G. Bawendi, W. L. Wilson, L. Rothberg, et al., Physical Review Letters **65**, 1623 (1990).

49 M. Kuno, J. K. Lee, B. O. Dabbousi, et al., Journal of Chemical Physics **106**, 9869 (1997).

50 A. L. Efros, M. Rosen, M. Kuno, et al., Physical Review B: Condensed Matter **54**, 4843 (1996).

51 D. J. Norris, A. L. Efros, M. Rosen, et al., Physical Review B: Condensed Matter **53**, 16347 (1996).

52 M. Nirmal, D. J. Norris, M. Kuno, et al., Physical Review Letters **75**, 3728 (1995).

53 L. Efros Al, in *Semiconductor and Metal Nanocrystals*, edited by I. Klimov Victor (Marcel Dekker, Inc. , New York, 2004).

54 V. I. Klimov and D. W. McBranch, Physical Review Letters **80**, 4028 (1998).

55 P. Guyot-Sionnest, M. Shim, C. Matranga, et al., Physical Review B: Condensed Matter and Materials Physics **60**, R2181 (1999).

56 V. I. Klimov, A. A. Mikhailovsky, D. W. McBranch, et al., Science **287**, 1011 (2000).

57 Y. Z. Hu, S. W. Koch, M. Lindberg, et al., Physical Review Letters **64**, 1805 (1990).

58 M. Achermann, J. A. Hollingsworth, and V. I. Klimov, Physical Review B: Condensed Matter and Materials Physics **68**, 245302/1 (2003).

59 K. I. Kang, A. D. Kepner, S. V. Gaponenko, et al., Physical Review B: Condensed Matter and Materials Physics **48**, 15449 (1993).

60 D. Scholes Gregory, The Journal of chemical physics **121**, 10104 (2004).

61 A. E. Colonna, X. Yang, and G. D. Scholes, Physica Status Solidi B: Basic Solid State Physics **242**, 990 (2005).

62 S. V. Nair and T. Takagahara, Physical Review B: Condensed Matter **55**, 5153 (1997).

63 A. V. Malko, A. A. Mikhailovsky, M. A. Petruska, et al., Journal of Physical Chemistry B **108**, 5250 (2004).

64 T. Aichele, G. Reinaudi, and O. Benson, Physical Review B: Condensed Matter and Materials Physics **70**, 235329/1 (2004).

65 B. Lounis, H. A. Bechtel, D. Gerion, et al., Chem. Phys. Lett. FIELD Full Journal Title:Chemical Physics Letters **329**, 399 (2000).

66 H. S. Shionoya, H. Hanamura, E. Akimoto, O., Solid State Commun. FIELD Full Journal Title:Solid State Communications **12** (1973).

67 U. Woggon, Springer Series in Solid-State Sciences **146**, 107 (2004).

68 L. Banyai, Y. Z. Hu, M. Lindberg, et al., Physical Review B (Condensed Matter and Materials Physics) **38** (1988).

69 T. Takagahara, Physical Review B (Condensed Matter and Materials Physics) **39**, 24 (1989).

70 A. Franceschetti, H. Fu, L. W. Wang, et al., Physical Review B: Condensed Matter and Materials Physics **60**, 1819 (1999).

71 J. Shumway, A. Franceschetti, and A. Zunger, Physical Review B: Condensed Matter and Materials Physics **63**, 155316/1 (2001).

72 S. V. Nair and T. Takagahara, Physical Review B: Condensed Matter **56**, 12652 (1997).

[73] J. Shumway, A. Franceschetti, and A. Zunger, Los Alamos National Laboratory, Preprint Archive, Condensed Matter, 1 (2000).

[74] A. L. Efros and A. V. Rodina, Solid State Commun. FIELD Full Journal Title:Solid State Communications **72**, 645 (1989).

[75] L. Banyai, Physical Review B (Condensed Matter and Materials Physics) **39**, 3 (1989).

[76] E. L. Pollock and S. W. Koch, Journal of Chemical Physics **94**, 6776 (1991).

[77] U. Woggon, H. Giessen, F. Gindele, et al., Physical Review B: Condensed Matter **54**, 17681 (1996).

[78] C. Burda, S. Link, T. C. Green, et al., Journal of Physical Chemistry B **103**, 10775 (1999).

[79] Y.-N. Hwang, K.-C. Je, D. Kim, et al., Physical Review B: Condensed Matter and Materials Physics **64**, 041305/1 (2001).

[80] V. I. Klimov, Journal of Physical Chemistry B **110**, 16827 (2006).

[81] C. Bonati, M. B. Mohamed, D. Tonti, et al., Physical Review B: Condensed Matter and Materials Physics **71**, 205317/1 (2005).

[82] B. Fisher, J.-M. Caruge, Y.-T. Chan, et al., Chemical Physics **318**, 71 (2005).

[83] B. Fisher, J. M. Caruge, D. Zehnder, et al., Physical Review Letters **94**, 087403/1 (2005).

[84] G. Nair and M. G. Bawendi, Phys. Rev. B: Condens. Matter Mater. Phys. FIELD Full Journal Title:Physical Review B: Condensed Matter and Materials Physics **76**, 081304/1 (2007).

[85] J. M. Caruge, Y. Chan, V. Sundar, et al., Physical Review B: Condensed Matter and Materials Physics **70**, 085316/1 (2004).

[86] Y. Chan, J. M. Caruge, P. T. Snee, et al., Applied Physics Letters **85**, 2460 (2004).

[87] Y. Chan, J. S. Steckel, P. T. Snee, et al., Applied Physics Letters **86**, 073102/1 (2005).

[88] B. Patton, W. Langbein, and U. Woggon, Physical Review B: Condensed Matter and Materials Physics **68**, 125316/1 (2003).

[89] I. A. Akimov, A. Hundt, T. Flissikowski, et al., Physica E (Amsterdam, Neth.) FIELD Full Journal Title:Physica E: Low-Dimensional Systems & Nanostructures (Amsterdam, Netherlands) **17**, 31 (2003).

[90] T. Flissikowski, A. Betke, I. A. Akimov, et al., Physica Status Solidi A: Applications and Materials Science **202**, 383 (2005).

[91] I. A. Akimov, J. T. Andrews, and F. Henneberger, Physical Review Letters **96**, 067401/1 (2006).

[92] A. Franceschetti and A. Zunger, Europhysics Letters **50**, 243 (2000).

[93] L. He, G. Bester, and A. Zunger, Physical Review Letters **95**, 246804/1 (2005).

[94] M. Ediger, K. Karrai, A. Badolato, et al., Phys. Status Solidi C FIELD Full Journal Title:Physica Status Solidi C: Current Topics in Solid State Physics **3**, 3806 (2006).

[95] A. J. Nozik, Physica E: Low-Dimensional Systems & Nanostructures (Amsterdam, Netherlands) **14**, 115 (2002).
[96] S. S. Prabhu, A. S. Vengurlekar, S. K. Roy, et al., Physical Review B: Condensed Matter and Materials Physics **51**, 14233 (1995).
[97] V. Klimov, P. H. Bolivar, and H. Kurz, Physical Review B: Condensed Matter **52**, 4728 (1995).
[98] U. Bockelmann and G. Bastard, Physical Review B: Condensed Matter and Materials Physics **42**, 8947 (1990).
[99] A. L. Efros, V. A. Kharchenko, and M. Rosen, Solid State Communications **93**, 281 (1995).
[100] H. Benisty, C. M. Sotomayor-Torres, and C. Weisbuch, Physical Review B: Condensed Matter and Materials Physics **44**, 10945 (1991).
[101] T. Inoshita and H. Sakaki, Physical Review B **46**, 7260 (1992).
[102] V. I. Klimov, D. W. McBranch, C. A. Leatherdale, et al., Physical Review B: Condensed Matter and Materials Physics **60**, 13740 (1999).
[103] M. Califano, G. Bester, and A. Zunger, Nano Letters **3**, 1197 (2003).
[104] L.-W. Wang, M. Califano, A. Zunger, et al., Physical Review Letters **91**, 056404/1 (2003).
[105] V. I. Klimov, A. A. Mikhailovsky, D. W. McBranch, et al., Physical Review B: Condensed Matter and Materials Physics **61**, R13349 (2000).
[106] P. Guyot-Sionnest, B. Wehrenberg, and D. Yu, Journal of Chemical Physics **123**, 074709/1 (2005).
[107] A. Pandey and P. Guyot-Sionnest, Science **322**, 4 (2008).
[108] S. Hunsche, T. Kedorsy, V. Klimov, et al., Applied Physics B: Lasers and Optics **62**, 3 (1996).
[109] V. Klimov, P. H. Bolivar, and H. Kurz, Physical Review B: Condensed Matter **53**, 1463 (1996).
[110] C. Burda, S. Link, M. Mohamed, et al., Journal of Physical Chemistry B **105**, 12286 (2001).
[111] V. I. Klimov, Optical Engineering (New York, NY, United States) **87**, 159 (2004).
[112] S. Xu, A. A. Mikhailovsky, J. A. Hollingsworth, et al., Physical Review B: Condensed Matter and Materials Physics **65**, 045319/1 (2002).
[113] E. Hendry, M. Koeberg, F. Wang, et al., Physical Review Letters **96**, 057408/1 (2006).

Chapter 2 Experimental Details

The data presented in this thesis concerns the non-linear optical response of the CdSe nanocrystals as measured using pump/probe spectroscopy. This requires measurements of ΔOD as a function of pump energy, probe energy, and time delay. The key results are obtained from tuning the pump energy to be resonant with the different excitonic states close to the band edge, and comparing the resulting data. Ideally there would be minimal opportunity for systematic experimental error in the comparison of the measurements.

The state selective measurements were taken using a home built adaptation of the standard pump/probe setup[1], which was designed to use 2 different pump pulses simultaneously. This allowed us to eliminate many of the problems which could contaminate an assessment of measurements when pumping into different states in a conventional setup.

The basis of our setup is a commercially available ultrafast system. A Kerr-lens mode locked Ti:Saph laser (Coherent Mira, outputs 20 fs pulses at 76 MHz) is powered by a diode pumped frequency doubled ND:YLF laser (Coherent Verdi). The output of this laser is amplified in a Ti:Saph regenerative amplifier (Coherent Legend USP), pumped by a Q-switched diode laser (Coherent Evolution-30, 527 nm center wavelength, 5 microsecond pulses at 1 kHz). The amplifier produces ~2.2 mJ pulses with a Gaussian spectrum of center wavelength of 800 nm and 25 nm bandwidth (FWHM). The output pulses were ~70 fs in duration (FWHM, Gaussian pulse envelope).

The majority of the output power is put into two optical parametric amplifiers (Coherent OPerA, SFG and UV/VIS output setups) which can be set to produce μJ pulses in energy and are tunable from 475 nm into the IR. The ability to tune our pump sources to be resonant with each transition is a major advantage of our setup. The OPA output pulses are collimated using spherical mirrors and passed through a compression setup[2, 3] using fused silica prisms (CVI Melles Griot) which produced transform limited pulses of ~45 fs (FWHM, Gaussian pulse shape). 400 nm pump is generated using second harmonic generation in a 0.1 mm BBO crystal.

The output of the Legend amplifier and all OPA pump pulse durations were measured by background free intensity autocorrelation in a home built setup based upon standard designs[4, 5]. This splits the pump pulse into an input and replica pulse. The replica pulse path includes a programmable delay stage (PM-500, Newport) which can be adjusted to give different delay times between the pulses by varying the path length of the replica pulse . The pulses are focused into a thin BBO crystal (0.3 mm, Newlight Photonics) in a noncollinear beam geometry. The crystal is on a rotation mount to achieve phase matching for second harmonic generation (SHG) using different wavelength pump pulses. In an autocorrelation measurement, the delay stage is scanned in order to measure the overlap of the pulses as a function of delay time, as detected by the intensity of sum frequency generation (SFG) arising from a photon from each pulse. The intensity of SFG is measured at a photodiode (PDA 25 K, Thorlabs) placed in the direction bisecting the two original pulses.

The power and polarization of the pulses are set using a waveplate/polarizer in combination (both CVI Melles Griot). The pump pulses are sent through mechanical choppers using a fan-like screen rotated at fixed frequency which periodically blocks the pulses, controlling pump on versus pump off in the measurements (New Focus 3.501 Optical Chopper). The delay time between the arrival of the pump and probe pulses was set using computer controlled delay stages (Newport PM-500 with precision up to 0.3 fs), with a retroreflector (PROSystems) mounted on them. The beams were aligned such that there was no change to the beam path as the position of the stage was varied, as measured using a CCD camera.

The probe pulse is derived from single filament white light continuum generated in a 1 mm sapphire plate (CVI). It was nJ in power, and spanned from 500 nm into the IR. It is sent using a concave mirror (Newport) into a compression setup using fused silica prism (CVI Melles Griot) so that probe wavelengths could be selected using a slit positioned at the folding mirror where the beam is focused[6]. In this way we could easily probe at any energy of interest using probes with near transform limited pulses (~50 fs, FWHM for Gaussian) over the entire visible portion of the spectrum.

The probe pulse duration and the overall time resolution of the instrument is set by the convolution of the pump and probe pulses, known as the instrument response function (IRF). The IRF of our setup was normally 65-80 fs, as measured using sum frequency generation of the probe and pump pulse inside a BBO crystal at the sample position, just as described for the autocorrelation setup (in this case the delay time is scanned by adjusting the position of the pump's delay stage). Early measurements had larger IRFs (110 - 130 fs), because of the use of lenses instead of concave mirrors in the probe setup.

Due to the relatively unstable nature of white light continuum, the probe beam ratiometry was performed to cancel power fluctuation from the generation process. The beam was split into a signal portion which passes through the sample before being detected, and reference beam which was sent directly to its detection photodiode. Irises were used to reduce background light and scatter reaching the photodiodes, and they were housed in a sealed, darkened container with small entrances for the beams to enter. Both signal and reference beam were passed through a holographic notch filter and 750 nm short pass filter (Newport) to remove residual 800 nm light and reduce background scatter.

The intensities of the beams were measured using a silicon photodiode (Thorlabs PDA-55) whose output was sent into a gated integrator. The signal and reference beams were focused gently to be slightly smaller than the active area of the photodiode, in order to capture the entire pulse but not locally saturate the photodiode response. The integrator holds a constant output corresponding to the area of the photodiode responses for approximately 50 microseconds, and was read in by a computer program. In this way the signal to noise ratio of the probe transmission could approach 10^3.

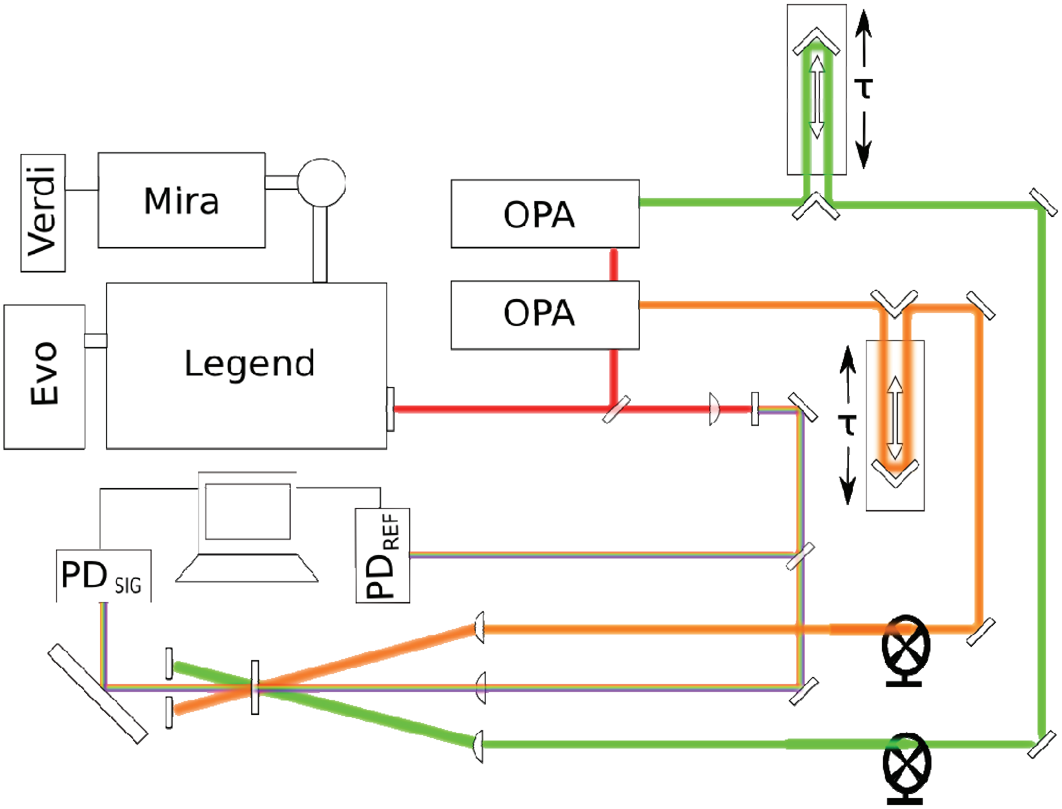

Figure 2.1: Generalized optical layout of the state selective ultrafast spectrometer used in this thesis. The output of the Legend regenerative amplifier is split to create two pump beams via optical parametric amplifier (OPA) and a broadband probe beam made from femtosecond continuum. Delay times are set using the stages in the path of the pump beams, pump on/pump off is controlled using the optical choppers.

A generalized diagram of our pump/probe setup with all the salient details is shown in figure 2.1. The components of the commercial system are shown, with the amplified pulses from the Legend being the red beam. This is split into the OPAs, creating two pumps (orange and green in the diagram). A third portion makes the continuum (rainbow coloured line), which is split into the signal and reference beams. The continuum is sent into photodiodes (PD_{sig} and PD_{ref}), which are read into the data acquisition system. The delay times of the pumps relative to the probe are set using the delay stages shown on the OPA lines, and Pump On conditions versus Pump Off conditions are set using the optical choppers shown. In the diagram lenses are shown focusing the probe and pump beams in the sample, however a concave mirror is actually used for the continuum in order to minimize pulse duration and problems arising from the chromatic aberration of a lens.

The probe pulse should measure a uniformly excited region of the sample in order to avoid systematic errors. Therefore the signal portion of the probe beam was focused to a 75 μm spot size using a spherical mirror, and directed into sample in a crystal quartz flow cell (Kaiser Optics). The pump pulses are focused down using lenses in order to set a beam size of 300-500 μm, and have crossing angles compared to the probe beam of less than 5 degrees. The beam sizes are reported as the FWHM assuming a Gaussian transverse mode. The beam waists are measured using a scanning blade technique which generates an inverse error function that can be fit to a Gaussian corresponding to the beam waist.

Samples were prepared by dissolving CdSe nanocrystals in a solution of HPLC grade toluene to reach an OD between 0.1-0.3 at the band edge, as measured by the difference between the absorbance of the sample cell when filled with a pure solvent and with the nanocrystal solution. The sample solution was flowed through the cell to avoid excessive photoexposure during measurements using a peristaltic pump (Masterflex from Cole-Parmer).

ΔOD is measured using a Labview program designed by Kevin Anderson in this group, which was used to collect all the measurements in this thesis. The program reads in the intensity of the signal and reference probe beams (I_{sig} and I_{ref}), which it uses to calculate the OD of the sample. The assignment of pump on versus pump off depends on whether the program receives a user defined sync pulse that is locked to the phase of the chopper.

A diagram showing the arrival of pulses at the sample is shown in figure 2.2 for a one pump experiment. Probe pulses arrive every millisecond at the sample. In an experiment using only one pump pulse each measurement of ΔOD occurs at 0.5 kHz , as it requires two sets of both probe measurements ($I_{sig,\ on}$ and $I_{ref,\ on}$ are read when the pump passes the chopper, followed by $I_{sig,off}$ and $I_{ref,off}$ when the pump is blocked). The computer program then calculates ΔOD using:

$$\Delta OD = -\log\left(\frac{I_{sig}^{on}}{I_{ref}^{on}}\right) + \log\left(\frac{I_{sig}^{off}}{I_{ref}^{off}}\right)$$

(1.19)

When acquiring data, the delay times are specified before beginning data acquisition. A typical file would consist of an average of 5 to 10 sweeps over the full range of time delays (for a kinetic transient) or probe wavelengths (for a TA spectrum), with each point of the sweep being an average consisting of 50 to 100 ΔOD measurements at a specific delay time. In both types of experiments, the program records each sweep graphically in real time, and reports the data for every sweep along with the average for all sweeps.

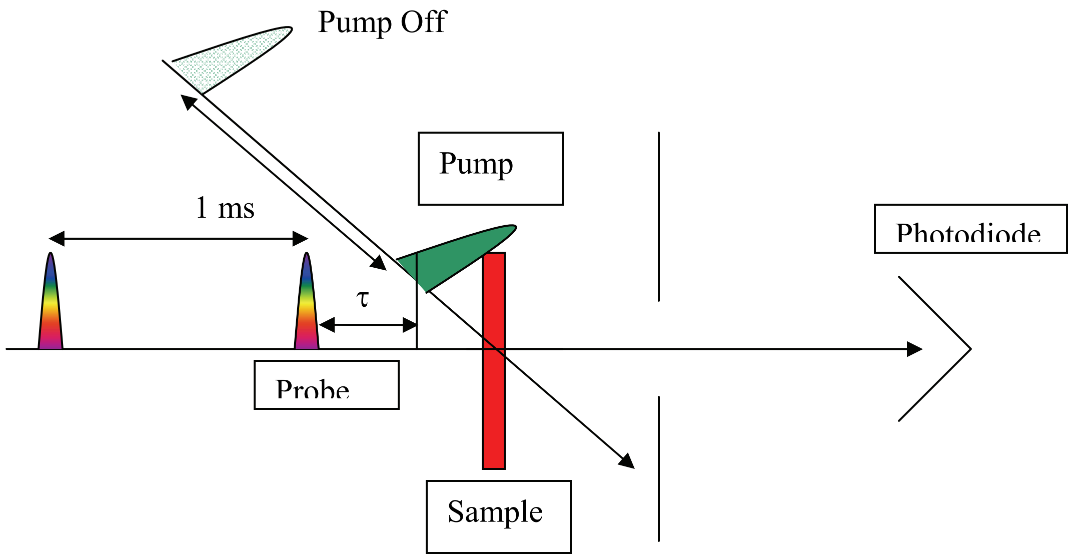

Figure 2.2 Pulse sequences arriving at the sample in a pump/probe experiment using one pump pulse. The delay time (τ) between pump and probe is set by the delay stage. Probe pulses arrive every millisecond, the pump beam is chopped at 0.5 kHz. ΔOD is then measured at 500 Hz.

In many of our experiments we used 2 different pumps alternated on a shot by shot basis in order to reduce the error associated with comparative techniques that could arise from sample aging, optical alignments, signal to noise considerations etc. In order to do we change the chopper frequency so as to pass only every third pulse (0.333 kHz). The pulse sequence in this case is shown in figure 2.3. In these experiments the sequence of pump pulses the sample then experiences is pump 1, pump 2, both pumps off. The probe still arrives a 1 kHz. The ΔOD data for each pump can then be read in separately at 333 Hz in a manner analogous to equation (1.19) above, where a second user defined input is used by the software to correctly designate between when pump 1 is passed, pump 2 is passed, and both are blocked.

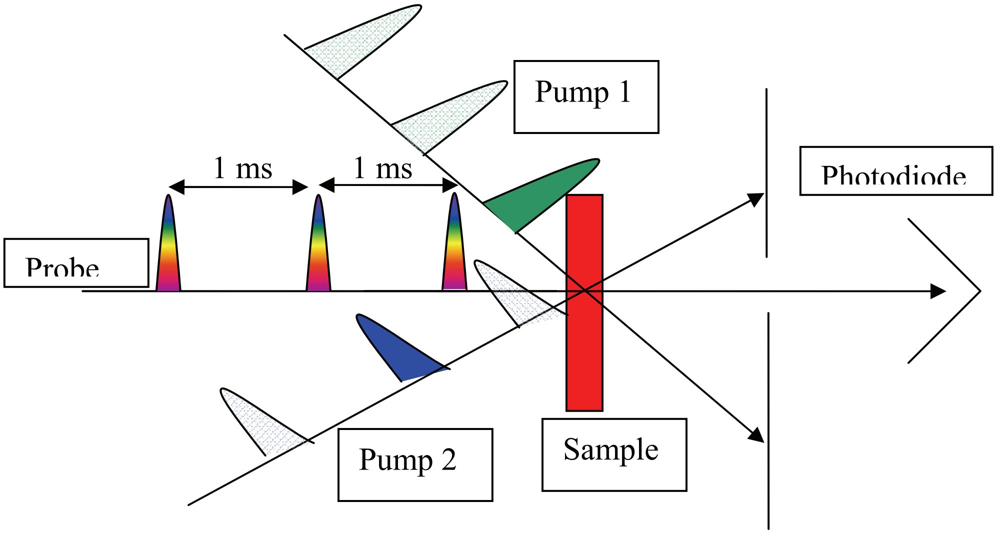

Figure 2.3: Pulse sequences arriving at the sample in a pump/probe experiment using two pump pulses. Probe pulses arrive every millisecond, the pump beams are chopped at 333 Hz. ΔOD for each pump is then measured at 333 Hz.

When necessary, data was pump normalized, which divides the ΔOD value by the pump power as detected by scatter into a separate set of photodiodes. This increased the signal to noise of the data by removing fluctuations due to small variations in the intensity of the pump. This would be done on a shot-by-shot basis.

To obtain chirp free highly resolved TA spectra, after the sample the signal beam is sent into an automated monochromator (DSS 15V, Horiba-Jvon), and read with an amplified Si photodiode (Eos Systems). The delay stage of the pump is moved to correct for this offset as the monochromator scans using calibration curves constructed from the relative delay times of different portions of the continuum as measured by cross correlation[7].

Fits of kinetic transients to obtain rate constants was done using a commercially available fitting program (SpectraSolve, Ames Photonics) which included convolution with the IRF of the sample. Population dynamics were simulated using ODE solving functions built into MATLAB.

References

[1] C. Rulliere, T. Amand, and M. X., in *Femtosecond Laser Pulses, Principles and Experiments*, edited by C. Rulliere (Springer, 2005).
[2] R. L. Fork, O. E. Martinez, and J. P. Gordon, Opt. Lett. **9**, 150 (1984).
[3] J. P. Gordon and R. L. Fork, Opt. Lett. **9**, 153 (1984).
[4] G. Steinmeyer, Journal of Optics A: Pure and Applied Optics **5** (2003).
[5] L. Sarger and J. Oberle, in *Femtosecond Laser Pulses: Principles and Experiments*, edited by C. Rulliere (Springer, 2005).
[6] R. L. Fork, Optics Lett. **11** (1986).
[7] V. I. Klimov and D. W. McBranch, Opt. Lett. **23**, 277 (1998).

Chapter 3:

State Specific Ultrafast Spectroscopy of Semiconductor Quantum Dots

This chapter adapts the text and contains figures from a previously published paper, reproduced with permission from Phys. Rev. B., ***2006****. 74 (235328) © 2006 The American Physical Society. It is co-authored by Ryan R. Cooney, Kevin E. H. Anderson, Eva A. Dias, and Patanjali Kambhampati. The text has been rewritten by the author to reflect the content of this thesis.*

In this chapter we establish the power of state selective spectroscopic methods when examining ultrafast processes in semiconductor nanocrystals. We examine carrier relaxation dynamics when pumping into the three lowest energy excitonic states of CdSe nanocrystals with R = 1.8 nm. These are compared with measurements using 400 nm pumping, in order to highlight the advantages of state specific pumping schemes over traditional near UV excitation. We show very clear differences between the different initially excited states in the early time dynamics, which allows us assign the contribution of electrons and holes to ΔOD in different spectral regions. This allows subtractive methods to be used in order isolate state specific relaxation dynamics for both types of charge carriers. These measurements also show state specific biexciton interactions, which is an important result to further studies of multiexciton complexes in quantum confined systems.

3.1 INTRODUCTION

As shown in the introduction, semiconductor nanocrystals (NCs) exhibit distinct electronic transitions, due their electronic structure lying between the bulk and molecular size regimes[1]. The electronic structure arises from quantum confinement of the charge carriers, with CdSe lying in the strong confinement regime where the electrons and holes can be considered to move independently of each other[2]. How charge carriers relax in these systems has been a subject of considerable investigation, necessary for both understanding the fundamental quantum mechanics of nanoscale materials and for incorporating them into devices.[3, 4]

Figure 3.1 reproduces the linear absorption spectrum of the sample used in these experiments. Recall from the introduction that according to the best assignments of electronic structure from theory, the conduction band states are relatively widely spaced, while the valence band states are much denser because of the higher degeneracy of the 4p orbitals from which these states derive. The transitions between the states are shown as assigned using the EMA approach[2, 5]. The electronic character of the lowest three transitions can be confidently assigned since there is general agreement between theoretical approaches along with considerable experimental support[6-9], and will be discussed more fully in the next chapter. There is some debate about the character of the higher excited states[6, 10], but experimental data shows that the excitonic transitions are closely spaced as in the higher regions of the absorption spectrum[5].

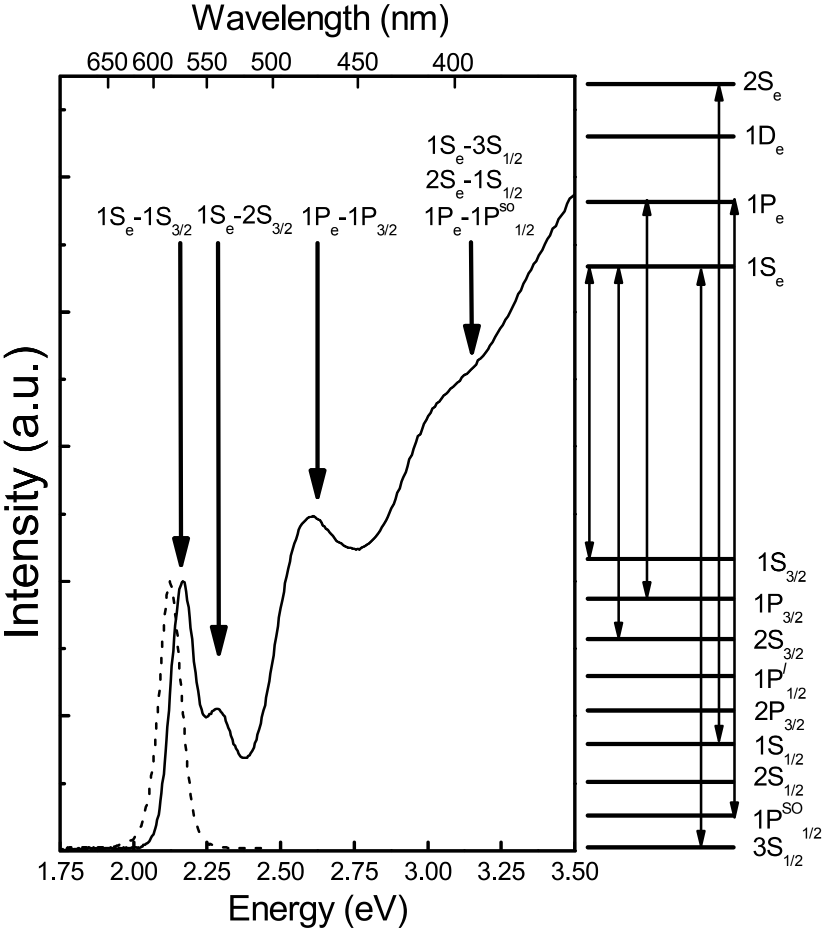

Figure 3.1. Absorption spectrum of CdSe quantum dots (black line) and photoluminescence spectrum (grey line). The pump wavelengths and the initially prepared excitonic states are noted in the figure. The level diagram shows the transitions into specific excitonic states using EMA notation (Ref 5). Assignments become ambiguous in the higher in energy ranges of the spectrum.

The congestion of the electronic states at higher energies leads to some experimental problems when using a fixed 400 nm pump source to examine relaxation dynamics. The distribution of initial states (1S, 1P, 2S, etc.) created using UV excitation will relax to the band edge state with different kinetics, depending how much excess energy must be given off. This would mean that the experimentally measured kinetics in a transient absorption experiments would correspond to the convolution of the instrument response function (IRF) with a complicated sum of several processes, whose amplitudes would depend on the initial distribution of states. This distribution cannot be accurately calculated for high energy regions of the spectrum. Furthermore, this will change in different sizes of nanocrystals, as the energy of the excitonic states change as a function of radius. All these factors make comparison of dynamics in different size of NCs subject to large uncertainties when using fixed UV excitation sources.

We show that preparing the system in a known initial excitonic state overcomes this challenge, by using pump pulses tuned to be resonant with different NC transitions. Under these conditions one measures the state-to-state dynamics of excited carriers, which can be held constant for any size of nanocrystal. This will greatly aid investigations of relaxation mechanisms in quantum dots.

In addition, the preparation of specific initial states allows the observation of specific multiexcitonic complexes in a pump/probe experiment. In our low fluence measurements these are biexcitons. This allows us to begin examinations of the biexciton spectrum of strongly confined charges in CdSe nanocrystals. By preparing specific biexciton states, we see marked changes in the dynamics depending on the initially prepared state showing the importance of excitation energy upon certain types of processes.

3.2 EXPERIMENTAL DETAILS

Samples of colloidal CdSe quantum dots were prepared using published procedures.[11] The samples had no apparent deep trap emission, and had absorption and emission linewidths characteristic of an ensemble dispersity of $\sigma <$ 10 %. The present work focuses on CdSe with an energy gap of 2.17 eV, and a corresponding radius of 1.8 nm.[12] For these measurements the nanocrystals were dissolved in toluene.

To facilitate precise comparisons of transients at different pump wavelengths, the 400 nm pump experiments were performed simultaneously with an OPA pump experiment by alternately chopping each of the pumps beams such that there was shot to shot alternation of the pump color as described in Chapter 2. We used an OPA tuned to be resonant with the three lowest energy transitions shown in figure 3.1, with center wavelengths 580 nm, 540 nm, and 475 nm. The IRF was 110-130 fs for all four pumps at each probe wavelength.

The pump fluence was set to maintain the same mean exciton occupancy, $\langle N \rangle = 0.5$.[3, 13] The OD of the sample was 0.2. Bleach magnitudes were ~50 mOD at the band edge and noise levels were typically ~0.2 mOD. Step sizes were 10 fs for the first two ps. Three separate days of experiments were done on each of three different syntheses of the same size of quantum dot to ensure reproducibility of the results.

3.3 STATE SPECIFIC DYNAMICS

3.3.1 Bleaching Signals and Electron Dynamics

Figure 3.2 shows the exciton dynamics as a function of initial excitonic state, when measured at the band edge (570 nm) and the first excited state (540 nm). We adopt a nomenclature to refer to our state selective measurements by assigning first the pump pulse and then the probe pulse, for example using a 400 nm pump and probing at 570 nm would be 400/570. In order remove XPM artifacts near time zero, pumps and probes were required to be ~10 nm different in wavelength, hence we used a 580 nm pump for the band edge instead of 570 nm, and probed the $1S_e$-$2S_{3/2}$ transition at 550 nm instead of 540 nm.

The 570 nm probe monitors bleaching of the band edge $1S_e$-$1S_{3/2}$ transition, while the 540 nm probe monitors the $1S_e$-$2S_{3/2}$ transition (B1 and B2 respectively, in the notation of Klimov et al)[3, 14]. It is clear in figure 3.2a that pumping resonant with the band edge (580 nm) produces exactly the same transient dynamics at the band edge (570 nm probe) as pumping resonant with the $1S_e$-$2S_{3/2}$ (540 nm), as the 580/570 and 540/570 transients are identical. In figure 3.2b we can see this is also true for both pumps when monitoring the $1S_e$-$2S_{3/2}$ transition (580/540 and 540/550 probe). The slight differences between probing these two different features has been observed previously, and reflects the more complicated contributions of overlapping transitions to measurements as higher energy probes are used[3].

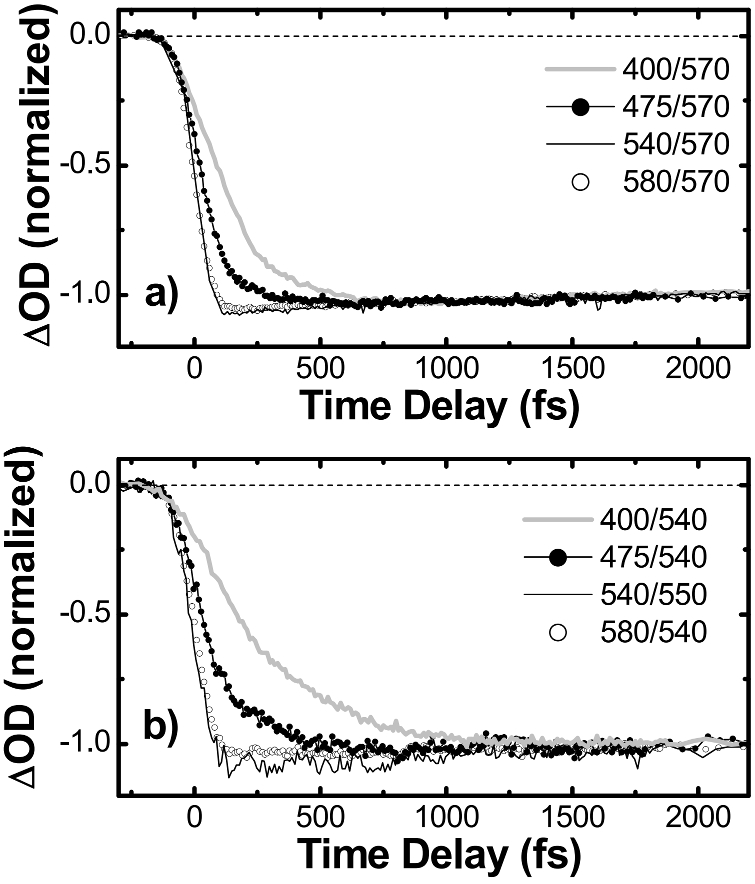

Figure 3.2 Femtosecond pump-probe transients noted by pump/probe wavelengths. The transients have been normalized to the bleach at 2 ps. Each pump wavelengths correspond to different initial excitonic states as noted in Fig. 1. Higher energy pumping at 475 and 400 nm corresponds to multiple initial states due to an increased density of states at higher energy. Panel a) corresponds to the band edge signal denoted B1 in Ref. [3]. Panel b) corresponds to the B2 feature.

Both pumps lead to IRF limited bleaches at the band edge, which as described in the introduction means that the signal reaches its maximum within the time resolution of our setup. The bleaching signal should be proportional to the carrier populations of both the holes and electrons, so while an IRF limited bleach is expected for the band edge (580 nm) pump, it is somewhat surprising for the $1S_e$-$2S_{3/2}$ pump where the hole is in an excited state.

Figure 3.3 shows the four different combinations in which this system could be prepared and measured with these pumps and probes wavelengths. While the hole state varies between them, the electron is always in the $1S_e$ state. The identical transients measured are then only monitoring the population of the $1S_e$ state, there is no contribution from state filling of hole populations in the valence band. Due the much higher density of states of valence band, it has been suggested that holes do not make significant contributions to bleaching signals[15]. This data unambiguously shows that the bleaching signals follow only the dynamics of electrons in the conduction band.

This begins to give us a clear window into intraband relaxation of electrons in nanocrystals. Also shown in figure 3.2, there are clear changes to the B1 and B2 transients when measured after pumping into the $1P_e$-$1P_{3/2}$ state (475 nm) and with 400 nm pump. Instead of an IRF limited bleach, the bleach shows a buildup time of 90 fs for 1P pumping and 200 fs for 400 nm pump. The 400 nm data reproduces earlier reports at all probe wavelengths monitored[3, 7, 14].

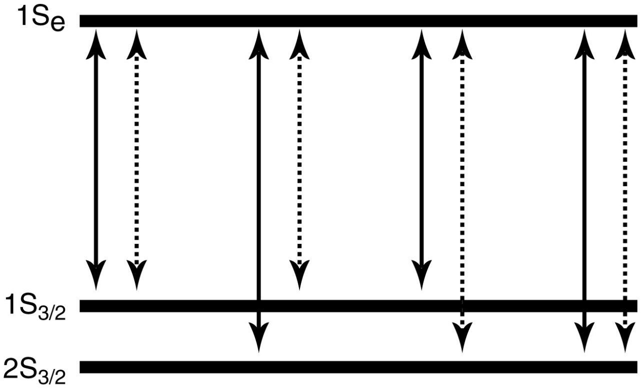

Figure 3.3. Selected transitions relevant to evaluating state-to-state electron and hole dynamics. The solid line corresponds to the pumped transition and the dashed line corresponds to the probed transition.

As discussed earlier, the 400 nm pump excites a distribution of initial states, which will each relax through the manifold of states to the band edge $1S_e$ state. There are obviously higher conduction band states than the 1P being populated, which lead to the larger buildup time as compared with the 475 nm pump data. Clearly, it would be difficult to determine what component of the 400 nm pump B1 transient follows 1P-1S relaxation.

For similar considerations, the 475 nm pump B1 transient buildup time is not a direct measure of electron relaxation time. There is an IRF limited component to the transient, which could be from the overlap of states coupled to both the $1P_e$ and $1S_e$ states in the spectral range of this transition[2, 5], or perhaps subtleties of the electronic structure which mixes states of even and odd angular momentum symmetry[6]. This means that the initial state of the pumped ensemble, and subsequent dynamics, appears to be a weighted average of the two transitions.

It will be shown in section 3.4 that subtractive methods can be used to obtain a direct measure of relaxation of the electrons from 1P to the 1S state.

All pump wavelengths showed identical B1 dynamics for delay times after the first few hundred femtoseconds, with our measurements going to almost 1 ns (figure 3.4). Dynamics on the picosecond to nanosecond timescales are assigned to recombination of electrons and holes[3] or trapping of electrons at surface states[3, 16, 17]. Our results indicate that these processes are not significantly affected by the initial excess energy of the electron, which would imply there no other competing pathways for electron intraband relaxation.

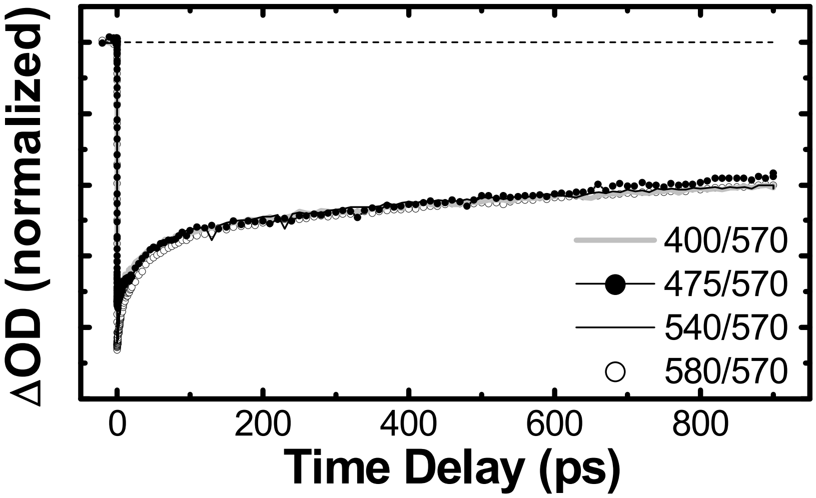

Figure 3.4 Long time dynamics of the band edge bleach (B1) as a function of initial state. All pumps show the same long time dynamics, which indicates that once intraband relaxation is complete all further processes are independent of the initial excess energy of the electron.

3.3.2 Induced Absorptions and Hole Dynamics

While the bleaching features reflect only electron dynamics, the absorptive features provide complementary information about nanoscale charge interactions and dynamics. Induced absorptions arise in pump/probe experiments as the results of excited state absorption (ESA) processes, discussed in the introduction. In nanocrystals these have been assigned to the formation of bound biexcitons[3, 18, 19], as intraband transitions take place at far in the NIR and IR regions[8, 16, 20, 21]. Indeed, our measurements showed no induced absorption between 650 nm and 800 nm, in agreement with previous measurements[3, 16].

The observed induced absorptions occur in the regions of the linear absorption spectrum with the lowest optical density, where ESA signals can overwhelm the bleaching contributions to ΔOD. These regions are on the red edge of the absorption onset (measured at 605 nm) and between the $1S_e$-$2S_{3/2}$ and $1P_e$-$1P_{3/2}$ features (measured at 520 nm). These are the A1 and A2 regions as labeled by Klimov et al[14].

Figure 3.5a shows the dynamics measured to the red of the band edge transition (A1 region) as a function of initial state using the same 4 pumps as for the bleaching data shown in figure 3.2. The transients are shown normalized to their magnitude relative to the band edge bleach, so that they correspond to the same average number of excitations (<N>) for each pump. There are clearly large differences between the transients for the different excitation energies.

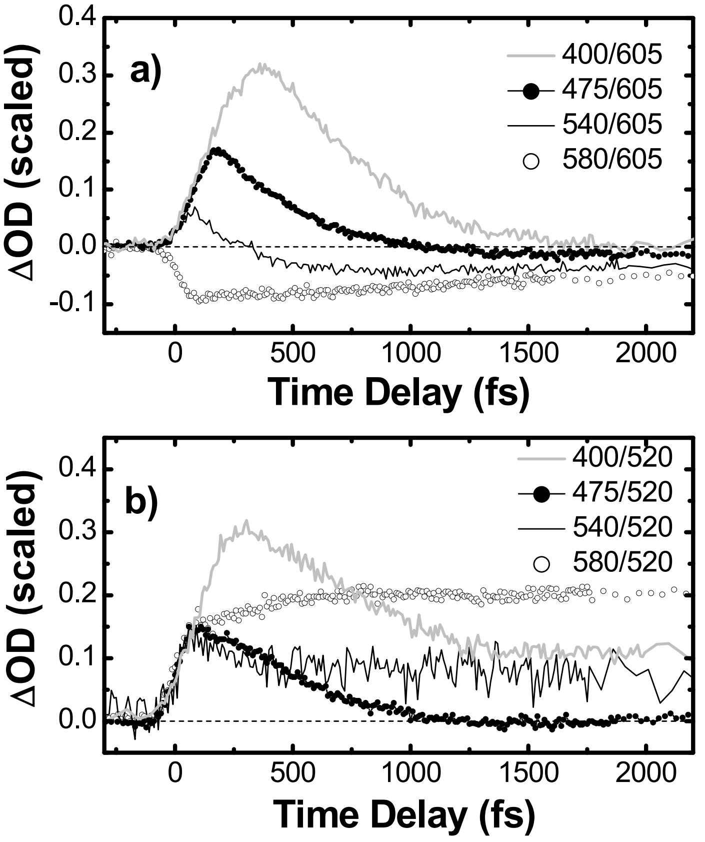

Figure 3.5. Femtosecond pump-probe transients noted by pump/probe wavelengths. The transients have been scaled to the band edge bleach at the corresponding pump wavelength, reflecting the mean exciton occupancy, <N>. The pump wavelengths correspond to different initial states as noted in Fig. 3.1. Higher energy pumping at 475 and 400 nm corresponds to multiple initial states due to an increased density of states at higher energy. Panel a) corresponds to the induced absorption, denoted A1. Panel b) corresponds to the A2 feature.

When using a $1S_e$-$1S_{3/2}$ band edge pump (580/605), the A1 is an IRF limited bleach, while pumping the $1S_e$-$2S_{3/2}$ leads to and IRF limited induced absorption which decays quickly into a bleach. As discussed in the previous section, both of these pumps place electrons into the lowest energy conduction band state, but the $1S_e$-$2S_{3/2}$ pump creates a hot hole with excess energy while the band edge pump creates a hole in its lowest energy state (see figure 3.3). This implies that the dynamics of the 605 nm transient are sensitive to the full eigenstate of the system, and comparison of 580 and 540 nm pumping monitors changes caused by an energetically hot hole relaxing through the valence band.

The induced absorptions, A1 and A2, are both very sensitive to the initial excitonic state, as can be seen by comparing the early time transients of the different pumps shown in figure 3.5a and b. Since the A2 region heavily overlaps with bleaching signal of both 1S and 1P types of electronic transitions, it is difficult to ascertain how much of each will contribute to the bleaching which competes with the absorptive signal. The A1 feature only overlaps with a small portion of the 1S transition so it can be more readily broken down into the contributions of bleaching and level shifting, which makes it a useful feature for monitoring relaxation dynamics since it is sensitive to the states of both charge carriers. It also shows continuous increases in the duration and magnitude of the induced absorption as pump energy is increased, while the A2 transients do not show any systematic variance, making it challenging to assign interpretation of its dynamics.

While the bleaching features in figure 3.2 were all were identical by 1 ps, the A1 features seen in figure 3.5 have not met up by 2 ps, with the offsets dependent upon the initial excess energy of the exciton. Figure 3.6 shows the A1 feature measured on a much longer timescale, where it can seen to evolve on multiple timescales. Since this feature is sensitive to full eigenstate of exciton and the transients of all for all the initial states all meet at ~60 ps, this implies that final state of relaxation is the same regardless of the initial pump states. However, the timescale with which this state is reached depends on the initial state. This can be assigned to hole trapping kinetics from excited states, and will be discussed further in chapter 5.

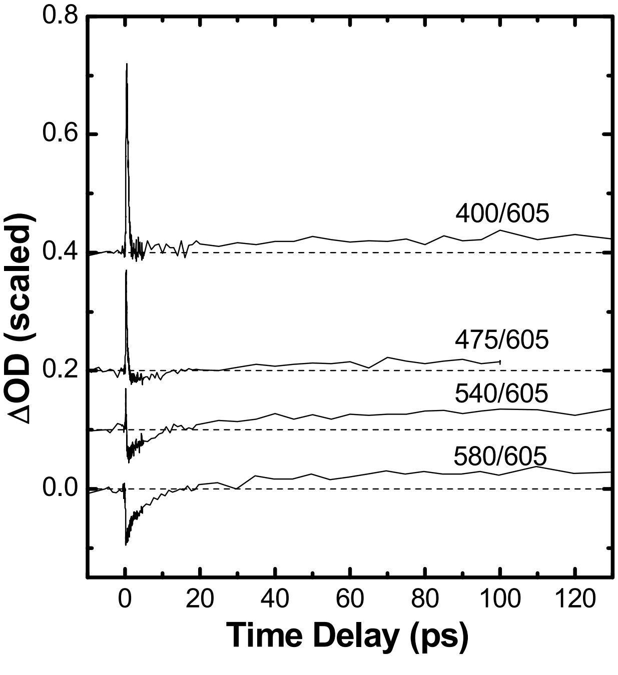

Figure 3.6. Long time scan of the A1 feature illustrating the presence of up to four timescales of processes. The pump-probe transients are noted by pump/probe wavelengths. Since this feature is sensitive to the full eigenstate of the system, it is clear that there is state dependent process which occurs on the ultrafast timescale that can effect how quickly the nanocrystals reach the final state.

The dynamics of the A1 feature will contain contributions on a variety of timescales from populations of the $1S_e$ conduction band state, induced absorption from biexciton formation, and relaxation into the final state. Because of this it cannot be used directly to monitor hole relaxation dynamics. We show in the following section how hole relaxation times can be extracted from the other contributions to the A1 features.

3.3.3 STATE-TO-STATE ELECTRON AND HOLE RELAXATION RATES

It was shown that electron dynamics as measured by probing B1 using higher energy pumps do not *directly* measure electron intraband relaxation. In the case of our 475 nm pump, we can see both an IRF limited portion and induction time to the bleaching signal (475/570 in figure 3.2), which is likely from overlapping of the states with the pump spectrum[2, 5] or subtleties of the electronic structure[6]. The S-type character of the transition leads to the IRF limited dynamics, which are identical to those measured using the band edge pump (580/570 in figure 3.2). We isolate the kinetics of $1P_e$ population relaxing to the $1S_e$ state by taking the difference of the 475/570 and 580/570 transients, producing a plot of ΔΔOD versus delay time, Figure 3.7a.

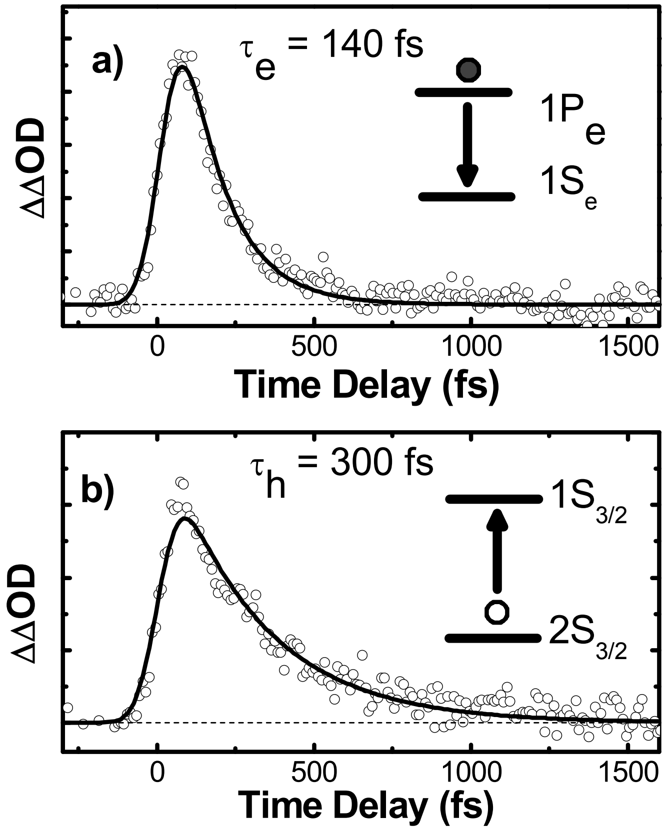

Figure 3.7 State-to-state relaxation dynamics. The ΔΔOD transient is the subtraction of two ΔOD transients reflecting specific initial excitonic states chosen to reflect either electron or hole dynamics. Panel a) shows the difference between the 475/570 and the 580/570 transients. Panel b) shows the difference between the 540/605 and the 580/605 transients the points are the data and the line is the fit.

This type of analysis of excess energy spectroscopy was used to analyze molecular systems[22]. The subtraction removes all contributions of states common to both pumps, leaving dynamics of ΔΔOD only reflecting the depopulation of 1P state electrons:

$$\Delta\Delta \mathrm{OD}(t) = e^{-kt} \otimes \mathrm{IRF}\,. \tag{3.1}$$

It can be seen that this depends only on the 1 parameter, the state-to-state transition rate, k.

Fitting this data requires only the use of a single exponential, which makes this method more robust than the sequential kinetic model with multiple initial states which is required to fit the raw ΔOD transients. This would be especially true for the 400 nm pump, where it is unclear how many states are initially populated and the distribution of their oscillator strengths. Our ΔΔOD measurement shows 1P to 1S relaxation takes place in 140 fs, with a precision of ~15 fs. The nanocrystal can dissipate excess electronic energy at a rate of 2.1 eV/ps when pumped into the 1P- much faster than the bulk value of 0.4-0.6 eV/ps[14]. This indicates how important confinement enhanced relaxation mechanisms such as Auger relaxation is in these systems.

A similar technique can be used to on the A1 data for pumping at 580 and 540 nm. The difference between these two is the initial state of the hole, so subtraction of their data leads to a ΔΔOD transient which directly measures hole relaxation, as seen in Fig 6b. Due our initial state specificity, we can assign a time constant of 300 fs +- 15 fs for hole relaxation between the $2S_{3/2}$ and $1S_{3/2}$ states of the valence band. The energy relaxation rate in this case is 0.4 eV/ps.

Our results are significantly shorter that those using femtosecond PL measurements and NIR transient absorption measurements, but these lack state specificity[23]. Time resolved THz experiments measure similar times for hot hole relaxation into the band edge states, with a somewhat well specified initial state[24].

3.4 STATE SPECIFIC BIEXCITON INTERACTIONS

The induced absorption measurements of nanocrystals prepared in the different excitonic states also shows state specific biexciton interactions. It has been well established that biexcitons in semiconductor NCs show relatively strong binding energies[19, 25-29 30-32], and that these will appear as induced absorptions near to time zero in ultrafast measurements[3, 7, 14]. Alternatively, some groups assigned these spectral signatures to a carrier induced Stark effect, as the TA spectra were similar to the changes of the absorption spectrum of nanocrystals in a strong electric fields (which follows the second derivative of the spectrum)[33-35]. While these terms are somewhat interchangeable, it has become more common to discuss the induced absorption as indicators of biexciton formation[18, 19, 25-29, 31, 32, 36-39].

By preparing the different initial states, we observe the level shifting caused by specific biexciton interactions. The 605 nm probes in figure 3.5a are clearly state dependent at early delay times. Level shifting on these timescales would correspond to lowering of the energy necessary to excite a $1S_e$-$1S_{3/2}$ transition in the presence of the charge carriers formed by the pump pulse, forming a complex composed of 4 particles (2 electrons, 2 holes).

Clearly the $1S_e$-$1S_{3/2}$ exciton (580 nm) produces little level shifting for biexciton formation, not enough to overcome the bleaching contributions. Much more pronounced A1 features are measured when exciting into the higher energy states, and the magnitude of the A1 signal increases with pump energy. The multi-particle interactions are much stronger for the $1S_e$-$2S_{3/2}$ exciton (540 nm pump), which produces the easily observable induced absorption feature which appears. Even larger signals are measured using the higher energy pumps.

It is interesting that the A1 transients for both $1P_e$-$1P_{3/2}$ and 400 nm pumps show buildup times much longer that the IRF of the system, and in fact are still evolving on the ultrafast timescale well after electronic relaxation is complete (which can be seen by comparing them with the transients in figure 3.2a). This suggests that while excitations relax and transiently populate different energy levels, the biexciton interactions sensitive enough to the specific states to produce measurable differences in level shifting. These state specific biexciton interactions are illustrated in figure 3.8. The magnitude of the state specific binding energies can be related to the magnitude of the A1 signal when different states are populated, which will be examined further in the following chapters.

As noted, the evolution of the A1 signal is not complete for the 1P and 400 nm pump even after 500 fs (fig 3.5a), when electronic relaxation is essentially complete. The A1 signals at these time delays then arise while the hole is still relaxing, with the probe pulse monitoring the transition energy into excited states of the biexciton consisting of a single energetically hot hole with the other charge carriers in the band edge states. While it is there are not specific states that can be assigned for the hot hole, enhanced biexciton binding energies in similar situations has been predicted from theory and observed previously[29].

A different interpretation is necessary to explain the picosecond of the A1 dynamics shown in figure 3.6, which depend strongly on the initial state. The signal magnitude here depends on how much state filling induced bleaching contributions are cancelled by biexciton induced level shifting. The biexcitonic contribution in the case of the lower energy pumps appears to be growing on the 10 ps timescale and the 605 nm transients all become positive by 50 ps. This can be explained by trapping of charge carriers[3, 14, 40], and the state dependent dynamics of carrier trapping will be explored in chapter 5.

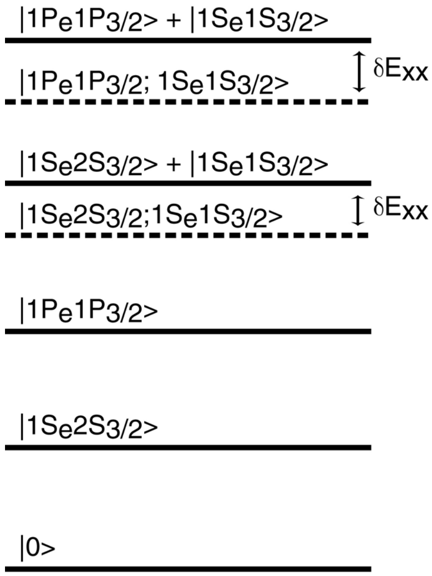

Fig. 3.8. Illustration of state specific biexciton interactions for two initial hot excitonic states, $1S_e$-$2S_{3/2}$, and $1P_e$-$1P_{3/2}$. Excited single exciton states are created by the pump pulse. Biexciton interactions with the $1S_e$-$1S_{3/2}$ exciton are monitored by timing the probe pulse prior to relaxation of the initial exciton. The biexiton binding energy, δE_{XX}, is specific to the four particle system.

3.5 CONCLUSIONS

Here we have shown how the transient dynamics of high quality CdSe nanocrystals depends on the initial excitonic state, in order to establish the advantages of using tunable pump and probe sources to investigate quantum confined systems instead of the traditional fixed UV excitation.

We were able to show conclusively that the band edge bleach (B1) monitors only populations of electrons in the conduction band, and is insensitive to the dynamics of the hole in the valence band. This allows us to disentangle the contribution of state filling caused by electronic populations from other factors contributing to the nonlinear optical response. This is a useful result for research into relaxation and recombination mechanisms, and will also be used in chapter 4 as a method of experimentally testing which types of states are optically coupled in the resolvable transitions of the absorption spectrum.

Subtractive methods using these state selective dynamics can be used to make *direct* relaxation measurements for electron and holes between well defined states. For electrons, this method gives enhanced precision over previous measurements which used 400 nm pumping, as it involves simple fitting models. For holes this is the first measurement of valence band relaxation rates using visible pumps and probes, and can be used to elucidate relaxation mechanisms available to holes[41, 42]. These results were applied to provide a comprehensive framework for understanding intraband relaxation dynamics which is beyond the scope of this thesis, but interested readers may wish to consult References [40] and [41].

The state specificity of biexciton interactions is apparent when comparing different signals of induced absorptions. State selective methods then provide a technique for measuring well specified excited states of the biexciton, allowing further understanding of multiexciton interactions in strongly confined systems. This explored in great detail chapters 4, 5 and 6.

There are also anomalies about the timescale of relaxation in the biexciton signals when pumping into different states. These signals show dynamics on a much longer timescale than can be assigned to intraband relaxation and the transients show a stark dependence on the initial state. We show how these techniques can be used to explore trapping processes of charge carriers in Chapter 5.

REFERENCES

[1] A. P. Alivisatos, Journal of Physical Chemistry **100**, 13226 (1996).

[2] A. L. Efros and M. Rosen, Annual Review of Materials Science **30**, 475 (2000).

[3] V. I. Klimov, Journal of Physical Chemistry B **104**, 6112 (2000).

[4] A. J. Nozik, Annual Review of Physical Chemistry **52**, 193 (2001).

[5] D. J. Norris and M. G. Bawendi, Physical Review B: Condensed Matter **53**, 16338 (1996).

[6] L.-W. Wang and A. Zunger, Journal of Physical Chemistry B **102**, 6449 (1998).

[7] V. I. Klimov and D. W. McBranch, Physical Review Letters **80**, 4028 (1998).

[8] P. Guyot-Sionnest, M. Shim, C. Matranga, et al., Physical Review B: Condensed Matter and Materials Physics **60**, R2181 (1999).

[9] P. Guyot-Sionnest, B. Wehrenberg, and D. Yu, Journal of Chemical Physics **123**, 074709/1 (2005).

[10] W. Hoheisel, V. L. Colvin, C. S. Johnson, et al., Journal of Chemical Physics **101**, 8455 (1994).

[11] J. J. Li, Y. A. Wang, W. Guo, et al., Journal of the American Chemical Society **125**, 12567 (2003).

[12] W. W. Yu, L. Qu, W. Guo, et al., Chemistry of Materials **15**, 2854 (2003).

[13] V. I. Klimov, C. J. Schwarz, D. W. McBranch, et al., Physical Review B: Condensed Matter and Materials Physics **60**, R2177 (1999).

[14] V. I. Klimov, D. W. McBranch, C. A. Leatherdale, et al., Physical Review B: Condensed Matter and Materials Physics **60**, 13740 (1999).

[15] S. Hunsche, T. Kedorsy, V. Klimov, et al., Applied Physics B: Lasers and Optics **62**, 3 (1996).

[16] C. Burda, S. Link, M. Mohamed, et al., Journal of Physical Chemistry B **105**, 12286 (2001).

[17] I. Klimov Victor, in *Semiconductor and Metal Nanocrystals*, edited by I. Klimov Victor (Marcel Dekker, Inc, New York, 2004), p. 159.

[18] V. Klimov, S. Hunsche, and H. Kurz, Physical Review B: Condensed Matter and Materials Physics **50**, 8110 (1994).

[19] U. Woggon, H. Giessen, F. Gindele, et al., Physical Review B: Condensed Matter **54**, 17681 (1996).

[20] C. Burda, S. Link, M. B. Mohamed, et al., Journal of Chemical Physics **116**, 3828 (2002).

[21] C. Burda, T. C. Green, S. Link, et al., Journal of Physical Chemistry B **103**, 1783 (1999).

[22] P. Kambhampati, D. H. Son, T. W. Kee, et al., Journal of Physical Chemistry A **104**, 10637 (2000).

[23] S. Xu, A. A. Mikhailovsky, J. A. Hollingsworth, et al., Phys. Rev. B: Condens. Matter Mater. Phys. FIELD Full Journal Title:Physical Review B: Condensed Matter and Materials Physics **65**, 045319/1 (2002).

[24] E. Hendry, M. Koeberg, F. Wang, et al., Physical Review Letters **96**, 057408/1 (2006).

[25] F. Gindele, U. Woggon, W. Langbein, et al., Physical Review B: Condensed Matter and Materials Physics **60**, 8773 (1999).

[26] B. Patton, W. Langbein, and U. Woggon, Physical Review B: Condensed Matter and Materials Physics **68**, 125316/1 (2003).

[27] Y. Z. Hu, S. W. Koch, M. Lindberg, et al., Physical Review Letters **64**, 1805 (1990).

[28] K. I. Kang, A. D. Kepner, S. V. Gaponenko, et al., Physical Review B: Condensed Matter and Materials Physics **48**, 15449 (1993).

[29] Y.-N. Hwang, K.-C. Je, D. Kim, et al., Physical Review B: Condensed Matter and Materials Physics **64**, 041305/1 (2001).

[30] C. Burda, S. Link, T. C. Green, et al., Journal of Physical Chemistry B **103**, 10775 (1999).

[31] C. Burda and M. A. El-Sayed, Pure and Applied Chemistry **72**, 165 (2000).

[32] U. Woggon, Springer Series in Solid-State Sciences **146**, 107 (2004).

[33] V. L. Colvin and A. P. Alivisatos, Journal of Chemical Physics **97**, 730 (1992).

[34] A. Sacra, D. J. Norris, C. B. Murray, et al., Journal of Chemical Physics **103**, 5236 (1995).

[35] S. A. Empedocles and M. G. Bawendi, Science (Washington, D. C.) **278**, 2114 (1997).

[36] J. Y. Bigot, A. Daunois, J. Oberle, et al., Physical Review Letters **71**, 1820 (1993).

[37] M. Achermann, J. A. Hollingsworth, and V. I. Klimov, Physical Review B: Condensed Matter and Materials Physics **68**, 245302/1 (2003).

[38] A. A. Rogachev, Progress in Quantum Electronics **25**, 141 (2001).

[39] U. Woggon, K. Hild, F. Gindele, et al., Physical Review B: Condensed Matter and Materials Physics **61**, 12632 (2000).

[40] D. J. Norris, A. Sacra, C. B. Murray, et al., Physical Review Letters **72**, 2612 (1994).

[41] R. R. Cooney, S. L. Sewall, K. E. H. Anderson, et al., Physical Review Letters **98**, 177403 (2007).

[42] R. R. Cooney, S. L. Sewall, E. A. Dias, et al., Physical Review B (Condensed Matter and Materials Physics) **75**, 245311 (2007).

Chapter 4:
Ordering of the Electronic States of Excitons and Biexcitons in CdSe Nanocrystals

Portions of this chapter have been previously published. These portions are reproduced with permission from App. Phys. Lett., ***2009****. 94 (243116) © 2009 The American Physical Society. It is co-authored by Ryan R. Cooney and Patanjali Kambhampati. The text below contains an adaptation of the published paper with additional sections in order to fit the continuity of this thesis.*

In the previous chapter we showed the advantages of using state selective spectroscopy over traditional UV excitation to investigate relaxation dynamics and state specific biexciton interactions. Here we use state-specific kinetic transients and TA spectra to measure dynamics, state filling and level shiftings and then use these results to assign the ordering of the single exciton and biexciton energy levels. These make up part of the coarse electronic structure of strongly confined charges, a rich and complicated system due to the high number of excitations which can be created in semiconductor nanocrystals[1] and the enhancement of various Coulomb, exchange and correlation effects due to quantum confinement[2, 3].

4.1. Electronic Structure in Strongly Confined Systems

Over the past two decades quantum confinement in semiconductor materials has been under intense investigation[4, 5]. Semiconductor nanocrystals (NCs) offer tunability by changing the size or geometry of the particle itself.

There is a tremendous amount of interest in incorporating these particles into devices to be used in broad range of fields including solar energy conversion, lasers, and optoelectronic devices[6-8]. To do so systematically will require researches to understand the electronic energy levels available to charges in quantum confined systems.

As shown in the introduction, in the strong confinement regime both electrons in the conduction band and holes in the valence band experience quantization of available energy levels. This leads to discrete eigenstates whose envelope functions are based upon the spherical harmonics with the familiar S, P, D type orbitals[2, 9, 10]. Strongly allowed one photon optical transitions in this system require the initial and final states to have the same symmetry, and will have the degeneracy associated with the envelope function[2, 10, 11].

While distinct single exciton states are clearly resolvable in the absorption spectrum[12] and photoluminescence excitation measurements[11], these linear spectroscopic methods can only determine the energy at which a transition occurs- they provide no information on which types of states (S, P etc) are coupled in the different transitions. It is important to assign the nature of the excitonic states in NCs as a test of theory, to identify the allowed number of excitations, and to interpret the relevant relaxation processes[13-17].

In addition to single exciton transitions, nanocrystals can support multiple excitations which create multiexciton complexes. The simplest multiexciton is the biexciton, discussed in the introduction and Chapter 3, which is made up of a total of 4 charge carriers distributed among the available states. It is agreed that the biexciton binding energy will be enhanced greatly over the bulk[1, 18-20], but there are expected to be many subtleties to the strength of interactions in biexciton complexes where carriers are distributed between different states[3, 21-23]. Therefore the ordering of biexciton levels between the various configurations of charges has yet to be determined. However, the available energy levels of the single exciton states must be understood before higher order multiexcitons can be systematically examined, so that it is clear into which valence and conduction band states populations are being created during photoexcitation.

Using state selective ultrafast spectroscopy we provide a direct experimental measurement of the conduction band state involved in the 4 lowest energy resolvable transitions, yielding unambiguous assignment of the ordering of level structure in colloidal CdSe quantum dots. These results provide an explicit test of the two prevailing theories of single exciton electronic structure in nanocrystals. Furthermore, these experiments allow us to measure the energy levels of both the band edge biexciton and the first three well resolved excited states of the biexciton, allowing us to build up the biexciton spectrum of strongly confined charges.

The proper descriptions of the single exciton electronic states yielded by these measurements are essential for interpretation of results in many of the most active areas of research involving nanocrystals. For intraband dynamics, the available relaxation pathways depend upon the excess energy of the charge carriers[13, 24-28]. For increased solar energy conversion, the Multiple Exciton Generation (MEG) process[29-31] must obey conservation of energy and the Pauli exclusion principle, so thresholds for increased quantum yield will be limited by which lower energy multiexciton states have the proper energy, degeneracy and symmetry to couple to a high energy exciton. To properly use these materials as gain media, one should take into account the degeneracy and excess energy carriers in the state which is pumped to create the population inversion, along with interfering induced absorptions from biexcitonic level shifting[7, 14, 32-35]. Understanding of the biexciton level structure is also essential for incorporating nanocrystals into other non-linear optical devices, not only in gain media but also for quantum information processing[36-40] and non-classical light sources[41, 42]. First we shall examine the single exciton states.

Figure 4.1 shows the linear absorption spectrum for a typical colloidal CdSe NC sample (R = 2.8 nm)[43]. Absorption of a photon creates an exciton comprised of an electron and hole each populating one of the available eigenstates. The linear absorption spectrum reveals discrete energy levels[11], but it has no information about the nature of the states (whether they are S or P, etc).

There have been two main theoretical approaches to describe the electronic structure of NCs leading to the features in Fig. 4.1. The first method, more widely used in the experimental literature for the type of colloidal NCs considered here, is the referred to as the effective mass approximation (EMA) method, and was described in some detail in the introduction. The second method is an atomistic approach using density functional theory, referred to as the direct diagonalization method (DDM). This was also described briefly in the introduction. Both approaches have been well described in reviews[2, 44, 45].

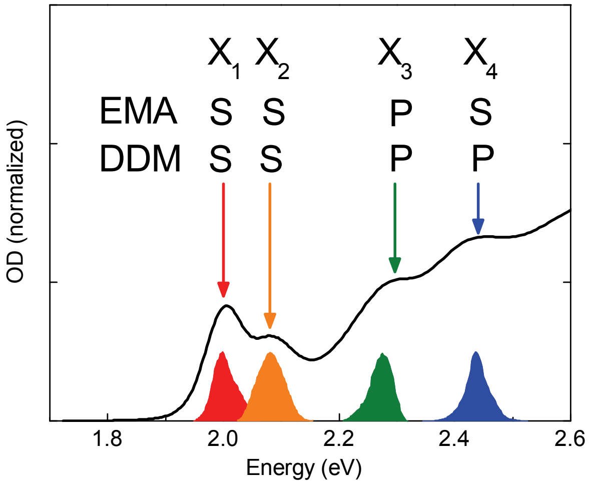

Figure 4.1. The linear absorption spectrum of CdSe quantum dots, R = 2.8 nm. There are 4 transitions in the visible window, labeled in order of increasing energy. The envelope function symmetry of the coupled states predicted using the EMA and DDM methods are indicated above each transition. S type transitions populate of the lowest energy conduction band state ($1S_e$), while P type transitions populate the $1P_e$ excited state. Pump spectra used in state-resolved experiments are shown beneath each transition.

While the EMA and DDM can both reproduce the experimentally determined energy levels and their size dependence, they differ in their descriptions of the underlying features from which these states arise[46-50]. It is beneficial for experimentalists to produce results which help resolve such discrepancies in order to test the fundamental soundness of the results. One of the inconsistencies between theories is the symmetry assignments of higher energy excitonic features[10], as shown in Fig. 4.1. These symmetries are crucial in both the design and interpretation of experiments[14, 24], as the symmetry determines both the degeneracy of the transition and how deep into each band the optically coupled electron and hole states are.

The DDM and EMA approaches yield different assignments of these higher energy peaks largely because of discrepancies in the number of states predicted in the valence band, discussed in detail in reference (10). It is shown that DDM calculations predict a very dense valence band, so higher energy peaks tend to arise from relatively shallow valence states coupling to higher energy conduction band states. The EMA yield fewer states over the same energy range, so it tends to assign the higher energy transitions to coupling between the lower energy conduction band states and very deep valence band states.

Due the difference in the density of states in the valence band, the DDM calculations predict that as photon energy is increased the populated electronic state changes sequentially. The 2 lowest energy strongly allowed transitions couple to the $1S_e$ state (2 fold spin degenerate), the next 3 transitions to the $1P_e$ state (6 fold spin degenerate), and higher transitions (beginning ~ 2.6 eV in the present sample) mainly to the $1D_e$ state[10]. In contrast, the EMA model predicts that over the same range of pump energies over half of the transitions are coupled to $1S_e$ state, so that there is not a clear correlation between pump energy and the symmetry of the coupled states[2, 11].

4.2 Determination of the Symmetry of Single Exciton Transitions

4.2.1 Transient Dynamics

Our excitonic state-resolved ultrafast pump/probe experiments introduced in Chapter 3 offer a method to distinguish eigenstate symmetry by looking at the dynamics of different specific states created using pump pulses resonant with their transition energies. The experimental details were described in chapter 2. The instrument response function (IRF) of the setup was 65-75 fs over all pump/probe combinations. The nanocrystals, purchased from NN Labs, have band edge exciton at 2.0 eV, corresponding to R = 2.8 nm.

The magnitude of ΔOD due to ground state bleaching (GSB) is proportional to the occupation numbers of carriers in the states coupled by the transition, determined by dividing the mean number of excitations per nanocrystal in that state by the degeneracy of the state[5, 14]. In CdSe nanocrystals ΔOD at the energy of the band edge transition (B1 nomenclature of Klimov et al.[5, 51]) is insensitive to valence band populations, and is proportional only to the population the $1S_e$ state in the conduction band[25, 51], as shown in the previous chapter. The dynamics of the B1 feature will then be identical for excitations which populate the same conduction band state[13, 16, 17] (seen previously in Figure 3.2 and 3.3). For a complete study of state-resolved exciton dynamics as reflected in the B1 signal using our methods, please refer to a set of papers by R. Cooney which are outside the scope of this theis[13, 25].

We have seen that a pump pulse resonant with S-type transitions excites electrons directly into the $1S_e$ state resulting in an IRF limited B1 feature, while in contrast P-type transitions populate the $1P_e$ state so the B1 feature exhibits an induction time during intraband relaxation[13, 16, 25, 51]. The clear distinction between IRF limited features and those with buildup times in pump/probe experiments allows assignment of which conduction band states are being populated by pump pulses resonant with the various transition frequencies seen in Fig. 4.1.

Using our state-resolved pumping scheme[13, 16, 25], we pump into each of the first 4 transitions labeled in Fig. 4.1 (pump spectra are shown beneath each transition) and monitor the dynamics of the B1 feature, shown in Fig. 4.2. Clearly pumping X_1 or X_2 both result in IRF limited bleaches, confirming that they directly populate the lowest energy $1S_e$ conduction band state as we saw in Chapter 3[13, 16, 25]. The transitions share the same final state but are at significantly different energies, and the excess energy of X_2 is due to excitation from an S-type state deeper in the valence band, resulting in an energetically hot hole, a fact which we used to investigate hole dynamics in the previous chapter.

When exciting transitions into X_3 and X_4 the bleach dynamics show identical build up times. Pump pulses resonant with either of these energies then populate the $1P_e$ state of the conduction band from P type valence band states of different energies, and the buildup time is caused by intraband electronic relaxation from $1P_e$ to $1S_e$ as we saw in chapter 3. When pumping into X_3 the excess energy is primarily due to the electron, the lowest energy P type hole state is relatively close to valence band according to both methods[2, 10, 11]. When pumping into X_4 both types of charge carriers will have significant amounts of excess energy.

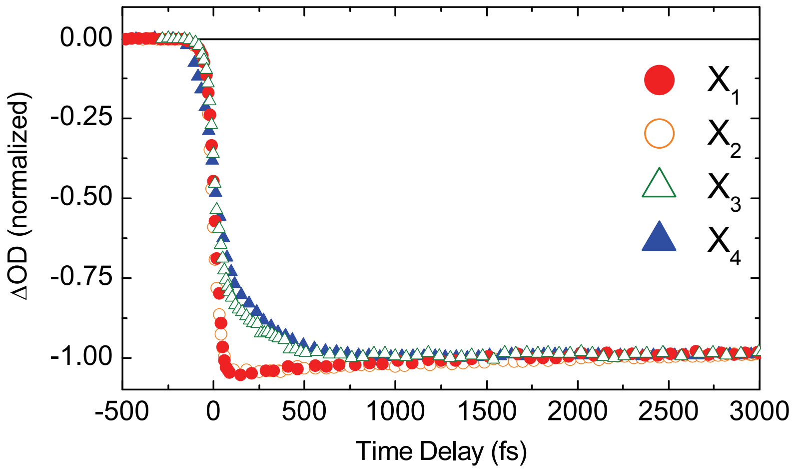

Figure 4.2. Transient dynamics of band edge (2.0 eV probe) when pumping into the first 4 excitonic states of CdSe quantum dots (R = 2.8 nm). The fluence was set to maintain <N> = 0.5 for each pump energy. All signals are normalized at late times (2500 fs) for comparison. S type excitons show an IRF limited bleach (X_1 and X_2). P type excitons have a build up time corresponding to relaxation from the $1P_e$ into the $1S_e$ state (X_3 and X_4).

The measured dynamics indicate a complete absence of overlapping states coupled to the $1S_e$ level in the spectral region of states X_3 and X_4. Such a state would be expected to decrease the induction time by directly populating the $1S_e$ state in a fraction of excited nanocrystals. This effect would be proportional to both the oscillator strength of the transition and its spectral overlap with the pump pulse. The pump spectra are well separated spectrally but the relaxation dynamics are identical, so if there are any unresolved transitions in this region they must also be coupled to the $1P_e$ state. These results are consistent only with the DDM calculations, and contradict the EMA results.

4.2.2 Non-linear Spectra

These assignments are further supported by the non-linear absorption spectrum upon exciting the different states in CdSe nanocrystals ($OD_{NL} = OD_0 + \Delta OD$). OD_{NL} for populated states decreases as a function of pump fluence, at high enough fluences the sample can approach optical transparency ($OD_{NL} = 0$) or show optical gain ($OD_{NL} < 0$). Figure 4.3 shows non linear spectra over a range pump pulse fluence when pumping into X_1, X_3 and X_4. The spectra were taken at 1 ps, after intraband relaxation is complete[13, 25].

When pumping into X_1 [Fig. 4.3(a)], at high pump powers *both* states X_1 and X_2 are nearly completely bleached due to state filling of the $1S_e$ level. There are small bleaches at the energies of states X_3 and X_4 which are primarily caused by multiexcitonic level shifting[52], which we will investigate further in the next portion of this chapter. These effects are proportional to the magnitude of the band edge bleach over the full range of pump power, which leads to the clear isosbestic points between X_2 and X_3. The lack of significant bleaching in the higher energy region of the spectrum indicates there are *no* S-type transitions with those energies, consistent with DDM predictions. Nearly identical results are obtained when pumping X_2.

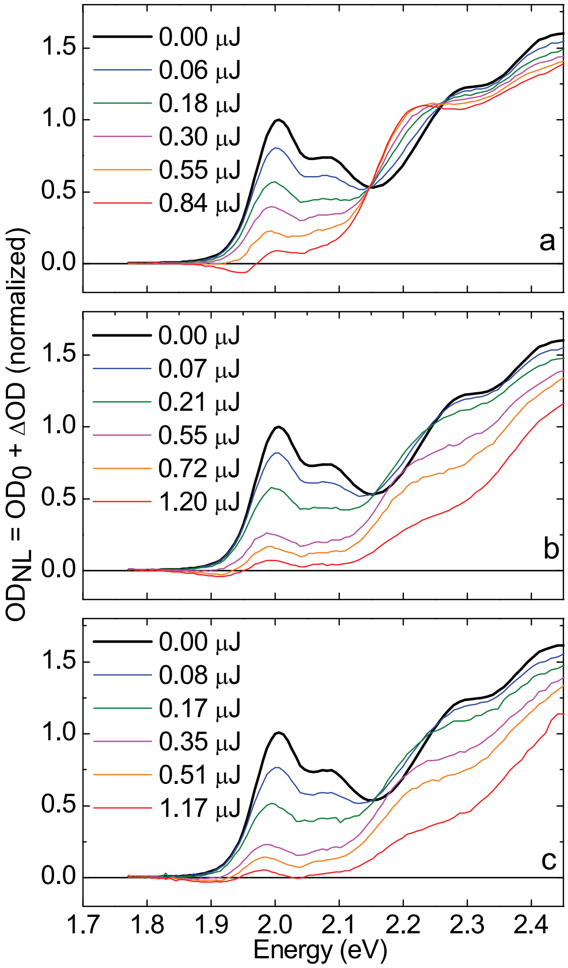

Figure 4.3. Nonlinear spectra ($OD_{NL} = OD_0 + \Delta OD$) of CdSe nanocrystals taken at 1 ps as a function of pump pulse energy when exciting resonant with a). X_1, b). X_3, c). X_4. When pumping into X_1 at high fluence the sample is almost transparent at the energies of X_1 *and* X_2, but the 2 highest energy states are not populated. When pumping into X_3 and X_4 there is significant bleaching of all transitions at high fluences due to filling of the $1P_e$ electronic state in QDs populated with more than 2 excitons.

When pumping into X_3 and X_4 the isosbestic points appear at lower fluences, but at higher excitation levels bleaching dominates $OD_{N.L.}$ of the higher energy region (Fig 4.3b, 4.3c). At low fluences photoexcited electrons can relax from the $1P_e$ to $1S_e$ level before 1 ps, but with more than 2 excitations the $1P_e$ level remains populated and this state filling decreases the absorbance of the sample at the energy of P-type transitions. With these pumps, we can see obvious fluence dependence to $OD_{N.L.}$ in the higher energy spectral range which is not proportional to the band edge bleach. Nanocrystals can clearly accommodate more than 2 excitons when pumped into X_3 and X_4, consistent with the 6 fold degeneracy of the P-type states.

4.3 State Specific Biexciton Binding Energies.

With proper descriptions of these single exciton states, we are able to examine how they interact when combined to form excitonic complexes. Multiexcitonic level shifting was discussed in the introductory chapter and in Chapter 3 to understand the origin of the inducted absorptions measurable in pump/probe experiments using visible light[18, 22, 53, 54]. These effects are quite interesting for both the understanding of the fundamental physics of confined charge carriers, and are also of technological importance since they make significant contribution to the nonlinear optical response of nanoscale semiconductor materials[38, 55-57].

Figure 4.3a showed how this type of level shifting can lead to serious changes in the absorption spectrum of a highly excited sample. When using the highest fluence pump, the band edge is over 90% bleached (in terms of the average excitations per particle, <N> = 1.84)[14]. Almost every nanocrystal has two excitons present so the S-type transitions are almost completely filled, and these populations lead to multiexcitonic interactions which shift the P-type transitions by over 50 meV from their original position[52]. It is difficult to systematically create higher order multiexcitonic complexes, so we focus on the simplest of these types of systems, the biexciton.

We use pump/probe measurements to generate biexcitons, via sequential absorption of photons from the pump and probe pulses[18, 53]. After the pump pulse is passed through the sample, some fraction of nanocrystals absorbs a photon and will be populated by excited charge carriers, and these nanocrystals will exhibit a new absorption spectrum as illustrated in figure 4.4a (dotted line) where the energy levels were shifted for the second excitation event (biexciton formation). The shift of the energy levels is the biexciton binding energy, Δ_{xx}, shown in the figure.

The results presented in the previous chapter showed that the magnitude of ΔOD measured in spectral regions sensitive to biexcitonic level shifting (A1, A2 features) is a function of excitonic state, allowing for optical measurements which can specify the particular biexciton complex created from many possible configurations. Here we focus on biexcitons made up of combinations of the band edge state (X1 in the terminology of the previous section, and $1S_e$-$1S_{3/2}$ using the EMA nomenclature standard in the literature[11]) with the 4 lowest energy excitations (as seen in the spectrum shown in figure 4.1). The method is illustrated in figure 4.4b.

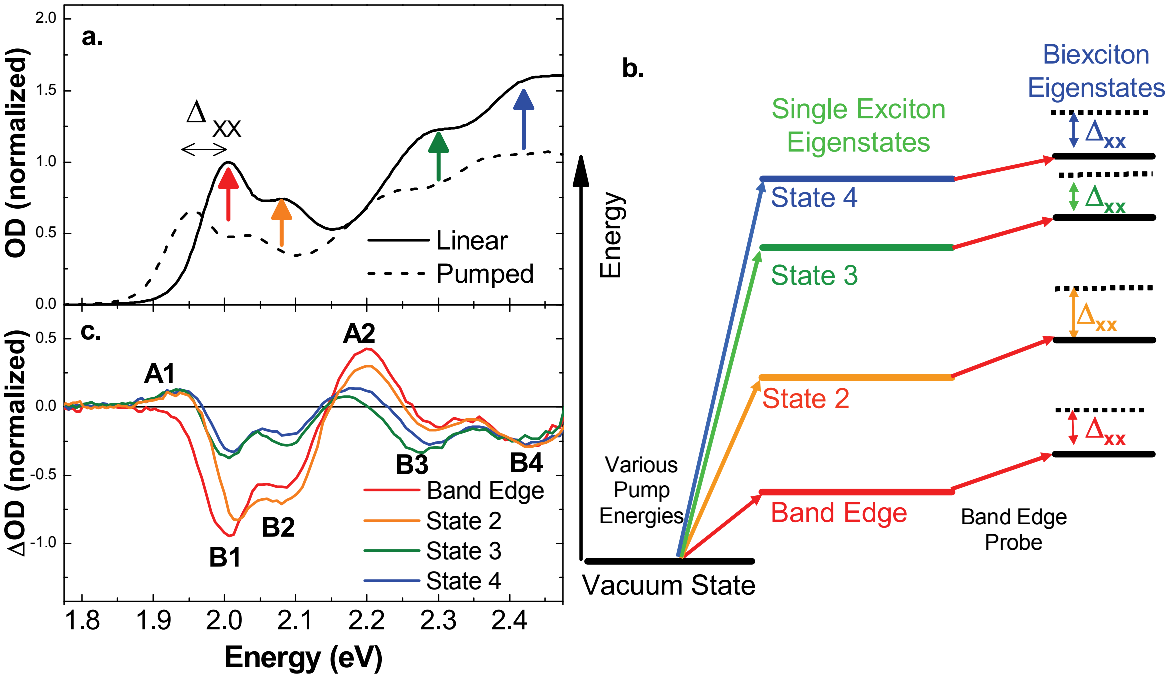

Figure 4.4: a). The linear absorption spectrum (solid line) and absorption spectrum of the fraction of the sample excited by the pump pulse (dotted line, energy shifting not to scale), R = 2.8 nm. The arrows indicate the four eigenstates optically excited (spectra shown in figure 4.1). The energy levels are shifted by biexciton binding energy Δ_{xx} in the pumped fraction of the sample (dashed line), which leads to the induced absorptions in the TA Spectrum.

b). Illustration of pump/probe sequences leading different biexcitons which are observed in the A1 region of the TA spectra.

c). TA spectra (τ = 75 fs) have bleaches (B1-B4) due to state filling of various conduction band states, and induced absorptions (A1, A2) due to level shifting via biexciton formation . The magnitude of the shift is the biexciton binding energy, Δ_{xx}, and is sensitive to the state prepared by the pump pulse. The bleach magnitude of each pump's data set reaches the same value at later time delays, the TA spectra are normalized to that magnitude.

As shown if figure 4.4 b, the biexcitons are created by sequential absorption during the pump/probe experiment, varying the wavelength of our excitation pulses and examining the low energy induced absorptions. In this manner we prepare each of the 4 different exciton states, then monitor transitions into the biexcitonic state, comprised of the original excitation and a second excitation in the band edge state, by the amount of level shifting.

These measurements must be done with the very short pulses as the excited states of the biexciton have relatively short lifetimes (~100-250 fs), decaying via Auger relaxation into a band edge electron and high energy hole state[51, 58, 59]. The hole can then relax through the valence band via emission of phonons or coupling to ligand vibrational modes, reaching the band edge by ~ 1 ps[13, 25, 26]. This data is for relatively large dots in which intraband relaxation is slower, giving us the best state resolution possible for the early time measurements. In smaller dots intraband relaxation is as fast as the time scale of our pump pulse, obscuring our ability to measure binding energies the specific states. The pump fluences were set so that <N> was ~0.5. This was done carefully to make sure any pumped particles should have only 1 excitation, so that the induced absorptions observed would be caused by transitions into the biexciton state.

Using the same sample of CdSe quantum dots (R =2.8 nm) as in figure 4.1, the TA spectra of when excited into each the 4 lowest eigenstates are shown if figure 4.4c. The spectra were taken at a time delay ~75 fs, just after the completion of the pump pulse and before relaxation processes have caused appreciable decay of excitonic state specificity. The spectra have features (B1-B4, A1-A2) labeled using the notation of Klimov et al. The bleaches are caused by state filling, as discussed previously.

The major difference between the TA spectra is in A1 region, on the low energy side of the band edge transition. This is the region where biexciton formation of the pump exciton and band edge probe exciton will cause positive deviations from the contours of the linear absorption spectrum. It is clear that the different initial excitonic states have dramatically different A1 signals, and allows us to measure the state specific binding energies.

An induced absorption in the TA spectra of nanocrystals is measurable when there is a significant change in the energy of the multiexciton particle complex compared to its component single excitons. For the combination of 2 excitons this is the biexciton binding energy as shown in fig 4.4a and b, defined as

$$\Delta_{XX} = (E_{x1} + E_{x2}) - E_{xx} \tag{4.1}$$

Equation (4.1) defines the biexciton binding energy as a positive number if the energy of the biexciton, E_{xx}, is lower than the sum of energies of the component single excitons, E_{x1} and E_{x2}, which would mean the 4 particle state is bound in some sense.

While in principle one could examine the binding energy of any combination of excitons by using different pumps and probes, in practice it proves problematic to use high energy probes since there are many different states that can contribute to signals in regions above the band edge. The most accessible biexcitons are therefore the ones which are made up of a pump exciton with a

$1S_e1S_{3/2}$ probe, as shown in 4.4b. As we are now interested in an energy shift, we can the equation used to describe ΔOD presented in section 1.4 in terms of energy such that it describes the change in absorption of a probe of energy $\hbar\omega$:

$$\Delta OD(\hbar\omega) = \sigma_{0\to1}(\hbar\omega) * (-2N_1) + \sigma_{1\to2}(\hbar\omega) * N_1 \tag{4.2}$$

This equation expresses ΔOD as function of probe frequency in terms of the linear absorption cross section $\sigma_{0\to1}(\hbar\omega)$, the concentration of excited nanocrystals N_1, and the absorption cross section for formation of biexciton $\sigma_{1\to2}(\hbar\omega)$. This equation should be valid for the TA spectrum of the band edge region (B1 and A1) at low fluences, in this case N_1 is the average number of excitations per nanocrystal (which can be determined from magnitude of the bleach[14, 51]).

The value of the binding energy can be extracted by modeling $\sigma_{1\to2}(\hbar\omega)$, the shifted absorption spectrum for transition of singly excited nanocrystals into the biexciton state, as the linear absorption spectrum displaced by the biexciton binding energy:

$$\sigma_{1\to2}(\hbar\omega) = \sigma_{0\to1}(\hbar\omega - \Delta_{XX}) \tag{4.3}$$

Using this definition, the TA spectrum for a $1S_e1S_{3/2}$ pump will be equal to

$$\Delta OD(\hbar\omega) = \sigma_{0\to1}(\hbar\omega) * (-2N_1) + \sigma_{0\to1}(\hbar\omega - \Delta_{XX}) * N_1 \tag{4.4}$$

Here the only unknown is then the displacement of the spectrum in the second term which describes the induced absorptions.

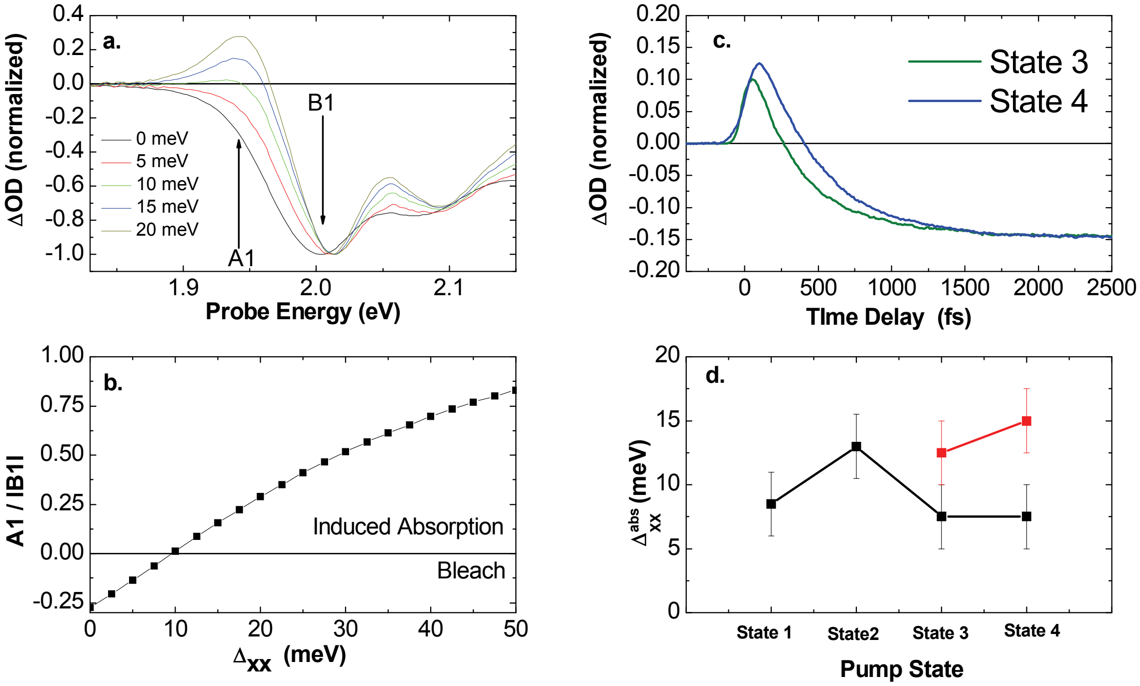

Figure 4.5: a). Calculated TA Spectrum for the band edge region (A1 and B1) of CdSe quantum dot (R = 2.8 nm) as a function of biexciton binding energy

b). Ratio of A1 and B1 features (as denoted by arrows in a).) as a function of biexciton binding energy.

c).The measured A1 traces when pumping into the P-type States 3 and 4. The biexciton binding energy for these states changes as different states are populated while charges undergo relaxation.

d). Extracted Δ_{xx} as a function of state. This shows the biexciton binding energies for formation of a biexciton using a pump exciton in each of the four lowest energy transitions with the $1S_e1S_{3/2}$ band edge state for R= 2.8 nm CdSe nanocrystals as a function of initial excitonic state. The black squares are calculated from the A1 data in Fig 4.4b, taken early times while the initial excitonic pump state is maintained. The red squares are calculated for the maximum A1 values seen in panel c, after up-pumping of the hole via Auger relaxation to higher energy states deep in the valence band.

The modeled A1 and B1 regions of the TA spectrum are shown in figure 4.5a for a variety of biexciton binding energies using equation (4.4). With no biexciton binding energy, the TA spectrum will simply follow the contours of the linear absorption spectrum. As the binding energy is increased the bleach becomes suppressed, and eventually becomes an induced absorption whose magnitude and spectral width are dependent on the amount of shifting.

Figure 4.5b. distills the spectral data into the ratio of the A1/B1, where the features are measured at positions indicated by the arrows in 4.5a. For binding energies below 10 meV the ΔOD spectrum will remain negative in the A1 region. For higher values an induced absorption should be visible, with a magnitude that depends on the amount of binding energy. For Δ_{xx} = 20 meV there should be an induced absorption that is ~ 25% the magnitude of the B1 feature.

In figure 4.5c the A1 signals for when pumping into the P-type states 3 and 4 is shown. It can be seen that the biexciton binding energy changes dramatically, and hits a maximum at a time delay of a few hundred femtoseconds, when the electron has relaxed by the Auger mechanism discussed in the previously, pumping the hole very deep into the valence band. While we cannot assign any symmetry of the hole states at these time delays, we can calculate their binding energy.

The biexciton binding energy as a function of state is shown in figure 4.5d. It is clear the initial state has an effect on the biexciton binding energy, and some interesting trends are revealed. The early time data where state specificity is maintained shows clearly that the first excited state of the biexciton arising from state 2 in combination with a band edge exciton has a much larger binding energy than the band edge biexciton itself, indicating that having a hole in its excited state is energetically favorable when both electrons occupy conduction band edge state.

At early times while state specificity is maintained, the combination of either P type state with a band edge excitation still have slightly lower biexciton binding energies than the band edge biexciton, even though they both exhibit noticeable induced absorptions in the A1 region. This is due to the fact that the electrons populate the 1P state at early times, so B1 is quite small when compared to S type transitions at the same time delay. This means there are less state filling contributions for the level shifting induced absorption to overcome in the A1 region, lowering the biexciton binding energy necessary to cause induced absorptions. This data indicates that when the charge carriers all occupy different states the overall interactions are not very pronounced.

The red data points in figure 4.5d show the biexciton binding energy for the maximum of the A1 peak measured for pumping into the states 3 and 4 (~ 250 fs as shown in figure 4.5c), after the initial exciton has relaxed to a band edge electron and high energy hole state. When the holes have been up-pumped deep into the valence band the binding energy is larger, which seems to further indicate that the energy of hole state when the other carriers are at the band edge correlates with the biexciton binding energy of the complex. This is in agreement with theoretical work based off measurements using a sample of a mixed composition $CdS_{0.6}Se_{0.4}$ nanocrystals in a glass matrix[21].

The theoretical calculation of the biexciton binding energies is quite difficult because it depends on many factors. To begin with the charge carrier wavefunctions should be well described, which was shown to be challenging in the first part of this chapter. To accurately calculate the Coulombic attractions and repulsions of the different carriers[9, 60] requires accurate inputs for the size dependence of the dielectric constant of the dot[61] and the dielectric environment created by the ligands[23]. Exchange interactions are enhanced in strongly confined systems[4, 62], and correlation factors have been predicted to contribute significantly[3]. It would be hoped that our measurements can provide a structure in which to begin a more thorough theoretical investigation of the multiexciton complexes that may shed light on these issues.

Section 4.4 Conclusions

This chapter aimed to show how state selective ultrafast spectroscopic methods can be used to investigate the electronic structure of the single exciton and biexciton states. While the energy levels of the single exciton states have been measured in great detail, these measurements do not describe the quantum mechanical nature of the transitions. Using our techniques, we show which types of states are coupled for the four lowest energy transitions.

Our results confirm the symmetry assignments of the DDM method, in which higher energy excitons have P type symmetry. This confirmation suggests that experimental investigations of other predictions unique to the DDM approach are warranted. While more widely used in interpreting the experimental literature, the EMA method does not correctly predict exciton symmetry in CdSe of states well above the band gap. While the EMA approach has greatly advanced the design of many experiments, these results suggest limitations which are relevant to the interpretation of nonlinear optical experiments on quantum dots[24, 63-65].

In contrast to the single exciton states, there have not been any measurements of the spectrum the biexciton in high quality colloidal nanocrystals. We have measured the biexciton binding energies of each of the 4 lowest energy states in the linear absorption spectrum with the band edge exciton. They were shown to be sensitive to the state of each charge carrier, with the general trend of having the highest binding energies for complexes in which the electrons both occupy the lowest energy conduction band state, and one of the holes is energetically hot. This provides an experimental benchmark for theoretical studies of multiexcitons in nanoscale systems.

References.

[1] M. Achermann, J. A. Hollingsworth, and V. I. Klimov, Phys. Rev. B **68**, 245302/1 (2003).

[2] A. L. Efros and M. Rosen, Annu. Rev. Mater. Sci. **30**, 475 (2000).

[3] J. Shumway, A. Franceschetti, and A. Zunger, Phys. Rev. B **63**, 155316/1 (2001).

[4] A. L. Efros, M. Rosen, M. Kuno, M. Nirmal, D. J. Norris, and M. Bawendi, Phys. Rev. B **54**, 4843 (1996).

[5] V. I. Klimov, Annu. Rev. Phys. Chem. **58**, 635 (2007).

[6] A. J. Nozik, Inorganic Chemistry **44**, 6893 (2005).

[7] V. I. Klimov, S. A. Ivanov, J. Nanda, M. Achermann, I. Bezel, J. A. McGuire, and A. Piryatinski, Nature **447**, 441 (2007).

[8] Y. Cui, U. Banin, M. T. Bjoerk, and A. P. Alivisatos, Nano Lett. **5**, 1519 (2005).

[9] L.-W. Wang and A. Zunger, Phys. Rev. B: Condens. Matter FIELD Full Journal Title:Physical Review B: Condensed Matter **53**, 9579 (1996).

[10] L.-W. Wang and A. Zunger, J. Phys. Chem. B **102**, 6449 (1998).

[11] D. J. Norris and M. G. Bawendi, Phys. Rev. B **53**, 16338 (1996).

[12] L. E. Brus, J. Chem. Phys. **80**, 4403 (1984).

[13] R. R. Cooney, S. L. Sewall, E. A. Dias, D. M. Sagar, K. E. H. Anderson, and P. Kambhampati, Phys. Rev. B **75**, 245311 (2007).

[14] R. R. Cooney, S. L. Sewall, D. M. Sagar, and P. Kambhampati, Phys. Rev. Lett. **102**, 127404 (2009).

[15] D. M. Sagar, R. R. Cooney, S. L. Sewall, E. A. Dias, M. M. Barsan, I. S. Butler, and P. Kambhampati, Phys. Rev. B **77**, 235321 (2008).

[16] S. L. Sewall, R. R. Cooney, K. E. H. Anderson, E. A. Dias, and P. Kambhampati, Phys. Rev. B **74**, 235328 (2006).

[17] S. L. Sewall, R. R. Cooney, K. E. H. Anderson, E. A. Dias, D. M. Sagar, and P. Kambhampati, J. Chem. Phys. **129**, 084701/1 (2008).

[18] V. Klimov, S. Hunsche, and H. Kurz, Phys. Rev. B **50**, 8110 (1994).

[19] C. Bonati, M. B. Mohamed, D. Tonti, G. Zgrablic, S. Haacke, F. van Mourik, and M. Chergui, Phys. Rev. B **71**, 205317/1 (2005).

[20] B. Fisher, J.-M. Caruge, Y.-T. Chan, J. Halpert, and M. G. Bawendi, Chem. Phys. **318**, 71 (2005).

[21] Y.-N. Hwang, K.-C. Je, D. Kim, and S.-H. Park, Phys. Rev. B **64**, 041305/1 (2001).

[22] U. Woggon, H. Giessen, F. Gindele, O. Wind, B. Fluegel, and N. Peyghambarian, Phys. Rev. B **54**, 17681 (1996).

[23] T. Takagahara, Phys. Rev. B **39**, 24 (1989).

[24] E. Hendry, M. Koeberg, F. Wang, H. Zhang, C. de Mello Donega, D. Vanmaekelbergh, and M. Bonn, Phys. Rev. Lett. **96**, 057408/1 (2006).

[25] R. R. Cooney, S. L. Sewall, K. E. H. Anderson, E. A. Dias, and P. Kambhampati, Phys. Rev. Lett. **98**, 177403 (2007).

[26] P. Guyot-Sionnest, B. Wehrenberg, and D. Yu, J. Chem. Phys. **123**, 074709/1 (2005).

[27] J. M. Harbold, H. Du, T. D. Krauss, K.-S. Cho, C. B. Murray, and F. W. Wise, Phys. Rev. B **72**, 195312/1 (2005).

[28] V. Klimov, A. Mikhailovsky, S. Xu, A. Malko, C. Leatherdale, and M. Bawendi, Trends in Optics and Photonics **46**, 140 (2000).

[29] R. D. Schaller and V. I. Klimov, Phys. Rev. Lett. **96**, 097402/1 (2006).

[30] R. J. Ellingson, M. C. Beard, J. C. Johnson, P. Yu, O. I. Micic, A. J. Nozik, A. Shabaev, and A. L. Efros, Nano Lett. **5**, 865 (2005).

[31] J. M. Luther, M. C. Beard, Q. Song, M. Law, R. J. Ellingson, and A. J. Nozik, Nano Lett. FIELD Full Journal Title:Nano Letters **7**, 1779 (2007).

[32] S. A. Ivanov, J. Nanda, A. Piryatinski, M. Achermann, L. P. Balet, I. V. Bezel, P. O. Anikeeva, S. Tretiak, and V. I. Klimov, J. Phys. Chem. B **108**, 10625 (2004).

[33] S. A. Ivanov, A. Piryatinski, J. Nanda, S. Tretiak, K. R. Zavadil, W. O. Wallace, D. Werder, and V. I. Klimov, J. Am. Chem. Soc. FIELD Full Journal Title:Journal of the American Chemical Society **129**, 11708 (2007).

[34] V. I. Klimov, Optical Engineering (New York, NY, United States) **87**, 159 (2004).

[35] A. V. Malko, A. A. Mikhailovsky, M. A. Petruska, J. A. Hollingsworth, and V. I. Klimov, J. Phys. Chem. B **108**, 5250 (2004).

[36] N. Akopian, N. H. Lindner, E. Poem, Y. Berlatzky, J. Avron, D. Gershoni, B. D. Gerardot, and P. M. Petroff, Phys. Rev. Lett. **96**, 130501/1 (2006).

[37] M. Bayer, et al., Advances in Solid State Physics **44**, 191 (2004).

[38] E. Biolatti, I. D'Amico, P. Zanardi, and F. Rossi, Phys. Rev. B **65**, 075306/1 (2002).

[39] G. Chen, T. H. Stievater, E. T. Batteh, X. Li, D. G. Steel, D. Gammon, D. S. Katzer, D. Park, and L. J. Sham, Phys. Rev. Lett. **88**, 117901/1 (2002).

[40] R. M. Stevenson, R. J. Young, P. Atkinson, K. Cooper, D. A. Ritchie, and A. J. Shields, Nature **439**, 179 (2006).

[41] B. Fisher, J. M. Caruge, D. Zehnder, and M. Bawendi, Phys. Rev. Lett. **94**, 087403/1 (2005).

[42] A. Malko, M. H. Baier, E. Pelucchi, D. Chek-al-kar, D. Y. Oberli, and E. Kapon, Physica E: Low-Dimensional Systems & Nanostructures (Amsterdam, Netherlands) **26**, 194 (2005).

[43] W. W. Yu, L. Qu, W. Guo, and X. Peng, Chem. Mater. **15**, 2854 (2003).

[44] A. Franceschetti and A. Zunger, Phys. Rev. Lett. **78**, 915 (1997).

[45] D. E. Gomez, M. Califano, and P. Mulvaney, Phys. Chem. Chem. Phys. **8**, 4989 (2006).

[46] A. Zunger, Physica Status Solidi A: Applied Research **190**, 467 (2002).

[47] H. Fu, L.-W. Wang, and A. Zunger, Appl. Phys. Lett. **71**, 3433 (1997).

[48] A. L. Efros and M. Rosen, Appl. Phys. Lett. **73**, 1155 (1998).

[49] L. W. Wang, A. J. Williamson, A. Zunger, H. Jiang, and J. Singh, Appl. Phys. Lett. **76**, 339 (2000).

[50] H. Fu, L.-W. Wang, and A. Zunger, Appl. Phys. Lett. **73**, 1157 (1998).

[51] V. I. Klimov, J. Phys. Chem. B **104**, 6112 (2000).

[52] A. Franceschetti and Y. Zhang, Phys. Rev. Lett. **100**, 136805 (2008).

[53] U. Woggon, Springer Series in Solid-State Sciences **146**, 107 (2004).
[54] K. I. Kang, A. D. Kepner, S. V. Gaponenko, S. W. Koch, Y. Z. Hu, and N. Peyghambarian, Phys. Rev. B **48**, 15449 (1993).
[55] A. E. Colonna, X. Yang, and G. D. Scholes, Physica Status Solidi B: Basic Solid State Physics **242**, 990 (2005).
[56] S. W. Koch, Y. Z. Hu, B. Fluegel, and N. Peyghambarian, Institute of Physics Conference Series **123**, 139 (1992).
[57] U. Hohenester, F. Rossi, and E. Molinari, Physica B: Condensed Matter (Amsterdam) **272**, 1 (1999).
[58] V. I. Klimov and D. W. McBranch, Phys. Rev. Lett. **80**, 4028 (1998).
[59] P. Guyot-Sionnest, M. Shim, C. Matranga, and M. Hines, Phys. Rev. B **60**, R2181 (1999).
[60] A. Franceschetti and A. Zunger, Phys. Rev. B **62**, R16287 (2000).
[61] A. Franceschetti, H. Fu, L. W. Wang, and A. Zunger, Phys. Rev. B **60**, 1819 (1999).
[62] A. Franceschetti, L. W. Wang, H. Fu, and A. Zunger, Phys. Rev. B **58**, R13367 (1998).
[63] R. D. Schaller, V. M. Agranovich, and V. I. Klimov, Nature Physics **1**, 189 (2005).
[64] S. Xu, A. A. Mikhailovsky, J. A. Hollingsworth, and V. I. Klimov, Phys. Rev. B **65**, 045319/1 (2002).
[65] C. Y. Wong, J. Kim, P. S. Nair, M. C. Nagy, and G. D. Scholes, J. Phys. Chem. C **113**, 675 (2009).

Chapter 5:
State-resolved studies of biexcitons and surface trapping dynamics in CdSe nanocrystals

*This chapter contains text and figures from a previously published paper, J. Chem. Phys., **2008**. 129 (084701) © 2008 American Institute of Physics. It is co-authored by Ryan R. Cooney, Kevin E. H. Anderson, Eva A. Dias, D.M. Sagar and Patanjali Kambhampati. The text was rewritten by the author with changes to reflect the content of this thesis.*

Biexcitons can be created with state specific pumping schemes, as described in the previous two chapters. We have previously examined the band edge biexciton and the first few excited states of the biexciton, but only in one size of quantum dot. We now focus our attention on how biexcitonic interactions vary with nanocrystal radius. The following chapter focuses on the properties of the band edge biexciton, while this chapter explores excited state biexcitons as a function of size.

The first excited state of the biexciton, comprised of charge carriers in the $1S_e$-$2S_{3/2}$ and $1S_e$-$1S_{3/2}$ states created by sequential absorption of photons in the pump/probe experiment, was chosen for these measurements because the only excited charge carrier is a hole which populates the $2S_{3/2}$ state ~50-150 meV below the valence band edge[1-3]. Using higher excited states would have involved excited electrons also, which decay via the Auger mechanism and would up-pump the hole more deeply into the valence band[4-6]. This would occur on timescales which would be dependent of the radius of the dot, and would make it difficult to have true state specificity for the measurements across all sizes of nanocrystal.

If the initially created exciton is allowed to relax to a surface trapped state, a mixed phase biexciton is created. The surfaces of nanocrystals are of great importance, but the states which arise from surface reconstruction and ligand passivation and how they affect the properties of the particle are poorly understood[7-10]. We show that surface trapping occurs in ligand passivated nanocrystals, and furthermore that there is enhanced rate for this process for higher excited states. We confirm prior assignment[5, 11-14] that it is primarily the hole which gets trapped on the picosecond timescale. This finding should be considered when discussing the time evolution of the biexcitonic states and exciton relaxation dynamics.

5.1 Biexcitons in Nanocrystals

It has been shown how semiconductor nanocrystals are promising new materials since they offer tunability of their electronic structure, and consequently their optical properties, by varying the geometry of the particle itself. The different descriptions of the core electronic states in these nanocrystals can somewhat be understood by applying the nearly spherical boundary conditions imposed by the size of the crystal upon the charge carriers, which results in envelope functions similar to those which arise in hydrogenic systems- it is these states which are resolvable in the linear absorption spectrum of a sample.[1, 15-18] It is also of great interest that multiple excitations can be contained inside one particle, where many charge carriers can be forced to interact by confinement[11, 18-33]. Bulk systems have a maximum density of excitons[23], so these higher order charge complexes and their effects on the properties of nanocrystals are relatively novel aspect of quantum confined systems.

We have examined the biexciton in some detail in the previous chapters, specifically sections 1.3, 3.4 and 4.3. In the bulk it can be weakly bound, and we showed in Chapter 4 that its binding energy is enhanced in nanocrystals because of the increased spatial overlap of the carrier wavefunctions[18, 25]. Prior works looked at the size dependence of the biexcitonic binding energy, both of the ground state and excited states, as well as measurements of the lifetime of the ground state biexciton[3, 11, 18, 20-22, 24-28, 34, 35]. It has also been shown how sensitive the biexciton binding energy is to state of the charge carriers in the previous chapter, so a large shortcoming of previous reports is a lack state specificity when examining excited state biexcitons in different sizes of dots, due to the use of fixed UV pumping.

The measurement of the size dependence of the biexciton binding energy with state selective control is an important benchmark for understanding many-body physics inside quantum confined systems. Understanding multiexcitons in semiconductor nanocrystal is important for many of their proposed applications, including single photon sources and quantum cryptography,[36-38] multiple exciton generation,[39-42] and quantum dot based gain media.[29-31, 43-47]

5.2 The Size Dependence of Biexciton Binding Energies

The measurements were made using the setup described in Chapter 2. The data focuses on a series of measurement taken with OPAs tuned to be resonant with the band edge transition, ($1S_e$-$1S_{3/2}$) and the first excited state ($1S_e$-$2S_{3/2}$) in each size of nanocrystal. The samples of the CdSe nanocrystals were synthesized using the techniques established by Peng et al[48], or purchased from NN Labs.

Bound states of biexcitons in quantum confined systems have been under investigation since their existence was predicted and measured in the 1990s[21, 22, 24, 25, 49]. The most easily resolved biexcitonic state in nanocrystals is the ground state, due to its relatively long lifetime[26]. Its binding energy has been measured in several different time resolved photoluminescence (PL) experiments[18, 23, 31, 32]. In these experiments a shoulder on the red edge of the PL can be assigned to the emission from the band edge biexciton, shifted by a binding energy of 10-40 meV, depending on the size of particle. Excited states of the biexciton have not been well studied, their short (<100 fs) lifetimes does not allow for measurable amounts of PL emission.

Beyond the band edge biexciton, the biexciton complexes have a spectrum consisting of the variety of two-body excitonic states which can comprise a four-body state. The biexciton spectrum will be distinct from the single exciton transition energies because of the level shifting characterized by the biexciton binding energy, as shown in section 4.3 of the previous chapter. Prior theory and experiments have discussed these excited biexcitons states[20-22, 50, 51]. Signals in the TA experiments of the prior literature reports have been assigned to excited biexciton states, but without spectral control of *both* the pump and probe pulses it is very difficult to cleanly probe these states due to the complications caused by spectral overlap from bleaching signals and overlapping of different transitions.

Our method achieves state selectivity by tuning our pump pulse to be resonant with the resolvable transitions, and probing in the appropriate spectral region. For the first excited state of the biexciton, we create a $1S_e$-$2S_{3/2}$ exciton with pump pulse tuned to the correct transition energy, and then monitor the region sub-resonant of the band edge with our probe pulse, detecting changes in absorption in the area caused by redshifting of the band edge transition when forming a $|1S_e$-$2S_{3/2}$; $1S_e$-$1S_{3/2}>$ biexciton. The only interfering signals are due the small amount of state filling of the band edge transition. The data can be analyzed at the earliest time delays (~50 fs) before extensive excitonic relaxation has occurred.

This is important because the state selectivity is quickly diminished due to relaxation processes, which occur on a variety of timescales in nanocrystals[3, 6, 11, 52, 53]. While the ground state biexciton has a lifetime of 10-100 ps[11, 26], the lifetime of the excited states is limited by the transition rates of the electrons and holes during relaxation between states[3, 6, 11, 52, 53] (100-500 fs). Accurate measurements of biexciton binding energy of these states must therefore have a better time resolution than the lifetime of the excited states of the biexciton.

5.2.1 Transient Data and Binding Energies

In figure 5.1, we show the A1 transients for the ground state and 1S-2$S_{3/2}$ pumps on the femtosecond timescale. The signals therefore correspond to the ground state and first excited state of the biexciton. These biexcitonic signals evolve over a broad range timescales from 50 fs to 100 ps. Experiments without femtosecond time resolution therefore contain some ambiguity in exactly which specific biexciton states are being probed. PL experiments with fs resolution can measure the binding energy of the ground state biexciton[18, 23, 31, 32], but excited states of the biexciton require both ultrafast time resolution and state selectivity in the initial excitonic state. The drawbacks of time resolved PL methods are discussed in the Chapter 6.

The transient data shows an obvious state dependence. While the band edge $|1S_e\text{-}1S_{3/2}; 1S_e\text{-}1S_{3/2}>$ biexciton transient has an instrument response function (IRF) limited bleach, the first excited state $|1S_e\text{-}2S_{3/2}; 1S_e\text{-}1S_{3/2}>$ data shows an IRF limited induced absorption. The magnitude of the signal in the A1 region will be proportional to the extent of level shifting upon formation of the biexciton[18], which means that the ground state biexciton has a lower binding energy than the excited state biexciton. The data for different sizes shows clearly that the excited state biexciton is bound more strongly in the smaller nanocrystals, meaning it is enhanced by forced overlap of charge carrier wavefunctions.

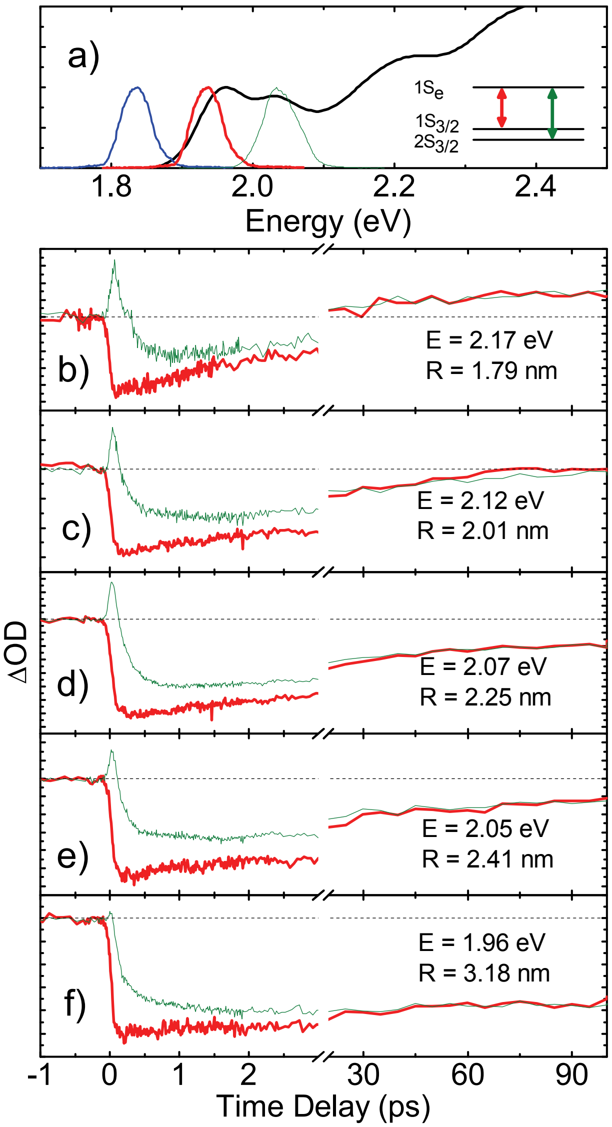

Figure 5.1. Spectra (a) and pump/probe transients (b-f) for the A1 spectral feature for five sizes of CdSe quantum dot. Panel a) shows the absorption spectrum and laser spectra used for one size of quantum dot to illustrate the experimental conditions. The sub-resonant (blue line) spectrum is the probe pulse. The two resonant spectra are the pump pulses. The colors of the pump/probe transients (b-f) correspond to the pump spectra in a). The energy of the band edge exciton $|1S_e\text{-}1S_{3/2}>$, and the quantum dot radius is denoted in each panel. The dashed line represents the zero level.

Previous methods explored in the section 4.3 of the last chapter the biexciton binding energy by defining the magnitude of ΔOD in the A1 region as a function of binding energy[13, 18, 49]. In the absence of biexciton level shifting, the A1 region would consist of small bleach proportional to the magnitude of the bleaching caused by state filling, and its contours would follow the linear absorption spectrum. As the binding energy is increased, the bleaching signal in the A1 region will be attenuated by increased absorption by excited nanocrystals, becoming a positive going induced absorption when the biexciton binding energy is large enough. The magnitude of the induce absorption is dependent on how far the spectrum of excited nanocrystals is shifted- the biexciton binding energy.

By modeling the ESA term as the linear absorption spectrum shifted by the biexciton binding energy, we showed in section 4.3 how the induced absorption signals (A1) grow in as a function of biexciton binding energy using the equation which will be restated here,

$$\Delta\mathrm{OD}(\omega) = -2\sigma_{0-1}(\omega)\times \mathrm{N}_1 + \sigma^{*}_{0-1}(\omega-\Delta_{\mathrm{XX}})\times \mathrm{N}_1 . \qquad (5.1)$$

The biexciton binding energy shifts the absorption spectrum. As Δ_{XX} increases, the signals change from negative to positive when the level shifting has a larger effect than state filling.

Figure 5.2 shows the extracted shifting and binding energies. The top panel illustrates the method. The magnitude of ΔOD in the absence of biexciton formation is set by the linear absorption spectrum and amount of state filling (proportional to B1), shown by the grey line in the top panel. Also shown is a transient when pumping into the first excited state, with the offset (δ) between the experimentally measured signal and the unshifted value measured for two different time delays. The time delay of 50 fs corresponds to the biexciton comprised of the 2 different excitations populating levels made up of excitons in the interior of the nanocrystal. At the time delay of 100 ps, relaxation into some kind of surface trapping state has occurred (discussed further in the next section of this chapter), so the level shifting is caused by formation of a mixed phase biexciton with charges in both interior and surface trapped states.

In 5.2b we show the offsets of the two types of excitons as a function of size. Using these offsets we extract the biexciton binding energy by shifting the linear absorption spectrum of the excited nanocrystals until the calculated A1 signal matches the measured values. The binding energies are plotted in the figure 4c. Neither the first excited state nor the mixed phase biexciton binding energies follow a strictly Coulombic 1/R functional form, indicating size dependent effects such as exchange factors strongly affect multiexcitonic complex stability[18, 23, 51]. Nonetheless, it is clear that the size dependence of binding energies for biexciton states other than the ground state biexciton can be measured.

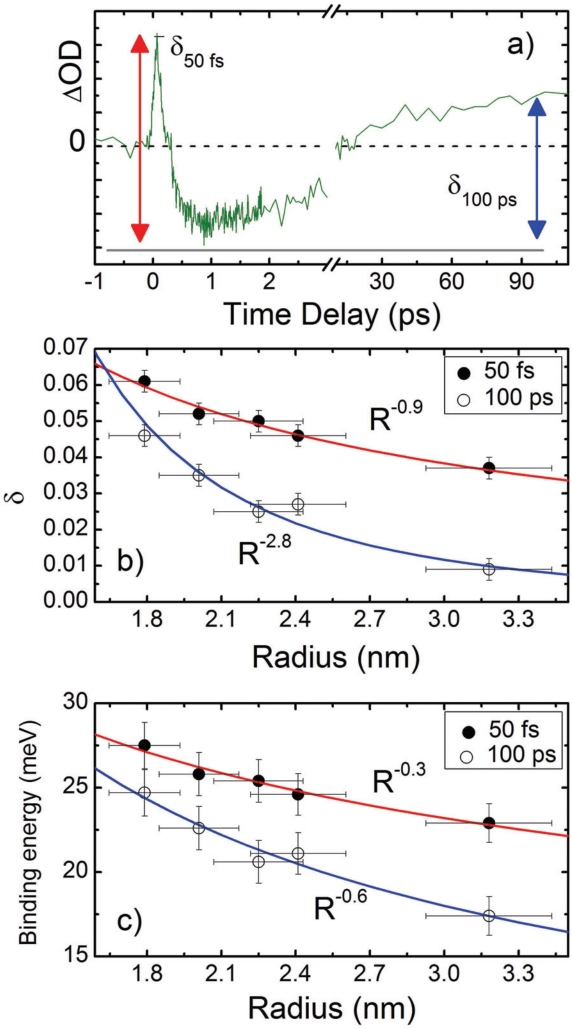

Figure 5.2 Size dependent biexciton interactions. Panel a) illustrates the experimentally determined ΔOD offsets (δ) in the A1 signal which are used to extract the biexciton binding energies. The grey line corresponds to the ΔOD with zero biexciton binding energy. The δ's reflect redshifting of the levels due to bound biexcitons. The size dependence of the experimental offsets is shown in b). Panel c) shows the extracted binding energies. Details of the analysis and the A1 spectral feature are described in the text. At early time (50 fs) the biexciton corresponds to the first excited state of the pure core biexciton, $|1S_e\text{-}2S_{3/2}; 1S_e\text{-}1S_{3/2}>$. At late time (100 ps) the biexciton corresponds to a mixed phase biexciton, $|\text{surface}; 1S_e\text{-}1S_{3/2}>$. The lines are power law fits as described in the text.

Our reported values for the specific biexcitons are consistent in magnitude with previous literature measurements of the ground state biexciton using time resolved PL[18, 23, 31, 32]. This is quite troublesome at first glance, as it was expected that there would be some state dependence for binding energies[18, 20, 54], and we showed in the previous chapter this true. Further investigation revealed the discrepancies arise due to splitting of the band edge biexciton into different levels, in an analogous manner to the fine structure of the single exciton described in section 1.2.4 of the introduction. This will be discussed further in the next chapter of this thesis.

5.2.2 Mixed surface-core biexcitons

According to the comprehensive studies of exciton dynamics in nanocrystals, intraband relaxation processes which occur in standard ligand passivated nanocrystals are on the ultrafast timescale[6, 11]. Provided both the electron and hole are photo-excited into the states above the band edge, the electron relaxes in a ~300 fs via an Auger process in which it transfers its excess energy to the hole and up-pumps it deeper into the valence band[6]. The hole then relaxes to the band edge by ~1 ps by coupling to a combination of vibrational modes of the ligands and crystal lattice[6, 52]. Both charge carriers will then reach the band edge very quickly, and any subsequent dynamics are related to either recombination[11, 26] or trapping of carriers into localized states related to nanocrystal surface[14, 53, 55-57].

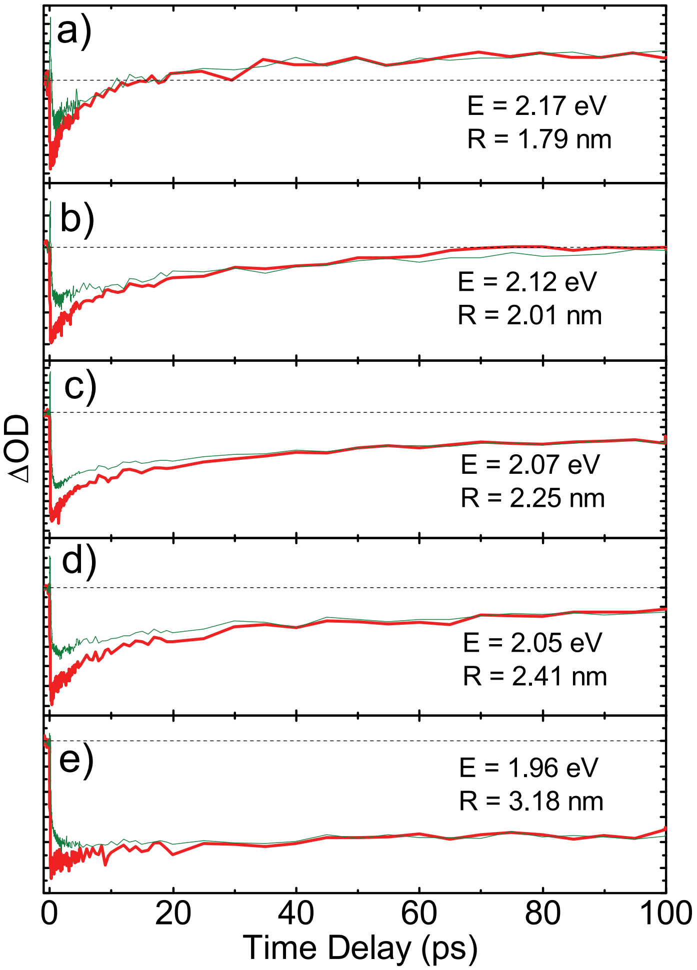

Figure 5.3. Long timescale pump/probe transients (a-e) for the A1 spectral feature for the five sizes of CdSe nanocrystals displayed if figure 5.1. The energy of the band edge exciton |$1S_e$-$1S_{3/2}$>, and the quantum dot radius is denoted in each panel. The dashed line represents the zero level. The smaller sizes show more prominent dynamics on this timescale, showing significant changes in the magnitude of ΔOD is the A1 region as a function of time over the first 50 ps.

The dynamics in figure 5.3 follow exciton relaxation. In all sizes of nanocrystal the A1 becomes negative within one ps. The signal the evolves on the 10-100 ps timescale, the dynamics of these changes are strongly size dependent. Previous literature reports suggest that dynamics on this timescale correspond to trapping processes of charge carriers into surface states[3, 11, 53]. This is consistent with the observed rates of intraband relaxation and carrier recombination[3, 6, 11, 52, 53].

It is clear in figure 5.3 that the signal at 100 ps is independent of the initial excitonic state, both band edge and first excited pump end up with identical final states. It is also quite obvious that the magnitude of the offset at 100 ps is strongly size dependent. This is consistent with the surface trapping process, and these measurements allow us to measure characteristics of biexcitons involving interior and surface trapped charges. The binding energies of these complexes are higher than the binding energy of the ground state biexciton, but lower than the first excited state biexciton. The binding energy has slightly stronger size dependence for the mixed phase biexciton than the first excited state biexciton, but still has contributions from non Coulombic interactions.

5.3. Surface trapping processes

5.3.1 Ground state trapping rate

Since charge carriers relax to the band edge by approximately 1 ps, further dynamics must correspond to processes which transfer population out of the intrinsic band edge states, either through recombination or migration into trap states[11, 14, 53]. In figure 5.3, the A1 signal can be seen to decay on the 100 ps timescale into some a long lived state- even when pumped directly into the band edge state (red traces). The dynamics of relaxation and the stability of this state indicate there is some kind trapping of the band edge exciton, most likely charge migration into a state associated with the surface atoms on the nanocrystal[7, 12, 58, 59].

This assignment is supported by considering the surface trapping rate obtained from the dynamics in figure 5.3 as a function of nanocrystal radius, which is plotted in figure 5.4. This rate follows an $R^{-1.5}$ size dependence. A simple model of the charge carrier wavefunctions developed to examine size dependent trends of radial charge density shows that the fraction of charge density at the surface of the nanocrystal has exactly the same trend[6, 52]. By excitation directly into the band edge, the dynamics of this process are more revealed in the A1 feature. Surface trapping processes are important for understanding recombination mechanisms and the types of mixed phase multiexcitonic complexes which may be formed[60, 61] and how they may effect technological applications[62, 63].

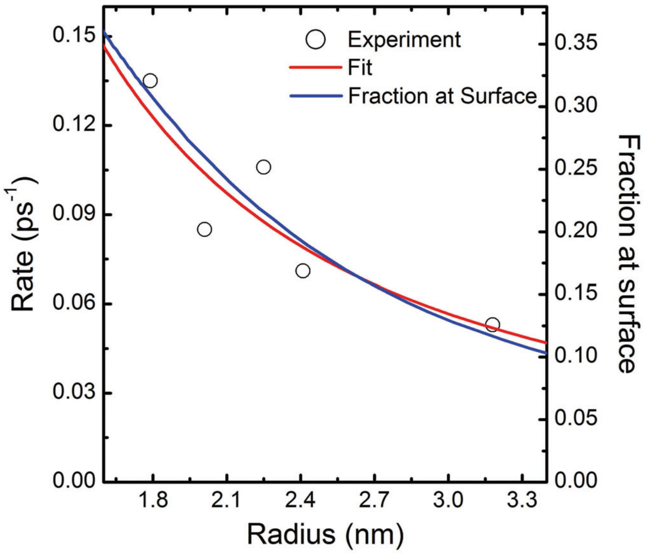

Figure 5.4 Surface trapping rate for the band edge exciton. The trapping rate follows an $R^{-1.5}$ functional form, as does the fraction of the 1S envelope function at the surface including tunneling.

5.3.2 Excited state trapping rate

Band edge pumping gives a straightforward picture of charge migration to trap states from the metastable band edge state[3], and excited state pumps are able to yield similar information since this process occurs after relaxation to the band edge[11, 53]. To examine trapping rates from excited states is more difficult due the sub-picosecond lifetime of the charge carriers in the states above the band edge. For a complete understanding of processes following photoexcitation, it should be assessed if excited state trapping can occur on a sufficiently fast timescale to compete with intraband relaxation of electrons or holes within the intrinsic core states.

Recall from Figure 3.6, it was shown in the A1 signal generated from pumping into different states that the transients evolve on a variety of timescales which depend upon the initial pump state. Similar behavior is seen in figure 5.3, where it is clear that the A1 signals when pumping into the two states do not meet up until some 20-50 ps after excitation, well after the hole intraband relaxation process is complete. In figure 5.5 we plot ΔΔOD, the subtraction of the two transients, (1S- 2S) for the R=1.8 nm nanocrystal (this method was described in section 3.3.3 in relation to intraband relaxation dynamics).

If exciton relaxation occurred in a completely sequential manner, then the transients should be identical following hole relaxation, thus the ΔΔOD signal would go to zero by ~1 ps. The data in figure 5.5 requires nearly 20 ps for the transients from the different states to meet. This data can be reproduced by allowing for excited states to trap directly, thus providing a second relaxation avenue which competes with intraband relaxation as illustrated in the figure inset.

A simple kinetic model in the hot hole first relaxes to the band edge state and is then trapped at the surface would predict an A1 ΔΔOD transient which would go to zero by 300 fs, and be easily fit using a single exponential that would correspond to intraband relaxation. This clearly does not agree with the data shown in figure 5.5. The excited state wavefunctions have larger charge densities near the surface of the nanocrystals[6], which would be expected to increase the surface trapping rate. It is possible to include trapping in a kinetic model which completely reproduces the observed kinetics of ΔΔOD.

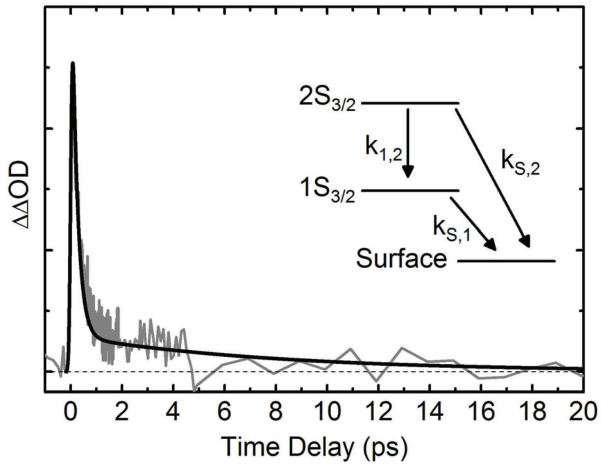

Figure 5.5 The difference between the ΔOD transients in Figure 5.1(b), ΔΔOD. The grey line is the experimental data and the black line is the model. The biexponential character of the ΔΔOD transient is due to the presence of two processes for the hot hole: relaxation ($k_{1,2}$) and excited state trapping ($k_{S,2}$) from the initial $2S_{3/2}$ state, where $k_{f,i}$ corresponds to the state-to-state transition rate. $k_{1,2}$ and $k_{S,1}$ were experimentally determined from fits to the raw data, whereas k_{S2} was obtained by varying this parameter in the kinetic model. The transition rates, $k_{f,i}$, are: $k_{1,2} = 4.0\ \text{ps}^{-1}$, $k_{S,1} = 0.125\ \text{ps}^{-1}$, $k_{S,2} = 0.65\ \text{ps}^{-1}$.

When exciting the band edge state, the ΔOD transient over time can be described in terms of the signal magnitude of the different states and the population between them. Under conditions of band edge pumping ($1S_e$-$1S_{3/2}$):

$$\Delta OD(t) = \left(A_{1S}P_{1S}(t) + A_{surface}P_{surface}(t)\right) \otimes IRF \tag{5.2}$$

Similarly, by including the excited state, then with 1Se-$2S_{3/2}$ pumping ΔOD can be described.

$$\Delta OD(t) = (A_{2S}P_{2S}(t) + A_{1S}P_{1S}(t) + A_{surface}P_{surface}(t)) \otimes IRF\,. \tag{5.3}$$

Here, 1S and 2S refer to the $1S_e$-$1S_{3/2}$ and $1S_e$-$2S_{3/2}$ excitons, described by the different hole state of the two pumps. The A values represent the experimentally determined amplitudes of the ΔOD for the A1 spectral feature at either 50 fs (core states) or 100 ps (surface states). The P values are the populations of each state, which are obviously functions of time.

These populations can be determined using a simple set of differential equations:

$$\frac{d}{dt}P_{2S} = -k_{1,2}P_{2S} - k_{S,2}P_{2S} \tag{5.4}$$

$$\frac{d}{dt}P_{1S} = -k_{S,1}P_{1S} + k_{1,2}P_{2S} \tag{5.5}$$

$$\frac{d}{dt}P_{Surface} = k_{S,1}P_{1S} + k_{S,2}P_{2S}\,. \tag{5.6}$$

The different k values correspond to the state-to-state transition rate, with the subscripts denoting the final and initial states, $k_{f,i}$. We determine $k_{S,1}$ experimentally from the A1 dynamics using band edge pump, shown in figure 5.3. The $k_{1,2}$ is the rate constant for intraband hole relaxation, determined from the femtosecond dynamic component which makes up the majority of the ΔΔOD transient[6, 52]. The minority picosecond component of ΔΔOD arises from the completion of the excited state trapping process, which occurs with a rate constant $k_{2,S}$ that can be varied to fit the experimental data.

This model (which is able to include the convolution with the instrument response function of the experimental apparatus) fits the ΔΔOD transient very accurately (gray line in figure 5.5). Since some of the excited state population is transferred directly to the surface without populating the band edge state, the A1 dynamics do meet up until later times for the two different pumps.

As seen in figure 5.2c the mixed phase biexciton has a larger binding energy than the band edge biexciton, so with excited state pumping the transient does not reach as negative a value of ΔOD as the band edge pump transient. This trend is exaggerated using higher energy pumps, as seen in figure 3.6. However, the A1 signal does reach the same final value regardless of which initial pump state is used, so the same total fraction of excitons become trapped at the surface in each case.

Similar biexponential signals have been observed in studies of dynamics in nanocrystals by Guyot-Sionnest[5] and Klimov[11, 12] which arose from re-excitation of electrons using IR pumps. These effects have also been seen for excitation of solvated electrons, where excited state detrapping processes could be measured[64]. In all these cases, the experimental signals were being affected by the removal of populations being probed so that they did not directly correspond to the excited state survival probability. Our state selective measurements have revealed that there is an enhancement of surface trapping rates when pumping into higher energy excited states, which can be quantified when the appropriate state-to-state transition rates are known. This should be taken into account in studies of exciton dynamics and optical gain[65-67].

5.3.3 Electron vs. hole trapping

There is not an inherent distinction in the A1 signal between electron and hole populations[11, 18, 21], as the signal is sensitive to the full eigenstate of the system. The trapping of either charge carrier would be expected to lead to a significantly altered charge distribution that could lead the measured signals. However, comparison with the band edge bleaching signal (B1) allows us to disentangle the dynamics of the two different charge carriers. As described in the previous two chapters, the B1 signal is sensitive only the electronic population of the lowest energy conduction band state. Its decay on the picosecond timescale will correspond to loss of electrons from this state[11, 53], whether by recombination or trapping.

In figure 5.6 we compare the A1 and B1 signals for four different sizes of quantum dots. It can be seen that the relative amplitude changes are size dependent, with smallest sizes showing the most prominent discrepancies. This is likely due to higher surface to volume ratio of the smaller crystals, exaggerating the effected of trapped charges.

It is very clear that in all cases the amplitude of the decay of B1 is much smaller than for A1. This implies that the electronic populations are relatively stable over this timescale, since the B1 monitors only state filling of the $1S_e$ level. This would mean that the majority of the surface trapping dynamics is due to holes. Prior works which examined nanocrystals using intraband transient absorption[11, 68] and photoluminescence[13] have also assigned trapping to primarily holes.

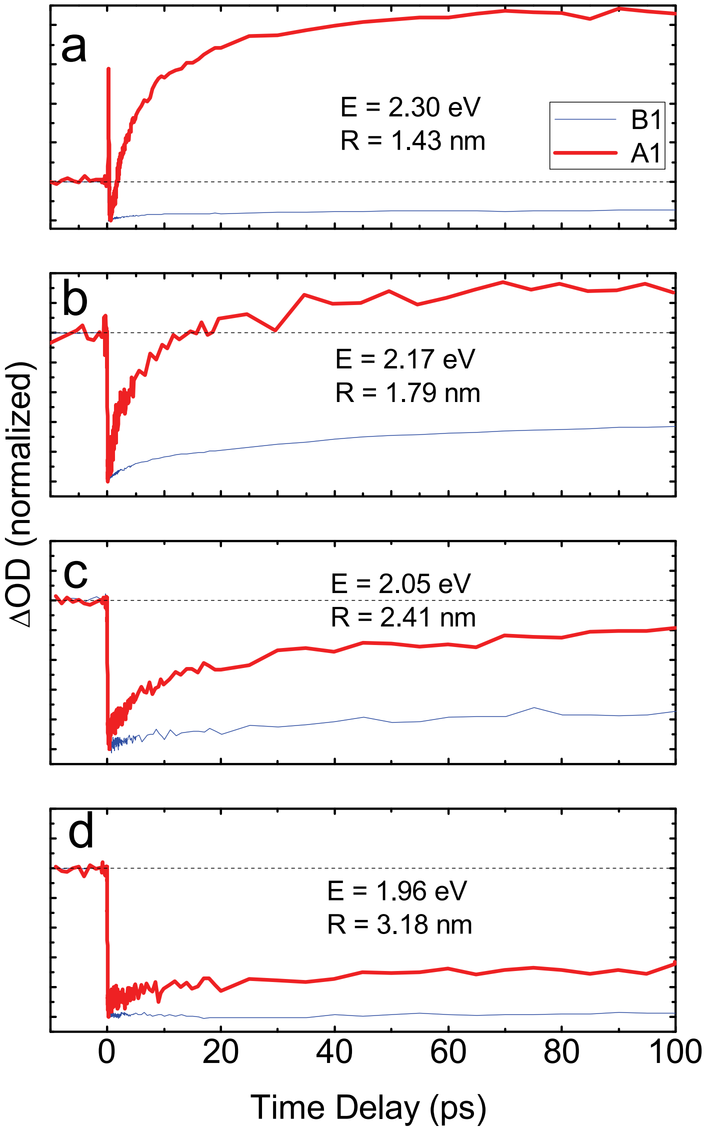

Figure 5.6 Decomposing electron and hole trapping at the surface by probing different spectral features. The B1 state-filling signal only monitors electron dynamics whereas the A1 biexciton signal arises from the charge distribution of the electrons and holes. The A1 signals decay with larger amplitude than the B1 signal, indicating a majority contribution from hole trapping dynamics. The signals are normalized for comparison of four sizes of CdSe quantum dots. In all cases, the offsets at 100 ps are larger for the smaller particles. The dashed line represents the zero level.

Passivation with a ZnS shell has been known to confine charges effectively to the interior of the nanocrystal[11, 53]. In figure 5.7 it can be seen that the overcoating of a nanocrystal with ZnS does not change the dynamics of the B1 signal, but does have a modest effect on the A1 transient. From the B1 data, we can conclude that the electron population dynamics are not altered by the ZnS shell, but it may change the hole trapping mechanism. It would be difficult to confidently make this assignment, as the charge distribution of the carriers which affects the amount of level shifting in biexciton formation[11, 18, 21, 25, 43, 54, 69] is likely different for core/shell systems. This would make it difficult to distinguish between fewer trapped charges at the surface, or changes to the charge distribution of the trap states available in core/shell systems.

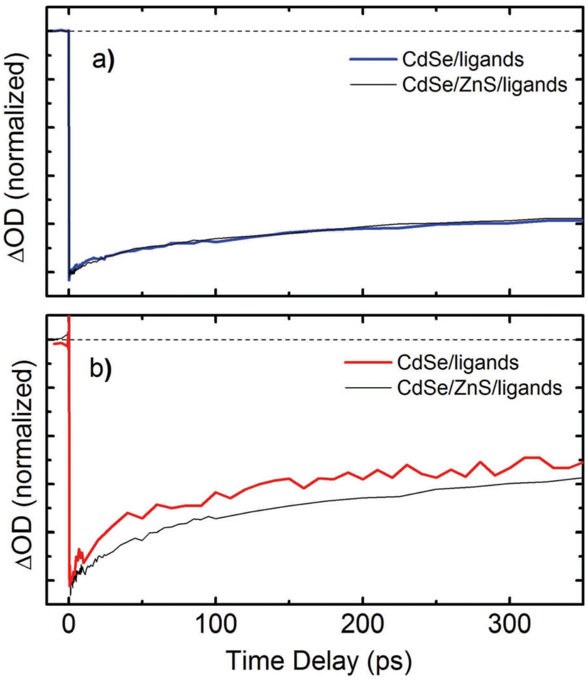

Figure 5.7. Comparison of the pump/probe transients for CdSe and CdSe/ZnS core/shell quantum dots. In both cases the band edge exciton was at 2.20 eV, with R = 2.80 nm. Panel a) monitors the B1 signal, reflecting only electron dynamics. Panel b) monitors the A1 signal, reflecting the charge distribution of the electron and hole. The dashed line represents the zero level. The ZnS Shell does not affect the electron dynamics but does affect the hole dynamics.

5.4 CONCLUSIONS

In this chapter, we report on measurements of the size dependence of excited states of the biexcitons. State selectivity must be maintained in order to accurately investigate the same state over a range of nanocrystals sizes. We are able to observe two different types of excited biexcitons: the first excited state of biexcitons in intrinsic core manifold of states ($|1S_e$-$2S_{3/2}$;$1S_e$-$1S_{3/2}>$) and a mixed phase biexciton where a hole has migrated into a surface trap state ($|1S_e$-

Surface;$1S_e$-$1S_{3/2}$>. Both of these show relatively large binding energies which increase dramatically as the size of nanocrystal is decreased.

Measurements of dynamics of formation for the mixed phase biexciton reveal that the rate of surface trapping is a size dependent *and* state dependent quantity. In particular, we show that with the higher energy excitonic states carrier trapping can compete very efficiently with intraband relaxation, while charge migration takes place on a much longer timescale for excitation directly into the band edge. Both of these processes occur more quickly in smaller nanocrystals where there is larger density of charge carrier wavefunctions at the surface. These effects are prominent over a broad range of timescales in A1 region, and will be important to consider when modeling carrier relaxation from excited states, biexciton interactions over the lifetime of an exciton, and depopulation mechanism in semiconductor nanocrystals.

REFERENCES:

[1] D. J. Norris and M. G. Bawendi, Physical Review B: Condensed Matter **53**, 16338 (1996).

[2] L.-W. Wang and A. Zunger, Journal of Physical Chemistry B **102**, 6449 (1998).

[3] S. L. Sewall, R. R. Cooney, K. E. H. Anderson, et al., Physical Review B: Condensed Matter and Materials Physics **74**, 235328 (2006).

[4] V. I. Klimov and D. W. McBranch, Physical Review Letters **80**, 4028 (1998).

[5] P. Guyot-Sionnest, M. Shim, C. Matranga, et al., Physical Review B: Condensed Matter and Materials Physics **60**, R2181 (1999).

[6] R. R. Cooney, S. L. Sewall, E. A. Dias, et al., Physical Review B (Condensed Matter and Materials Physics) **75**, 245311 (2007).

[7] M. Califano, A. Franceschetti, and A. Zunger, Nano Letters **5**, 2360 (2005).

[8] D. E. Gomez, M. Califano, and P. Mulvaney, Physical Chemistry Chemical Physics **8**, 4989 (2006).

[9] K. W. Leung, K.B, Journal of Chemical Physics **110**, 11 (1999).

[10] M. L. Huxter Vanessa, Anna Lo, Shun S Scholes, Gregory D., Nano Lett **9**, 4 (2008).

[11] V. I. Klimov, Journal of Physical Chemistry B **104**, 6112 (2000).

[12] V. I. Klimov, A. A. Mikhailovsky, D. W. McBranch, et al., Physical Review B: Condensed Matter and Materials Physics **61**, R13349 (2000).

[13] V. I. Klimov, *Semiconductor and Metal nanocrystals: Synthesis and Electronic and Optical Properties.* (Marcel Dekker, New York, 2004).

[14] C. Burda, S. Link, M. Mohamed, et al., Journal of Physical Chemistry B **105**, 12286 (2001).

[15] D. J. Norris, A. L. Efros, M. Rosen, et al., Physical Review B: Condensed Matter **53**, 16347 (1996).

[16] A. I. Ekimov, F. Hache, M. C. Schanne-Klein, et al., Journal of the Optical Society of America B: Optical Physics **10**, 100 (1993).

[17] A. L. Efros and M. Rosen, Annual Review of Materials Science **30**, 475 (2000).

[18] V. I. Klimov, Annual Review of Physical Chemistry **58**, 635 (2007).

[19] D. H. Son, J. S. Wittenberg, and A. P. Alivisatos, Physical Review Letters **92**, 127406/1 (2004).

[20] Y.-N. Hwang, K.-C. Je, D. Kim, et al., Physical Review B: Condensed Matter and Materials Physics **64**, 041305/1 (2001).

[21] Y. Z. Hu, S. W. Koch, M. Lindberg, et al., Physical Review Letters **64**, 1805 (1990).

[22] K. I. Kang, A. D. Kepner, S. V. Gaponenko, et al., Physical Review B: Condensed Matter and Materials Physics **48**, 15449 (1993).

[23] M. Achermann, J. A. Hollingsworth, and V. I. Klimov, Physical Review B: Condensed Matter and Materials Physics **68**, 245302/1 (2003).

[24] U. Woggon, H. Giessen, F. Gindele, et al., Physical Review B: Condensed Matter **54**, 17681 (1996).

[25] U. Woggon, Springer Series in Solid-State Sciences **146**, 107 (2004).

[26] V. I. Klimov, A. A. Mikhailovsky, D. W. McBranch, et al., Science **287**, 1011 (2000).

[27] C. Burda, S. Link, T. C. Green, et al., Journal of Physical Chemistry B **103**, 10775 (1999).

[28] P. Borri, W. Langbein, S. Schneider, et al., Physical Review Letters **89**, 187401/1 (2002).

[29] B. Fisher, J. M. Caruge, D. Zehnder, et al., Physical Review Letters **94**, 087403/1 (2005).

[30] B. Fisher, J.-M. Caruge, Y.-T. Chan, et al., Chemical Physics **318**, 71 (2005).

[31] J. M. Caruge, Y. Chan, V. Sundar, et al., Physical Review B: Condensed Matter and Materials Physics **70**, 085316/1 (2004).

[32] C. Bonati, M. B. Mohamed, D. Tonti, et al., Physical Review B: Condensed Matter and Materials Physics **71**, 205317/1 (2005).

[33] D. Oron, M. Kazes, I. Shweky, et al., Phys. Rev. B: Condens. Matter Mater. Phys. FIELD Full Journal Title:Physical Review B: Condensed Matter and Materials Physics **74**, 115333/1 (2006).

[34] F. Gindele, U. Woggon, W. Langbein, et al., Physical Review B: Condensed Matter and Materials Physics **60**, 8773 (1999).

[35] B. Patton, W. Langbein, and U. Woggon, Physical Review B: Condensed Matter and Materials Physics **68**, 125316/1 (2003).

[36] X. Xu, I. Toft, R. T. Phillips, et al., Applied Physics Letters **90**, 061103/1 (2007).

[37] X. Li, Y. Wu, D. Steel, et al., Science **301**, 809 (2003).

[38] R. M. Stevenson, R. J. Young, P. Atkinson, et al., Nature (London, United Kingdom) **439**, 179 (2006).

[39] R. D. Schaller, M. Sykora, S. Jeong, et al., Journal of Physical Chemistry B **110**, 25332 (2006).

[40] A. Shabaev, A. L. Efros, and A. J. Nozik, Nano Letters **6**, 2856 (2006).

[41] R. D. Schaller, V. M. Agranovich, and V. I. Klimov, Nature Physics **1**, 189 (2005).

[42] J. Ellingson Randy, C. Beard Matthew, C. Johnson Justin, et al., Nano letters **5**, 865 (2005).

[43] V. I. Klimov, S. A. Ivanov, J. Nanda, et al., Nature **447**, 441 (2007).

[44] S. Link and M. A. El-Sayed, Journal of Applied Physics **92**, 6799 (2002).

[45] G. Chen, R. Rapaport, D. T. Fuchs, et al., Applied Physics Letters **87**, 251108/1 (2005).

[46] C. E. Finlayson, D. M. Russell, C. M. Ramsdale, et al., Advanced Functional Materials **12**, 537 (2002).

[47] H. Giessen, U. Woggon, B. Fluegel, et al., Optics Letters **21**, 1043 (1996).

[48] Z. A. Peng and X. Peng, Journal of the American Chemical Society **123**, 183 (2001).

[49] V. Klimov, S. Hunsche, and H. Kurz, Physical Review B: Condensed Matter and Materials Physics **50**, 8110 (1994).

[50] R. Perez and A. Gonzalez, Journal of Physics: Condensed Matter **13**, L539 (2001).

[51] J. Shumway, A. Franceschetti, and A. Zunger, Physical Review B: Condensed Matter and Materials Physics **63**, 155316/1 (2001).

[52] R. R. Cooney, S. L. Sewall, K. E. H. Anderson, et al., Physical Review Letters **98**, 177403 (2007).

[53] V. I. Klimov, D. W. McBranch, C. A. Leatherdale, et al., Physical Review B: Condensed Matter and Materials Physics **60**, 13740 (1999).

[54] A. L. Efros, Private communication. (2007).

[55] S. A. Majetich and A. C. Carter, Journal of Physical Chemistry **97**, 8727 (1993).

[56] C. Burda, R. B. Little, S. Link, et al., Proceedings of the International Conference on Lasers **21st**, 85 (1999).

[57] C. Burda, T. C. Green, S. Link, et al., Materials Research Society Symposium Proceedings **536**, 419 (1999).

[58] A. Franceschetti and A. Zunger, Physical Review B: Condensed Matter and Materials Physics **62**, R16287 (2000).

[59] S. Xu, A. A. Mikhailovsky, J. A. Hollingsworth, et al., Phys. Rev. B: Condens. Matter Mater. Phys. FIELD Full Journal Title:Physical Review B: Condensed Matter and Materials Physics **65**, 045319/1 (2002).

[60] S. Empedocles and M. Bawendi, Accounts of Chemical Research **32**, 389 (1999).

[61] M. C. Troparevsky and A. Franceschetti, Applied Physics Letters **87**, 263115/1 (2005).

[62] A. J. Nozik, Proceedings - Electrochemical Society **2001-10**, 61 (2001).

[63] R. G. Neuhauser, K. T. Shimizu, W. K. Woo, et al., Physical Review Letters **85**, 3301 (2000).

[64] P. Kambhampati, D. H. Son, T. W. Kee, et al., Journal of Physical Chemistry A **104**, 10637 (2000).

[65] A. V. Malko, A. A. Mikhailovsky, M. A. Petruska, et al., Journal of Physical Chemistry B **108**, 5250 (2004).

[66] V. I. Klimov, Optical Engineering (New York, NY, United States) **87**, 159 (2004).

[67] V. I. Klimov, A. A. Mikhailovsky, S. Xu, et al., Science **290**, 314 (2000).

[68] V. I. Klimov, C. J. Schwarz, D. W. McBranch, et al., Physical Review B: Condensed Matter and Materials Physics **60**, R2177 (1999).

[69] V. I. Klimov, Private communication. (2007).

Chapter 6:
The Ground State Biexciton: Binding Energy and Stokes Shift

The results presented in this chapter have been published previously and are reproduced with permission from Phys. Rev. B., ***2009****. 80 © 2009 American Physical Society. The co-authors are Alberto Franceschetti, Ryan R. Cooney, Alex Zunger, and Patanjali Kambhampati. The text has been rewritten and enlarged by the author, removing sections concerning theoretical calculations, in order to more appropriately present these results for this thesis.*

In this chapter it will be shown that the state selective measurements can be used to reveal electronic sub-structure of the band edge biexciton. The fact that the band edge biexciton has an electronic structure which is distinct from that of the single exciton is an important result that had not been observed previously.

It was shown in the introduction that many emissive properties of a single exciton in semiconductor nanocrystals could only be explained by including the different factors which split the degeneracy of the band edge state, producing a fine structure on top of the coarse structure determined by quantum confinement alone[1, 2] (see section 1.2.4). This allowed for absorptive and emissive transitions to occur at different energies and this leads to the large, size dependent Stokes shift which is relatively insensitive to solvent and ligand termination[3].

In this chapter we show that anomalies between the biexciton binding energies when measured using absorptive and emissive experiments can be explained by a fine structure of sorts to the band edge biexciton, which can easily be understood as arising due splitting caused by the wurzite lattice and shape asymmetry of a real nanocrystal. This will be referred to from this point forward as substructure (as opposed to fine structure), since this effect does not arise from considerations of spin orientations as in the case of the single exciton.

This is a very important finding, for any applications requiring multiple excitations to be present in a single nanocrystal. When using these materials for optical gain, the energy shift between absorptive and emissive states of the biexciton is probably the most important factor in determining the balance of gain and losses when optically pumping the system[4, 5]. Many of the quantum computing applications envisioned for these materials require the formation of qbits using entangled states of the biexciton[6, 7]. Obviously, this would require a thorough understanding of the electronic structure of biexcitonic energy levels.

Section 6.1 The Band Edge State of the Exciton and Biexciton

As the reader hopefully acknowledges by this point, quantum confinement of charge carriers in CdSe nanocrystals leads to the distinct states visible in the absorption spectrum which correspond to different excitonic states[8, 9]. The band edge state, which is commonly designated as $1S_e$-$1S_{3/2}$ in the literature[10], is well known to have distinctly different absorptive and emissive energies[1, 11]. This fine structure of the band edge state arises from different perturbations which lifts the degeneracy of the state and leads to emission occurring from an optically dark state which is lower in energy than the optically bright state into which optical absorption occurs[3, 8]. The three dominant contributions to the level splitting are the electron/hole exchange interaction, crystal field splitting, and deviations from spherical symmetry in the shapes of real nanocrystal[1, 2, 8, 11, 12] (see section 1.2.4).

The Stokes shift can be measured in two different regimes: the resonant case or as a global parameter[9]. Resonant measurements have complete resolution of fine structure states. For instance, the resonant Stokes shift of the single exciton is the energy difference between the lowest energy absorptive and emissive state within the fine structure of the band edge. Resonant measurements can be obtained by steady state methods using narrow linewidth excitation sources[1], but these lack any time resolution. They can also be obtained with single molecule measurements[13], which is very difficult to set up for transient absorption or time resolved PL experiments in colloidal systems. An advantage of resonant measurements is that they can be compared directly to theoretical predictions which include full resolution of states.

The global case defines its parameters as the shifts between the peaks as measured of the full ensemble (the difference between broadened transitions made up of multiple states) without any narrowing techniques. The global Stokes shift of the single exciton is simply the energy difference between the peak of the P.L. emission and the first peak of the linear absorption spectrum.

While the theoretical models using the described asymmetry and exchange factors successfully predict the resonant stokes shift observed in low temperature fluorescence line narrowing experiments[1], to correctly calculate the global stokes shift requires the inclusion of phonon contributions[3] and/or contributions from surface states[14, 15]. This is done in a somewhat phenomenological manner, as it is not entirely clear why the global Stokes shift is so much larger than the resonant Stokes shift. Since there is not a direct relationship between the two, both the resonant and global Stokes shifts are important parameters when discussing the optical properties of nanocrystals.

While the linear optical properties of the nanocrystals are determined by coarse and fine structure of the single exciton states, in a similar manner the non-linear optical properties will be largely determined from the level structure of the multiexcitonic states (since these make up the excited state absorption contribution to the non-linear optical response in the visible region)[9, 16, 17]. There has been a significant amount of research into multiexcitonic energy levels in quantum confined structures[9, 18], driven by their importance in understanding the fundamental physics of charge carriers in these materials. Much effort has been put into studies of self assembled quantum dots (SAQD) [16, 18-23], and they offer some experimental advantages for doing controlled charging and single particle experiments, but there has also been a significant amount of interest in colloidal systems[9, 24-27].

There are many important distinctions between SAQDs and colloidal nanocrystals, including different shapes, selection rules, relaxation rates, and interaction strengths. It is not straightforward to extrapolate the results obtained in SAQD measurements to colloidal systems or vice versa, so studying each system should be thought of as providing complimentary rather than redundant information.

The coarse structure of the biexciton manifold in colloidal nanocrystals was determined by the measurement of state specific biexciton binding energies in Chapter 4. The biexciton states can be highly degenerate, to first approximation they consist of two separate single excitons of varying degeneracy. The excited states of the biexciton decay too quickly to resolve any level of detail about possible splitting of their degeneracy, but the band edge state can be examined in more detail.

The biexcitonic transitions in colloidal nanocrystals have always been assumed to occur to/from an unsplit biexciton state. This is likely because subtleties to their electronic structure from exchange type splitting are precluded by the closed shell configuration of the $1S_e$ state when populated by two electrons. However there exist in CdSe nanocrystals other possible contributions to substructure to the band edge biexciton, due to the contributions of the crystal field and shape asymmetry in splitting degenerate levels[28, 29].

Section 6.2 Irreconcilable Differences: Absorptive and Emissive Binding Energies

6.2.1 Literature Discrepancies

Experiments in colloidal systems generally examine multiexcitons either using transient absorption (TA) experiments[9, 18, 30] or complementary techniques to obtain time resolved photoluminescence (tr-PL) measurements[24-27]. Historically the first experiments used TA measurements, and observed the formation of multiexciton complexes with shifted energy levels that resulted in induced absorptions when performing pump/probe experiments[30-32]. In general, these experiments measured binding energies which were enhanced significantly over the bulk phase value of ~4.5 meV[33], but the measured values ranged greatly in value. This was due in part to the fact that the actual states populated were ambiguous due to excitation in the UV, and also because early glass samples had significant inhomogeneous broadening. The most complete set of measurements using TA methods on high quality colloidal systems measured a binding energy of 12 meV, with no apparent size dependence over a nanocrystal radius range of 1-5 nm[9].

Measurements from the same group using tr-PL gave much different results. Here they observe a shoulder to the lower energy side of the band edge photoluminescence which is only seen at early delay times and has a supralinear power dependence, and they assign this to ground state biexciton emission[24]. By extracting the peak from the overall signal, they obtain binding energies ranging ~12-35 meV which show complicated size dependence that rises to maximum binding energy at 1.7 nm, and decreases sharply to either side[24]. While these results are contradictory with the values and size dependence of the same groups TA measurements, the tr-PL values are in close agreement with other literature reports in which various multiexciton states have been assigned to different spectral regions of the tr-PL measurements[25-27].

These reported binding energies using tr-PL techniques have less ambiguity than the TA methods, but the use of UV excitation in both cases precludes any claims of complete state specificity. In the tr-PL measurements, the emission measured is from electrons from the conduction band edge recombining with holes that may be distributed in a few different ways. The holes may be at valence band edge state ($1S_{3/2}$) in the interior of the NC, trapped at the surface due the enhanced surface trapping rates described in the previous chapter[34, 35], or there could be combinations of a surface trapped hole and a hole remaining in the interior of the crystal. Theory has shown these types of effects may have a significant effect on emission energy[36, 37].

Furthermore, by excitation high above the band edge it is not possible to control conditions to exclude higher numbers of excitons being formed. Indeed, there will be a significant number of higher order multiexcitons using 400 nm pumping, and the overall ensemble should be populated according to Poissonian statistics[38, 39]. It would be expected that that higher order multiexcitons would perturb the energy of emission[4, 27], and they have been shown to completely alter the TA spectral features[40, 41]. This makes it even more difficult to assign which states emission is being measured from in the tr-PL experiments reported in the literature.

Our state selective pumping allows us to improve upon previous reports by examining the time resolved absorption and emission spectra of the band edge biexciton exclusively. This will allow us to obtain a clearer picture. By excitation with a band edge pump, we can measure the binding energy of the ground state biexciton from the magnitude of the signal in the A1 region, as shown in the previous chapters. The key is that our emissive data uses a high fluence *band edge* pump to heavily excite the sample, allowing us to measure the stimulated emission (S.E.) spectrum of the band edge biexciton. The S.E. spectrum can be measured with very sensitive temporal and spectral resolution.

The S.E. signal obtained with band edge pumping has some important advantages over tr-PL measurements using UV excitation sources. First is that our data is essentially background free, as the only competing signal is a small amount of residual absorption (~10-15%) on the blue edge of the S.E. spectrum, from the portion of the sample which did not absorbed two photons from the pump pulse. This may be easily subtracted, yielding a small change which improves the spectral symmetry but does not significantly alter the peak position of the S.E. spectrum. Our method also allows for specificity for the number of excitations, since with band edge pumping we are limited to maximum of

2 excitations, due to the 2 fold degeneracy of the $1S_e$ state. Furthermore, using the band edge pump and measuring the SE at early times we minimize the contribution of any hole trapped complexes, giving us the best possible state specificity.

On a more practical level, our techniques require no changes the experimental setup. The data for both absorptive and emissive experiments is taken on the same samples, using the same optical setup, and often on the same day- reducing any systematic errors due aging or experimental drift. Any discrepancies in our data can therefore be confidently assigned to the intrinsic properties of the nanocrystals as opposed to some systematic problem arising from comparing data obtained with different techniques.

6.2.2 State Selective Transient Absorption

For these experiments, samples of colloidal CdSe quantum dots passivated with organic ligands (octadecylamine and trioctylphosphine oxide) were used, purchased from NN Labs. The spectroscopic measurements were made in the pump/probe configuration, the details of which were previously described in Chapter 2. The instrument response functions were ~ 65 fs (FWHM) for all pump/probe wavelengths.

The ground state biexciton is made up of 2 electrons in the $1S_e$ ground state of the conduction band and 2 holes in $1S_{3/2}$ state at the top of the valence band. It has a much longer lifetime than both the excited state biexcitons discussed previously and higher order complexes[42], which makes it the most accessible and therefore important multiparticle state for technological applications.

Figure 6.1a shows TA spectra at ~100 fs using a band edge pump compared with the linear absorption spectrum for 3 sizes of CdSe nanocrystals. None of the sizes show an actual induced absorption in the A1 region at this time delay, but clearly the discrepancy between the contours of the linear absorption spectrum and the TA spectra become more pronounced as the radius of the dot decreases. This is not due to any sort of line narrowing due to pump bandwidth, as we have the same spectral widths when pumping into higher excited states on all sizes nanocrystals.

The binding energy of the ground state biexciton as a function of size is calculated using the methods discussed in section 4.3, and is displayed in figure 6.1b. Because we are examining the band edge state, we can define the biexciton binding energy in this case as

$$\Delta_{\mathrm{xx}}^{\mathrm{abs}} = 2 * \mathrm{E}_{1\mathrm{S}-1\mathrm{S}_{3/2}} - \mathrm{E}_{\mathrm{XX}}^{\mathrm{abs}} \tag{6.1}$$

In this equation, Δ_{xx}^{abs} refers to the biexciton binding energy measure by transient absorptive techniques, $E_{1S-1S_{3/2}}$ is the energy of the band edge transition as measured from the linear absorption spectrum, and E_{XX}^{abs} is the energy of a transition into the band edge biexciton state.

The binding energies ranged from ~8 to 17 meV over the range of quantum dots studied. The binding energy increases in smaller dots, a trend that has been seen many other NC properties such as the band gap[43], Stokes shift[11], intraband relaxation[44-46] and multiexciton Auger recombination rates[38, 42]. Confinement increases Δ_{xx} because the carrier-carrier interactions (Coulomb, Exchange) that contribute to level shifting of exciton complexes are enhanced in smaller dots due to greater carrier wavefunction overlap, however assigning the various contributions of different factors is a formidable task for theoreticians[47, 48].

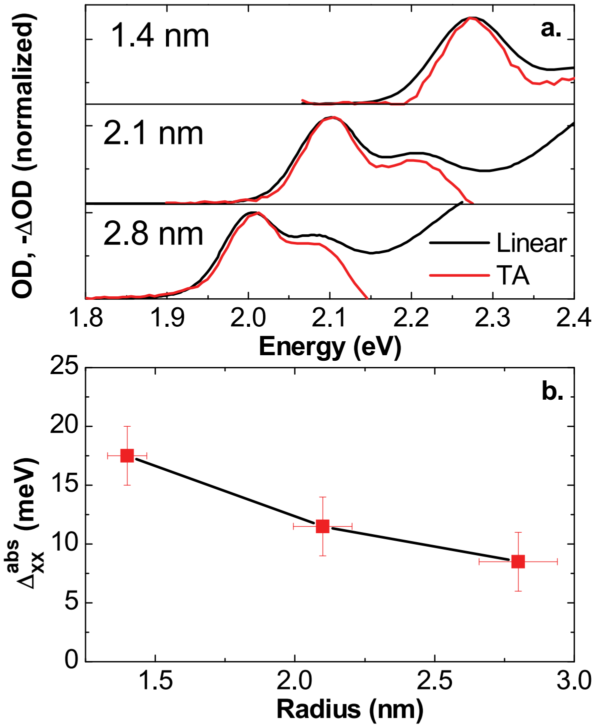

Figure 6.1: Band Edge pump TA spectrum compared with Linear Absorption Spectrum for 3 sizes of CdSe quantum dots a)., Δ_{XX}^{abs} as a function of size b). The contour of the TA spectrum of largest size dot matches the linear absorption spectrum very closely, and deviations become progressively more pronounced as the dot becomes smaller. As seen shown in previous chapters, we can extract the biexciton binding energy for the ground state from these measurements. Δ_{XX}^{abs} is larger in smaller quantum dot samples, due to enhanced multiparticle interactions.

The magnitude of measured values is fairly consistent with the most comprehensive previous literature report when using TA techniques[9]- though they lacked state specificity. The size dependence has been predicted by certain theoretical treatments of these systems[31, 49]. However, our measured biexciton binding energies are much smaller than the literature reports of several groups which measure the binding energy using tr-PL. This led us to examine the same phenomena using state-resolved emissive techniques, which we describe next.

Section 6.2.3 State Selective Stimulated Emission Measurements

Measuring the emission spectrum of band edge biexcitons is another method of looking for level shifting. In numerous tr-PL measurements[24, 26, 27], a redshift of biexciton emission compared with the single exciton PL spectrum has been observed. The size dependence and magnitude of previous measurements are in good agreement with each other, but as we have seen are in disagreement with measurements of the binding energy using transient absorptive techniques.

The biexciton binding energy in an emissive experiment is defined as

$$\Delta_{xx}^{em} = E_{PL} - E_{XX}^{em} \tag{6.2}$$

In this equation Δ_{xx}^{em}, the biexciton binding energy as measured by emissive techniques, is defined as the energy difference between E_{PL}, the energy of the single exciton photoluminescence peak, and the E_{XX}^{em}, the energy of the measured biexciton emission.

In our state selective experiments using the band edge pump it is not possible to exceed 2 excitations per particle, due to the 2-fold degeneracy of the $1S_e$ conduction band state. High pump fluence almost completely bleaches the first absorption feature of the sample, and one can observe a distinct negative going stimulated emission feature in the non-linear spectrum (where the sample emits more probe light than entered). The lineshape of the SE contribution to the TA spectrum is simply the biexciton emission spectrum.

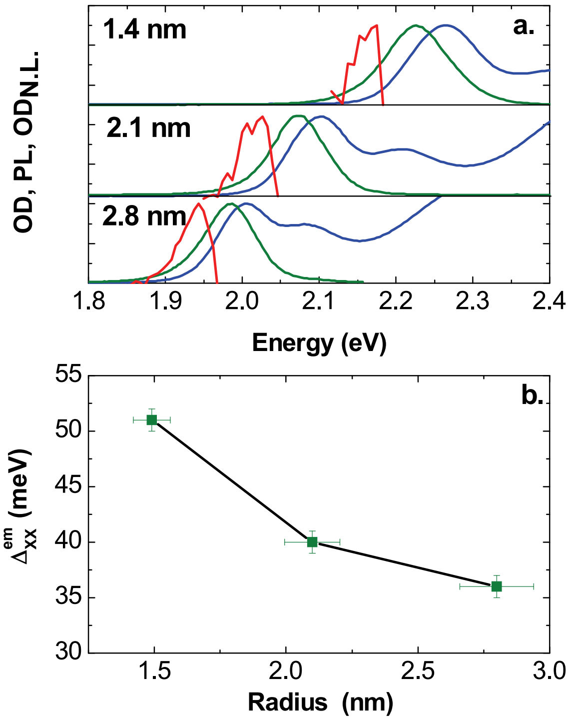

Figure 2: Linear Absorption (blue), Photoluminescence (dark green), and Stimulated Emission Spectrum (red) using band edge pump for 3 sizes of CdSe quantum dots a). Emissive biexciton binding energy, the difference between PL and SE peaks, as a function of radius b). The SE spectrum is the negative portion of the Non-Linear spectrum ($OD_{N.L.} = OD_0 + \Delta OD$). The value of the biexciton binding energy measured comparing emission peaks Δ_{xx}^{em} is much larger than Δ_{XX}^{abs}.

Figure 6.2a. shows absorption, PL and SE spectra for 3 sizes of nanocrystals. The SE spectrum is clearly redshifted from both single exciton absorptive and emissive energy levels. The emissive binding energy as defined in equation (6.2) is plotted below, ranging from 35-50 meV in the size range examined. The magnitudes of the values are consistent with previous measurements tr-PL measurements, but are around three times larger than the binding energies seen in the absorptive experiments (figure 6.1b).

The size dependence of Δ_{xx}^{em} measured in our SE experiments continuously increases as the size of the particle decreases, just as seen in the absorptive case. The most comprehensive previous measurement had a complicated size dependence[24] over the same size range, where the binding energy grew as radius is decreased until a critical size, and then decreased in the smallest sized dots. This was assigned to a regime change where repulsion of like carriers overwhelms attractive biexcitonic interactions[9, 24].

The difference between our data and that shown in Ref (23) is likely due to the different methods abilities to resolve the true size dependent trends. As described previously, using a UV excitation source obscures the actual states being measured due to probably contributions of higher order multiexcitons formed during pumping and enhanced hole trapping at the surfaces, and it is also difficult to extract the true biexciton emission spectrum from the large PL back ground in the tr-PL technique. Our pump probe measurements have almost no competing signals in the energy range of the SE, and are necessarily of the biexciton state with minimal possible hole trapping.

Section 6.2.4: Implications of the Emissive Binding Energy Methods

The emissive binding energy is much too large to be consistent with our absorptive experiments. We examined the relationship of binding energy to induced absorption magnitude in the A1 feature previously, as shown in figure 4.5b (the numerical results in the figure applies to the R = 2.8 nm NC, but would be similar in other sizes). If the band edge biexciton was as strongly bound as suggested by the emissive measurements, the A1 region should consist of a long lived induced absorption of significant magnitude (50% the size of the B1 feature). This is completely inconsistent with all our data, and there are no reports of such features in the literature.

However, our data and the previous literature reports agree on the magnitude of the absorptive *and* emissive binding energy. Since our absorptive measurements are consistent with the spectral characteristics of the A1 region measured under conditions where charges populate the band edge states, this implies that there is some fundamental problem with characterizing the level shifting of the biexciton energy level by the emissive techniques using equation (6.2), instead of an equation similar to (6.1). It is then of interest to consider the implication of comparing the emissive energy levels of the biexciton and single exciton states in order to calculate the biexciton binding energy. In order to extract a meaningful parameter, this implies one of two possibilities which are both shown to be unsatisfactory upon careful consideration.

The first possibility is that the biexciton has no substructure, implying that $E_{XX}^{abs} \approx E_{XX}^{em}$. In this case, one could predict the absorptive binding energy to the energy difference between the biexciton level measured by emission and the linear absorption peak of the band edge state:

$$\Delta_{\mathrm{XX}}^{\mathrm{abs}} = 2 * \mathrm{E}_{1\mathrm{S}-1\mathrm{S}_{3/2}} - \mathrm{E}_{\mathrm{XX}}^{\mathrm{em}} \tag{6.3}$$

This model then requires that the binding energy measured in TA experiments should be even larger than measured in emissive experiments. This is the exact opposite of all reported data, and would yield such large binding energies that the predicted large induced absorptions in the A1 region would be unmistakable in the TA spectrum.

The second possibility is then that the biexciton level structure is the same as that of the single exciton, and that the induced level shifting between the biexciton emissive states would be the same as that of the biexciton absorptive states. However, it is well known that the level structure of the single exciton state is partially determined by e/h exchange[8, 50, 51]. In the biexciton state, this effect is cancelled by symmetry because the 2 fold spin degenerate ground state of the conduction band ($1S_e$) is completely filled. This implies that the level structure must be somewhat different. Furthermore, these experiments measure the binding energy using the ensemble P.L. spectrum, which for the single exciton can have significant contributions from phonons or surface states[3, 14, 15, 52, 53]. How biexciton emission is coupled to these degrees of freedom is not at all clear.

While the emissive binding energy may be experimentally useful, it is clear that there are fundamental problems with using it as a metric for the level shifting in nanocrystals. From the arguments above, we must then consider a case where E_{XX}^{abs} is not equal to E_{XX}^{em}, which would arise from some kind of level splitting which must be distinct from that of the single exciton. The absorptive and emissive experimental results can be reconciled by investigating the substructure of the exciton and biexciton states.

Section 6.3. Reconciliation: Stokes Shift of the Band edge Biexciton

The fine structure of the band edge of the exciton in CdSe NCs has been described previously in great detail, and is illustrated in the lower portion of figure 6.3. It is based upon the energy levels as labeled by the inset to the right hand side. It is accepted that there are 3 optically active states separated in energy by some tens of meV, along with 2 optically dark states[1, 2].

The splitting is caused by both spin (e/h exchange) and the asymmetry of the real Hamiltonian (wurzite lattice, elliptical shape)[8]. The asymmetry results in splitting of the valence band edge $1S_{3/2}$ level into two states, designated as h_1 and h_2 for this discussion (comparable to the light-hole and heavy-hole subbands in bulk semiconductors). The conduction band is not affected by the asymmetry so there is only the $1S_e$ state to consider, designated as e_1. Shown in figure 6.3, this leads to 2 manifolds of single exciton states, (h_1, e_1) and (h_2, e1), depending on which state the hole is populating. At room temperature there is significant population of both states[29].

The electron/hole exchange interaction contributes an optically dark state for each manifold (dashed lines in figure 6.3), depending on the relative orientation of the spins of the electron and hole. The lowest energy state is optically dark, leading to the relatively long P.L lifetime of CdSe nanocrystals[2], and the energy separation between the lowest energy optically active transition and the dark state describes the size dependence of the resonant Stokes shift[1, 3].

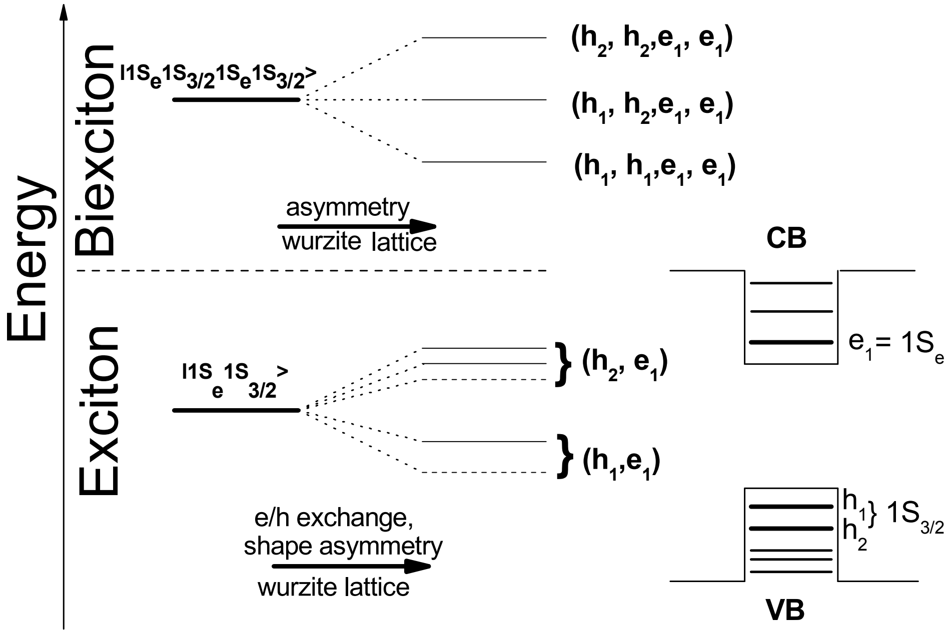

Figure 6.3: Illustration of the splitting of the single exciton and biexciton states. The relevant energy levels are shown on the inset to the right, where e_1 stands for the only state available to electrons ($1S_e$) in the conduction band, while there are 2 different hole state, h_1 and h_2, arising from the splitting of the $1S_{3/2}$ state by the crystal field and deviation from spherical symmetry of the nanocrystal.

For the single exciton, the splitting leads to 5 states, with optically dark states are indicated by dashed lines. The biexciton is split into 3 states, depending upon the configuration of holes. Any analogous splitting in the band edge biexciton has previously been unobserved, yet we can understand what states must be available by considering the same component levels of the conduction and valence band. While the electrons completely fill the e_1 state for the band edge biexciton, the valence subband splitting remains so there are different possibilities for how the two holes can populate the available states. This leads to three states for the biexciton energy level, as seen in the upper portion of figure 6.3. These states correspond to the 3 possible configurations of 2 holes among the valence band edge states.

From the two different single exciton manifolds not all transitions into the biexciton states are allowed. For the states in the (h_1, e_1) manifold there may be transitions into either the (h_1, h_1, e_1, e_1) or (h_1, h_2, e_1, e_1) biexciton state depending on the selection rules, but it is not possible to optically couple the (h_1, e_1) states to (h_2, h_2, e_1, e_1). Similar considerations apply for the (h_2, e_1) single exciton states, which may be excited into (h_1, h_2, e_1, e_1) or (h_2, h_2, e_1, e_1) but not to the (h_1, h_1, e_1, e_1) state.

Examining absorptive transitions from the single exciton to the biexciton using pulsed light will measure a combination of allowed transitions from the different states making up the single exciton fine structure due to the broad bandwidth necessary to maintain femtosecond time resolution. The absorptive binding energy measurements will then have considerable contributions of high energy transitions, both from the populations of holes deeper valence band state (h_2, e_1) making direct transitions into the (h_2, h_2, e_1, e_1) state and indirect transitions into the (h_1, h_2, e_1, e_1) state from (h_1, e_1).

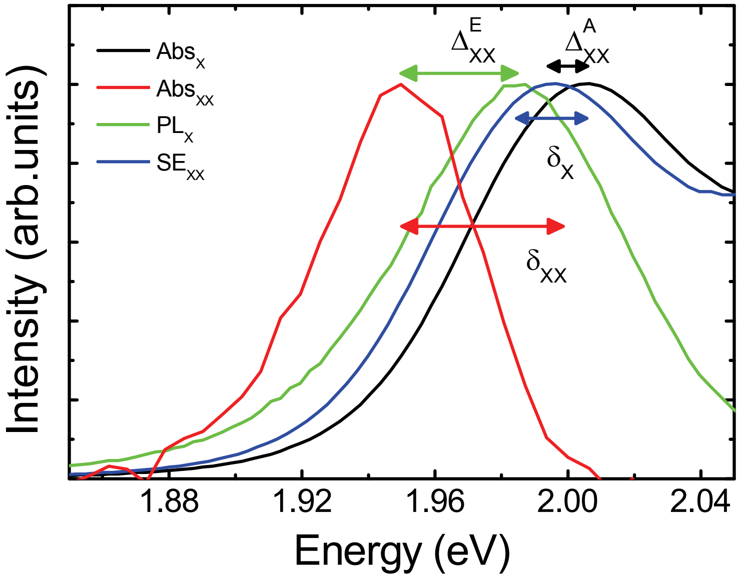

Figure 6.4: The various observable parameters between the measured absorption and emission spectra of the single exciton (X) and biexciton (XX) band edge states. The radius of the nanocrystal is 2.8 nm. The absorptive binding energy was measured via TA measurements (Figure 1), while the emissive binding energies come from the comparison of the stimulated emission spectrum and the single exciton PL. We define the Stokes shift of each state as the energy difference between the absorbing and emitting transition for X and XX.

Following excitation in to the biexciton states, the ensemble relaxes into the Boltzmann distribution. The lowest biexciton level, (h_1, h_1, e_1, e_1) will then be the most heavily populated and make the greatest contribution to stimulated emission in the transition back to states in the (h_1, e_1) manifold. The valence band splitting therefore allows absorptive transitions into the biexciton state to be at a higher energy as emissive transitions back to the single exciton state. Because of this, one can measure different binding energies in the two different experiments.

The biexciton Stokes shift, δ_{xx}, can be defined as the difference in energy between absorption and emission of the biexciton state, just as with the single exciton.

$$\delta_{xx} = E_{XX}^{abs} - E_{XX}^{em} \tag{6.4}$$

Figure 6.4 illustrates these results for one size of NC (R = 2.7 nm). Here we have labeled the 4 observables from the data presented in this chapter: the absorptive and emissive biexciton binding energies, and the global stokes of the single exciton and biexciton.

The single exciton and biexciton Stokes shifts are plotted in figure 6.5a and 6.5b respectively. Both show the same trend of increasing as radius decreases, but the magnitude of the biexciton Stokes shift is much larger than the in the single exciton. Pseudopotential calculations have shown that the biexciton will have a larger Stokes Shift than the single exciton, and predicts the same size dependence[54].

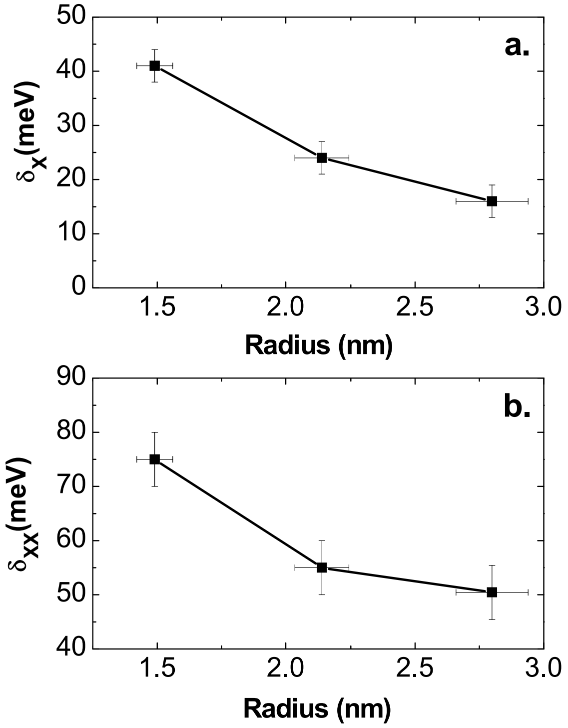

Figure 6.5: Single Exciton Stokes shift (δ_x) as a function of radius a). Biexciton Stokes shift (δ_{xx}) as a function of radius b). The Stokes shift of both band edge exciton and biexciton are greater in smaller nanocrystals, due increased the splitting between bright and dark states. In the biexciton this is due to orbital effects, while in the single exciton the exchange interaction plays a large role.

Since we use TA spectra to obtain the absorptive and emissive spectra of the band edge biexciton, we obtain the global biexciton stokes shift. Our absorption spectra measurements obviously have not resolved the three optically active states making up the $1S_e$-$1S_{3/2}$ transition, but instead measure a transition peak which reflects their energy separation and oscillator strengths. This is also true of the TA and tr-PL experiments, as they use broad bandwidth excitation sources in order to maintain appropriate time resolution. This factor, along with the inhomogeneous broadening of the sample, means that it is not possible to distinguish individual states in the substructure of the levels in order to obtain resonant Stokes shift values. Still, the global biexciton Stokes shift is an important parameter for determining the emissive properties of highly excited samples, especially for optical gain[4, 5].

Section 6.4. Exciton Thermalization

In analogy to the global Stokes shift, it should be noted that we measure the "apparent" biexciton binding energies as there is no resolution of the different transitions which make up the spectral peaks. Each of the optically allowed transitions out of the single exciton state could be in principle assigned a different biexciton binding energy, and our measurement contains a weighted average of the allowed transitions. The model proposed for the electronic structure of the states can be further validated by considering the time dependence of the apparent biexciton binding energy. This also provides a method to measure spin relaxation rates in nanocrystals, which are important potential spintronic applications[55-57].

Upon excitation with our spectrally broad pump pulse into the single exciton state, on the ensemble level there is a distribution of initial states based upon the oscillator strengths of the allowed transitions in the (h_1, e_1) and (h_2, e_1) manifolds. In smaller dots this initial distribution is strongly weighted towards the higher energy transitions, because the e/h exchange interaction skews the oscillator strength towards to upper states as the size of the nanocrystal is decreased[1, 8]. This distribution then will undergo relaxation between fine structure states via spin flipping processes until it reaches the Boltzmann distribution based upon the temperature and energy spacing between the sub levels, favoring the lower energy states. This redistribution of population will cause the biexciton binding energy to give the impression that it is evolving, but this is actually due to changes in the apparent biexciton binding energy as relaxation takes place.

As biexciton interactions are enhanced in the smaller sizes of quantum dots, we are able to observe this relaxation as it occurs. Figure 6.6 shows the kinetic transient taken in the A1 region for a nanocrystal of R = 1.4 nm using a pump pulse resonant with the band edge. As expected from the proposed level structure, there is a very small induced absorption which relaxes into attenuated bleaching with a $\tau \sim 80$ fs, indicating ultrafast relaxation is occurring within the band edge level on this timescale.

Using the method described in section 4.3, the apparent biexciton binding energy is calculated and ranges from 21-17 meV over the first few hundred femtoseconds. This process doesn't measure actual level shifting, but instead reflects the thermalization of excitons within the fine structure of the band edge state. The 80 fs time constant gives us information on the timescale of spin flipping processes in CdSe quantum dots[58], and agrees with measurements of the same processes using an elegant transient grating technique developed by the Scholes group[59, 60]. Unfortunately it is only in the smallest sizes of nanocrystal that this signal is measurable using our technique. In larger sizes these effects are obscured by the difficulty resolving such a fast process in the absence of a positive going signal against the bleaching contribution of the state-filling signals.

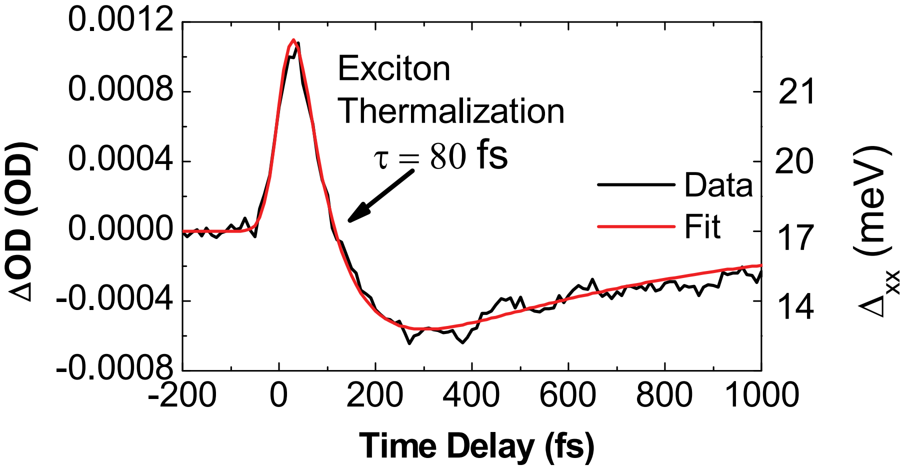

Figure 6.6: A1 Transient when using band edge pump on R = 1.4 nm CdSe quantum dots. The decay time of the feature corresponds to exciton thermalization time of the band edge exciton as the distribution of population among substructure states goes from being weighted by the oscillator strength of the transitions (favoring higher energy states) to the thermal Boltzmann distribution (favoring lower energy states). This shifts the apparent binding energy.

Section 6.5: Conclusions

There had been many reports about the binding energy of the ground state biexciton in colloidal semiconductor nanocrystals, but there was no consensus about the magnitude or size dependence of this parameter. We applied our state selective techniques to measure this parameter, using both the TA techniques seen in chapters 4 and 5, and by measuring the stimulated emission spectrum of the biexciton. Our results for absorptive and emissive binding energy measurements were incompatible, but each agreed in turn with the relevant literature values.

We have shown that in order to understand the band edge biexciton state, one has to consider its substructure. This arises from the splitting of the valence band edge state by asymmetry of the Hamiltonian due to the crystal field of the wurzite lattice and the slightly elliptical symmetry of the nanocrystal, which allows for various possibilities of filling in hole states in the biexciton.

This leads to three separate biexciton states distinguished by the configuration of holes between the available states, which causes the absorptive and emissive techniques to measure very different values for the biexciton binding energy. In essence, these effects can be captured by having the ground state biexciton split by a global Stokes shift between the absorptive and emissive energy levels. This is an important parameter when considering nanocrystals for gain applications[4, 5].

To the best of our knowledge this was the first report of biexciton electronic structure in colloidal quantum dots. Furthermore, we were able to measure the thermalization time for excitons within the fine structure of the band edge state in small NCs to be 80 fs at room temperature. This very fast process occurs via spin flipping, which sets limits upon how these materials can be used in spintronic applications.

References.

[1] D. J. Norris, A. L. Efros, M. Rosen, et al., Physical Review B: Condensed Matter **53**, 16347 (1996).

[2] M. Nirmal, D. J. Norris, M. Kuno, et al., Physical Review Letters **75**, 3728 (1995).

[3] M. Kuno, J. K. Lee, B. O. Dabbousi, et al., Journal of Chemical Physics **106**, 9869 (1997).

[4] R. R. Cooney, S. L. Sewall, D. M. Sagar, et al., Physical Review Letters **102**, 127404 (2009).

[5] A. V. Malko, A. A. Mikhailovsky, M. A. Petruska, et al., Journal of Physical Chemistry B **108**, 5250 (2004).

[6] E. Biolatti, I. D'Amico, P. Zanardi, et al., Physical Review B: Condensed Matter and Materials Physics **65**, 075306/1 (2002).

[7] R. J. Young, R. M. Stevenson, A. J. Shields, et al., J. Appl. Phys. FIELD Full Journal Title:Journal of Applied Physics **101**, 081711/1 (2007).

[8] A. L. Efros and M. Rosen, Annual Review of Materials Science **30**, 475 (2000).

[9] V. I. Klimov, Annual Review of Physical Chemistry **58**, 635 (2007).

[10] D. J. Norris and M. G. Bawendi, Physical Review B: Condensed Matter **53**, 16338 (1996).

[11] A. L. Efros, M. Rosen, M. Kuno, et al., Physical Review B: Condensed Matter **54**, 4843 (1996).

[12] N. Le Thomas, E. Herz, O. Schops, et al., Physical review letters **94**, 016803 (2005).

[13] H. Htoon, P. J. Cox, and V. I. Klimov, Physical Review Letters **93**, 187402/1 (2004).

[14] K. W. Leung, K.B, Journal of Chemical Physics **110**, 11 (1999).

[15] K. Leung, S. Pokrant, and K. B. Whaley, Phys. Rev. B: Condens. Matter Mater. Phys. FIELD Full Journal Title:Physical Review B: Condensed Matter and Materials Physics **57**, 12291 (1998).

[16] M. Bayer, O. Stern, P. Hawrylak, et al., Nature (London) **405**, 923 (2000).

[17] A. E. Colonna, X. Yang, and G. D. Scholes, Physica Status Solidi B: Basic Solid State Physics **242**, 990 (2005).

[18] U. Woggon, Springer Series in Solid-State Sciences **146**, 107 (2004).

[19] I. A. Akimov, A. Hundt, T. Flissikowski, et al., Applied Physics Letters **81**, 4730 (2002).

[20] V. D. Kulakovskii, G. Bacher, R. Weigand, et al., Physical Review Letters **82**, 1780 (1999).

[21] B. Urbaszek, R. J. Warburton, K. Karrai, et al., Physical review letters **90**, 247403 (2003).

[22] M. Ediger, G. Bester, A. Badolato, et al., Nature Physics **3**, 774 (2007).

[23] M. Ediger, G. Bester, B. D. Gerardot, et al., Physical Review Letters **98**, 036808/1 (2007).

[24] M. Achermann, J. A. Hollingsworth, and V. I. Klimov, Physical Review B: Condensed Matter and Materials Physics **68**, 245302/1 (2003).

[25] B. Fisher, J.-M. Caruge, Y.-T. Chan, et al., Chemical Physics **318**, 71 (2005).

[26] J. M. Caruge, Y. Chan, V. Sundar, et al., Physical Review B: Condensed Matter and Materials Physics **70**, 085316/1 (2004).

[27] C. Bonati, M. B. Mohamed, D. Tonti, et al., Physical Review B: Condensed Matter and Materials Physics **71**, 205317/1 (2005).

[28] A. Franceschetti and M. C. Troparevsky, Journal of Physical Chemistry C **111**, 6154 (2007).

[29] A. Franceschetti and Y. Zhang, Physical Review Letters **100**, 136805 (2008).

[30] Y. Z. Hu, S. W. Koch, M. Lindberg, et al., Physical Review Letters **64**, 1805 (1990).

[31] K. I. Kang, A. D. Kepner, S. V. Gaponenko, et al., Physical Review B: Condensed Matter and Materials Physics **48**, 15449 (1993).

[32] V. Klimov, S. Hunsche, and H. Kurz, Physical Review B: Condensed Matter and Materials Physics **50**, 8110 (1994).

[33] H. S. Shionoya, H. Hanamura, E. Akimoto, O., Solid State Commun. FIELD Full Journal Title:Solid State Communications **12** (1973).

[34] S. L. Sewall, R. R. Cooney, K. E. H. Anderson, et al., Journal of Chemical Physics **129**, 084701/1 (2008).

[35] S. L. Sewall, R. R. Cooney, K. E. H. Anderson, et al., Physical Review B: Condensed Matter and Materials Physics **74**, 235328 (2006).

[36] M. C. Troparevsky and A. Franceschetti, Applied Physics Letters **87**, 263115/1 (2005).

[37] A. Franceschetti and A. Zunger, Physical Review B: Condensed Matter and Materials Physics **62**, R16287 (2000).

[38] V. I. Klimov, Journal of Physical Chemistry B **104**, 6112 (2000).

[39] V. I. Klimov, A. A. Mikhailovsky, S. Xu, et al., Science **290**, 314 (2000).

[40] C. Burda, S. Link, T. C. Green, et al., Journal of Physical Chemistry B **103**, 10775 (1999).

[41] D. H. Son, J. S. Wittenberg, and A. P. Alivisatos, Physical Review Letters **92**, 127406/1 (2004).

[42] V. I. Klimov, A. A. Mikhailovsky, D. W. McBranch, et al., Science **287**, 1011 (2000).

[43] L. E. Brus, Journal of Chemical Physics **80**, 4403 (1984).

[44] V. I. Klimov and D. W. McBranch, Physical Review Letters **80**, 4028 (1998).

[45] V. I. Klimov, C. Schwarz, X. Yang, et al., Materials Research Society Symposium Proceedings **536**, 211 (1999).

[46] P. Guyot-Sionnest, M. Shim, C. Matranga, et al., Physical Review B: Condensed Matter and Materials Physics **60**, R2181 (1999).

[47] J. Shumway, A. Franceschetti, and A. Zunger, Physical Review B: Condensed Matter and Materials Physics **63**, 155316/1 (2001).

[48] A. Zunger, Physica Status Solidi B: Basic Research **224**, 727 (2001).

[49] Y.-N. Hwang, K.-C. Je, D. Kim, et al., Physical Review B: Condensed Matter and Materials Physics **64**, 041305/1 (2001).

[50] A. Franceschetti and A. Zunger, Physical Review Letters **78**, 915 (1997).

[51] A. Franceschetti, L. W. Wang, H. Fu, et al., Physical Review B: Condensed Matter and Materials Physics **58**, R13367 (1998).

[52] M. G. Bawendi, P. J. Carroll, W. L. Wilson, et al., Journal of Chemical Physics **96**, 946 (1992).

[53] M. Nirmal, C. B. Murray, and M. G. Bawendi, Physical Review B: Condensed Matter and Materials Physics **50**, 2293 (1994).

[54] L. Sewall Samuel, A. Franceschetti, R. Cooney Ryan, et al., Physical Review B (Condensed Matter and Materials Physics) **80**, 4 (2009).

[55] S. A. Wolf, D. D. Awschalom, R. A. Buhrman, et al., Science (Washington, DC, United States) **294**, 1488 (2001).

[56] M. Ouyang and D. D. Awschalom, Science (Washington, DC, United States) **301**, 1074 (2003).

[57] X. Li, Y. Wu, D. Steel, et al., Science **301**, 809 (2003).

[58] J. Kim, Y. Wong Cathy, P. S. Nair, et al., J Phys Chem B FIELD Full Journal Title:The journal of physical chemistry. B **110**, 25371 (2006).

[59] V. M. Huxter, V. Kovalevskij, and G. D. Scholes, Journal of Physical Chemistry B **109**, 20060 (2005).

[60] C. Y. Wong, J. Kim, P. S. Nair, et al., Journal of Physical Chemistry C **113**, 675 (2009).

Chapter 7: Conclusions and Future Directions

The ability to control the electronic structure of colloidal semiconductor materials by tuning quantum confinement conditions offers intriguing potential technological applications. To use these materials effectively, we must understand the energy levels available, and how the system evolves when excited into these states. Broadly, we must understand how quantum confined charges behave in systems of low dimensionality, which show characteristics intermediate between the bulk and molecular limits. This will allow researchers to determine how to enhance the process desired for a specific application via specific choices of material size and geometry.

Femtosecond time resolution is necessary to follow many of the important processes which occur after optical excitation. Ultrafast measurements in these systems are complicated by the overlap of bleaching caused by population changes and absorptions due to level shifting in transitions made into multiexcitonic states. It is imperative to disentangle these contributions in order to understand both dynamical processes (such as charge carrier relaxation and recombination), and the electronic level structure of the available states.

This thesis was concerned with the development of exciton selective spectroscopy for the measurement of specific dynamical processes and multiexcitonic states in CdSe nanocrystals. It endeavored to show the power of this method over fixed UV excitation pump/probe experiments in addressing some of the long standing problem areas of research into strongly confined systems. It was shown that our methods, while technically challenging, offer a straight forward method of determining the electronic structure of the single exciton and biexciton states and the rates of electron and hole relaxation.

Chapter 3 presented an introduction to the different features of the nonlinear optical response of CdSe nanocrystals, and how they depend on the wavelength of the pump pulse[1]. Pumping into the three lowest energy excitonic states via pulses from an OPA source was compared with UV excitation using 400 nm light. The lowest energy bleaching features, B1 and B2, conclusively showed how state filling signals in these systems follow only the populations of electrons, and are completely insensitive to the dynamics of holes in the valence band. The induced absorption to the red edge of the absorption onset, A1, was shown to be sensitive to the full eigenstate of the system. A subtractive method for examination of state-to-state dynamics of electrons and holes was shown, and it yields high precision time constants for intraband relaxation of each type of charge carrier. Furthermore, the A1 signals had state dependent magnitudes and dynamics, which imply that the biexcitons should be discussed with specificity of the configuration of charges which make up the complex.

Chapter 4 used these results to experimentally determine the types of states coupled in the four lowest energy single exciton transitions visible in the absorption spectrum of CdSe nanocrystals[2], and to determine the biexciton binding energies of the lowest energy intrinsic biexciton states. It was shown that that conventional assignment[3] of the exciton states using the effective mass approximation is not correct for higher excited states, and that the more complicated level structure predicted by semiempirical modeling gives more accurate results[4]. This is an important result for researchers in the design and interpretation of experiments. The lowest levels of the biexciton spectrum were also examined, revealing a somewhat stronger dependence upon the energy of the hole state than of the electron populations. This sets an experimental benchmark for theoretical modeling of these complicated multiexcitonic complexes to take into account.

In chapter 5 the size dependence of excited state biexcitonic interactions was examined[5]. Intrinsic core states were examined by pumping the $1S_e$-$2S_{3/2}$ state in various sizes of CdSe nanocrystals and looking at the magnitude of ΔOD in the A1 region at early times (~50 fs). A new type of mixed phase biexciton where one of the holes is trapped at the surface was also measured at later time (50 ps). Both types had larger binding energies in smaller nanocrystals, showing how confinement enhances the formation of multiexcitonic complexes over wide range of sizes. The dynamics of the surface trapping process was shown to be both size dependent and state dependent. Trapping occurs more quickly from the band edge state in smaller sizes of nanocrystal, consistent with the amount of wavefunction amplitude at the surface. In excited states surface trapping competes effectively with intraband relaxation of holes, leading to the formation of significant amounts of trapped carriers at early times.

In Chapter 6 the band edge biexciton was investigated with complete state specificity using both absorptive and emissive measurements[6]. Our results, which agreed with previous literature results for both techniques, showed a large discrepancy between the observed values for the binding energy of band edge biexciton. This was shown to arise from the electronic substructure of the biexciton, which is split into 3 separate states by the crystal field of the lattice and the elliptical shape of real nanocrystals. This allows for absorption into the biexciton from the single exciton to occur at different energies than emission from the biexciton- in essence there is a Stokes shift for the biexciton in analogy with that of the single exciton.

While this thesis has focused mainly upon multiexciton interactions and dynamics, these techniques have been successfully applied by our group to examine intraband relaxation processes[7, 8], phonon coupling[9, 10], and optical gain[11] in these systems. In each case using state-selective measurements has been shown to provide a clearer picture of the underlying physics behind each of these processes in nanoscale systems than experiments which did not spectrally select their excitation pulses. There are many directions that could be developed further within this framework.

It would be very interesting to see how our results apply to another material. For instance, comparing our predictions with measurements of CdTe or zinc blend CdSe nanocrystals would explore how differences in the strength of spin orbit coupling or changes to the lattice structure effect the electronic structure of the single exciton and biexciton states. The lead salt systems are also of great interest, with a completely different level structure and band gaps in the IR.

Another area in which our method can be applied is investigations of multiexciton formation and recombination. There has been some controversy in the literature concerning the analysis of data looking for evidence of multiexciton generation (MEG), the formation of the multiple lower energy excitations from one high energy excitation[12], as manifested in the magnitude and dynamics of the B1 feature. This has obvious implications for nanotechnology to be used to greatly improve solar cell efficiency. Once formed by MEG or high intensity pumping, the recombination of multiexcitons in nanoscale systems has been assigned to an Auger type of process based upon the changing dynamics of the B1 feature[13], but there is some data which would contradict such a mechanism[14]. However, is it not clear how to correlate the magnitude of the state filling signals measured by the B1 feature to the average number of excitations per particle in highly excited samples[15]. This is a serious problem, which makes it somewhat unclear how to interpret the data shown in both types of experiments. State-selective spectroscopy using combinations of band edge pumping and higher excited pumps offers one way to obtain more specific data, which could help untangle the different contributions to the B1 signal of various multiexcitonic complexes.

The surface of the nanocrystal is also poorly understood, and how much surface states couple to the interior states of a nanocrystal[16-18]. It would be of great interest to determine the different types of surface states which could be involved in the trapping process examined in chapter 5, which would involve a careful examination of the effects of different passivating ligands and overcoating techniques, along with temperature dependent studies. Doing this in conjunction with conventional quantum yield and Stokes shift measurements would be one way to explore how much such states contribute to the global ensemble photoluminescence spectrum, and could help determine the different contributions of acoustic and optical phonons versus surface states to the global Stokes shift[19, 20].

More complicated materials where different layers are deposited upon the nanocrystal have been shown to be useful in tuning charge carrier interactions[21], but there has not been any state-selective investigation. There are also near limitless possibilities as synthetic procedures become more developed for linking different type of nanocrystals together, forming artificial solids or superlattices[22-26]. Such a system created from building blocks which have distinct transitions would be best investigated using sources tuned to create specific excited states, in order to understand the complicated interactions that will likely arise.

Nanoscale semiconductor materials are poised to become one of the foundations of next generation technologies. By examining the specific states that can be formed in these strongly confined systems, this thesis has shown that one should consider excitonic state as a key factor in designing experiments and applications of these materials, in many cases just as important as particle size or composition.

References

[1] S. L. Sewall, R. R. Cooney, K. E. H. Anderson, et al., Physical Review B: Condensed Matter and Materials Physics 74, 235328 (2006).
[2] L. Sewall Samuel, R. Cooney Ryan, and P. Kambamphati, Applied Physics Letters 94 (2009).
[3] D. J. Norris and M. G. Bawendi, Physical Review B: Condensed Matter 53, 16338 (1996).
[4] L.-W. Wang and A. Zunger, Journal of Physical Chemistry B 102, 6449 (1998).
[5] S. L. Sewall, R. R. Cooney, K. E. H. Anderson, et al., Journal of Chemical Physics 129, 084701/1 (2008).
[6] L. Sewall Samuel, A. Franceschetti, R. Cooney Ryan, et al., Physical Review B (Condensed Matter and Materials Physics) 80, 4 (2009).
[7] R. R. Cooney, S. L. Sewall, K. E. H. Anderson, et al., Physical Review Letters 98, 177403 (2007).
[8] R. R. Cooney, S. L. Sewall, E. A. Dias, et al., Physical Review B (Condensed Matter and Materials Physics) 75, 245311 (2007).
[9] D. M. Sagar, R. R. Cooney, S. L. Sewall, et al., Journal of Physical Chemistry C 112, 9124 (2008).
[10] D. M. Sagar, R. R. Cooney, S. L. Sewall, et al., Physical Review B (Condensed Matter and Materials Physics) 77, 235321 (2008).
[11] R. R. Cooney, S. L. Sewall, D. M. Sagar, et al., Physical Review Letters 102, 127404 (2009).
[12] R. D. Schaller, V. M. Agranovich, and V. I. Klimov, Nature Physics 1, 189 (2005).
[13] V. I. Klimov, A. A. Mikhailovsky, D. W. McBranch, et al., Science 287, 1011 (2000).

[14] A. Pandey and P. Guyot-Sionnest, J. Chem. Phys. FIELD Full Journal Title:Journal of Chemical Physics 127, 111104/1 (2007).

[15] A. Franceschetti and Y. Zhang, Physical Review Letters 100, 136805 (2008).

[16] N. A. Hill and K. B. Whaley, J. Chem. Phys. FIELD Full Journal Title:Journal of Chemical Physics 100, 2831 (1994).

[17] K. W. Leung, K.B, Journal of Chemical Physics 110, 11 (1999).

[18] M. Califano, A. Franceschetti, and A. Zunger, Nano Letters 5, 2360 (2005).

[19] D. Valerini, A. Creti, M. Lomascolo, et al., Physical Review B: Condensed Matter and Materials Physics 71, 235409/1 (2005).

[20] T. J. Liptay, L. F. Marshall, P. S. Rao, et al., Physical Review B (Condensed Matter and Materials Physics) 76, 155314 (2007).

[21] L. P. Balet, S. A. Ivanov, A. Piryatinski, et al., Nano Letters 4, 1485 (2004).

[22] M. Ouyang and D. D. Awschalom, Science (Washington, DC, United States) 301, 1074 (2003).

[23] M. Drndic, M. V. Jarosz, N. Y. Morgan, et al., Journal of Applied Physics 92, 7498 (2002).

[24] P. Guyot-Sionnest and C. Wang, Journal of Physical Chemistry B 107, 7355 (2003).

[25] I. Gur, N. A. Fromer, and A. P. Alivisatos, J. Phys. Chem. B FIELD Full Journal Title:Journal of Physical Chemistry B 110, 25543 (2006).

[26] H. Doellefeld, H. Weller, and A. Eychmueller, Nano Letters 1, 267 (2001).